Czech Technical University in Prague
Faculty of Electrical Engineering
Department of Cybernetics

COMPREHENSIVE AUTOMATIC EVALUATION OF SURFACE EMG SIGNAL AND HIGH-DENSITY EMG

by

IVA MILERSKÁ

A dissertation thesis submitted to
the Faculty of Electrical Engineering, Czech Technical University in Prague,
in partial fulfilment of the requirements for the degree of Doctor.

Dissertation degree study programme: Electrical Engineering and Information Technology

Prague, August 2020

Supervisor:
doc. Ing. Lenka Lhotská, CSc.
Department of Natural Sciences
Faculty of Biomedical Engineering
and Czech Institute of Informatics, Robotics and Cybernetics
Czech Technical University in Prague
Jugoslávských partyzánů 1580/3
160 00 Prague 6
Czech Republic

Co-Supervisor:
doc. Ing. Václav Křemen, Ph.D.
Czech Institute of Informatics, Robotics and Cybernetics
Czech Technical University in Prague
Jugoslávských partyzánů 1580/3
160 00 Prague 6
Czech Republic
and Department of Neurology
Mayo Clinic
Rochester, MN 55905
United States of America

Declaration

I hereby declare I have written this doctoral thesis independently and quoted all the sources of information used in accordance with methodological instructions on ethical principles for writing an academic thesis. Moreover, I state that this thesis has neither been submitted nor accepted for any other degree.

In Prague,.....

.....

Ing. Iva Milerská

Abstract

Musculoskeletal problems are widespread throughout the world. Sedentary jobs are currently increasing. Lack of movement leads to a gradual loss of muscles and builds up their imbalance. This results in muscle shortening and poor spine stabilization. Sooner or later, unpleasant complications of the musculoskeletal apparatus such as muscle blockages, neck or lumbar spine pain, head or shoulder pain will occur. Sleep disorders, which negatively affect the physical health of a person, occur more and more frequently. For these reasons, the number of sleep laboratories, rehabilitation and health centers dealing with the causes and consequences of musculoskeletal problems is also increasing. The electromyographic approach and the measurement of muscle tone by so-called myotonometry are mainly used to obtain muscle parameters. However, the development of new devices for these measurements also brings a larger increase in data, which must be processed in both analysis and graphical evaluation of results. Our proposed methods utilize the latest approaches to the processing of electomyographic signals in combination with methods used in electroencephalography and electrocardiography. We also focus on analyzing the processing of myotonometric parameters, which helps us to expand our knowledge of the current state of muscle. The main aim of this work is to propose an effective and non-invasive approach (method) of measuring muscle activity for use in clinical and rehabilitation practice.

Keywords:

SEMG, HD SEMG, myotonometry, joint patterns, REM sleep behavioral disorders, muscle imbalance.

Abstrakt

Problémy s pohybovým aparátem jsou rozšířené po celém světě. Sedavých zaměstnání v současné době stále přibývá. Nedostatek pohybu vede k postupnému úbytku svalů a vytváření jejich dysbalance. To má za následek zkracování svalů a špatnou stabilizaci páteře. Dříve či později se objeví nepříjemné komplikace pohybového aparátu, jako například svalové blokády, bolest krční či bederní páteře, bolesti hlavy nebo ramen. Stále častěji se vyskytují i spánkové poruchy, které negativně ovlivňují psychické i fyzické zdraví člověka. Z těchto důvodů roste i počet spánkových laboratoří, rehabilitačních a zdravotnických center, zabývajících se příčinami a následky muskuloskeletárních problémů. Pro získání svalových parametrů se nejčastěji využívá elektromyografický přístup a měření svalového tonu pomocí takzvané myotonometrie. Vývoj nových zařízení pro tato měření však přináší i větší nárůst dat, která se musejí zpracovávat jak při analýze, tak při grafickém vyhodnocování výsledků. Námi navrhované metody využívají nejnovější přístupy zpracování elektomyografických signálů v kombinaci s metodami používanými v elektroencefalografii a elektrokardiografii. Zaměřujeme se také na analýzu zpracování myotonometrických parametrů, která nám pomáhá rozšířit znalost o aktuálním stavu svalu. Hlavním cílem této práce je navrhnout efektivní a neinvazivní přístup (metodu) měření svalové aktivity pro použití v klinické a rehabilitační praxi.

Klíčová slova:
SEMG, HD SEMG, myotonometrie, kloubní vzorce, spánkové poruchy v REM fázi, svalová dysbalance.

Acknowledgements

I would like to express my thanks to my supervisor doc. Ing. Lenka Lhotská, PhD. for advices given throughout the studies and to my supervisor-specialist Ing. Václav Křemen, PhD. for a constant insight during my research and helping me with numerous problems and professional advancements.

Special thanks go to my friend and colleague Ing. Pavel Vlk for his dedication to the secrets of the programming and to MUDr. Ing. David Macků for consulting and maintaining a healthy perspective.

My research has also been partially supported by the Grant Agency of the Czech Technical University in Prague, grant No.SGS17/216/OHK4/3T/37.

I would like to express thanks to my colleagues for their valuable comments and proofreading.

Finally, my greatest thanks go to my family members, for their infinite patience and care.

List of Tables

List of Figures

Acronyms

ACh acetylcholine. 5–7

AChE acetylcholinesterase. 6, 7

AChRs acetylcholine receptors. 6

Ag-AgCl silver-silver chloride. 8

ANOVA analysis of variance. 31, 41

AP action potential. 6

APs action potentials. 5

DFT Discrete Fourier Transform. 19

DMS deep muscle system. 72

DWT discrete wavelet transformation. 51, 52

ECG electrocardiogram. 13, 46–49, 51–53, 57

EEG electroencephalography. 45, 48

EMG electromyography. 8, 13, 14, 16, 21, 32, 45–48, 53, 58

EO external oblique. 68, 69

EOG electrooculography. 45, 48

EPP end plate potential. 7

ES erector spinea. 68, 69

FFT Fast Fourier Transform. 19, 22

FT Fourier Transform. 19

GM gluteus maximus. 72

GML gluteus maximus left. 62, 63

GMR gluteus maximus right. 62

GUI graphical user interface. 72

HD SEMG high density SEMG. 32, 36, 41

IDWT inverse discrete wavelet transformation. 51, 52

IZ innervation zone. 10, 11, 28

KCl potassium chloride. 8

LBP low back pain. 67, 68

MA moving average. 53, 56, 57

MUAPs motor unit action potentials. 9

MUs motor units. 5, 8

MVC maximum voluntary contraction. 29, 30, 33, 41

NMJ neuromuscular junction. 5, 10

NREM non-rapid eye movement. 45, 48

PHP pronation heel pad. 29, 35

PKS peak interpolation. 53

PM pectoral major. 72

PSD power spectral density. 19, 20, 31

PSG polysomnography. 45–47, 49, 53, 56, 58, 60, 80

RA rectus abdominis. 68, 69

RBD REM sleep behavior disorder. 45–47, 56, 58, 60

RC resistor-capacitor. 15

REM rapid eye movement. 45, 46, 48, 49, 53, 56, 58, 80

RF rectus femoris. 33, 34

RP relaxation phase. 63

RSWA REM sleep without atonia. 45–47, 49, 53, 55–60, 80, 81

SA active sportsmen. 62–66

SavGol Savitzky-Golay. 53, 56

SD standard deviations. 30, 34, 46, 62, 63

SEMG surface EMG. 8–13, 16, 17, 19, 21, 28, 30–33, 35, 38, 39, 41, 45, 47, 49, 51, 53, 57, 58, 60, 79–82

SENIAM Non-Invasive Assessment of Muscles. 10

SHP supination heel pad. 29, 35

SI inactive sportsmen. 62–67

SP squat phase. 62, 63

TL lower trapezius. 68, 69

TM middle trapezius. 68, 69

TU upper trapezius. 68, 69

VGCCs voltage-gated calcium channels. 6

VGKCs voltage-gated potassium channels. 7

VL vastus lateralis. 28, 31

VLL vastus lateralis left. 62

VLR vastus lateralis right. 62

VM vastus medialis. 28, 29, 31, 33, 34

VML vastus medialis left. 62

VMR vastus medialis right. 62

WF wavelet function. 21

WHP without heel pad. 29, 35

WT wavelet transform. 21

Contents

Chapter 1

Introduction

All parts of the body which have a function if used in moderation and exercised in labors in which each is accustomed, become thereby healthy, well developed and age more slowly; but if unused and left idle they become liable to disease, defective in growth and age quickly.

—*Hippocrates, c. 450 B.C.*

Musculoskeletal problems are widespread throughout the world. There are more and more professions characterized by sitting. Sedentary occupation and lack of exercise lead to the gradual muscle wasting and the development of muscle imbalance. Muscle imbalance involves a weakening of muscles, shortening of muscles and impaired spine statics and dynamics in a long-term sitting position. Sooner or later, unpleasant complications in the locomotor system will occur. This can be a muscle block, a neck or chest pain, a headache or a shoulder pain. Increasingly, sleep disorders occur which negatively affects the physical health of a person.

1.1 Motivation

The number of sleep laboratories, rehabilitation and health centres using electromyography (mostly non-invasive surface electromyography - SEMG) approach is rising. They use this method for diagnosis of various disorders such as dysfunction of posture, coordination or sleep disorders. Development of new devices for measurement brings more and more data growth. Thus time demands for classic processing are growing too. This places increasing demands on the processor. New methods are looking for reducing the time required not only for mathematical analysis but also for imaging methods that quickly and efficiently process large amounts of data. The number of companies and software vendors for diagnostic tools already in use is growing. However, not every software is user-friendly and tends to delay its use. When developing new devices or user interfaces, the most important thing is good cooperation with the end-user.

This thesis deals with the processing of SEMG signal according to predefined needs of physiotherapists and doctors for a given diagnostic problem. There are used both classical methods of SEMG signal processing in the time domain and less used spectral analysis. A multi-channel electrode was designed for this purpose. Based on the deep search, charged knowledge and case studies, a muscle contraction detector was designed for muscle timing analysis. This detector has been modified to detect REM sleep behaviour disorder.

By definition, electromyographic measurements cannot be used outside the laboratory or diagnostics department. It is therefore an attempt to replace this expensive and time-consuming measurement with another, less demanding method that meets the required parameters. Information about total muscle load and fatigue can be complement by measuring biomechanical parameters. A myotonometric measurement was designed using a MyotonPro device for this purpose.

On the basis of cooperation with physiotherapists and doctors, three non-binding topics were created, whose task is to understand, simplify and facilitate the time-consuming evaluation of the issues.

1.2 Goals of the Dissertation Thesis

The main goal of the thesis is to propose effective non-invasive methods for measuring muscle activity for use in clinical and rehabilitation practice. In the described research, we investigate measurement problems of joint patterns, muscle parameters and detection of REM sleep behaviour disorder. The main goal is divided into three subgoals, formulated as follows:

- To investigate the representation of joint patterns. To study the problem of detection muscle activity. To propose a method for measuring and detecting muscle contractions.
- To propose a detection method for REM sleep behavioral disorders. To implement a designed solution and test it on the real polysomnographic data from several subjects suffering from sleep disorders.
- To study the problem of measuring biomechanical muscle parameters to complement electromyographic measurement. To design the measurement, test it on the subjects and to create methods for results evaluation.

1.3 Structure of the Dissertation Thesis

Pursuing the goals, the thesis is structured in the following way: Chapter 2 provides medical and technical background for measurement of muscle parameters, electromyography and myotonometry. Representation of joint patterns by using surface electromyography

and high-density surface electromyography is presented in Chapter 3. Methods for detecting muscle contractions and developing multichannel electrodes are also described herein. Chapter 4 deals with a novel semi-automated detection of polysomnographic REM sleep without atonia in REM sleep behavioral disorder based on charged knowledge and a previously designed detector of muscle contractions. Chapter 5 focuses on measuring biomechanical parameters of muscle by using MyotonPro device. This chapter tries to find a method which can substitute the time-consuming SEMG measurement for physiotherapeutic practice. A graphical user interface is designed for this purpose too. The last Chapter 6 provides an overview of succeeding in achievements of goals stated in Section 1.2 and discuss the possibilities of future work.

1.4 List of Author's Publications

Publications Related to the Dissertation Topic

Impact Factor Journals

- Milerská, I., Křemen, V., Gerla, V., St Louis, E.K. and Lhotská, L. "Semi-automated detection of polysomnographic REM sleep without atonia (RSWA) in REM sleep behavioral disorder", *Biomedical Signal Processing and Control.* 2019, 51, 243-252, ISSN 1746- 8094, DOI 10.1016/j.bspc.2019.02.023, IF 3.137, Q2.

Peer-review Journals

- Daniel, M., Tomanová, M., Hornová, J., Novotná, I. and Lhotská, L. "Biomechanical analysis of INFINITY rehabilitation method for treatment of low back pain", *Journal of Physical Therapy Science.* 2017, 29(5), 832-838, ISSN 0915-5287 DOI 10.1589/jpts.29.832.

Conferences

- Milerská, I., Saifutdinova, E., Jelínek, M., and Lhotská, L. "Representation of Joint Patterns in HD SEMG: A Case Study", *Proceedings.* 2019, 31(1), ISSN 2504-3900, DOI 10.3390/proceedings2019031045.

- Milerská, I., Lhotská, L. and Macaš, M. "Biomechanical Parameters of Muscles, Objective Assessment Using MyotonPRO", In: *2018 IEEE International Conference on Bioinformatics and Biomedicine (BIBM) - Proceedings.* Madrid 2018, p. 1522-1525. ISBN 978-1-5386-5488-0. DOI 10.1109/BIBM.2018.8621074.

- Novotná, I., Tomanová, M. and Lhotská, L. "Statistical Evaluation of Objectivisation of Rehabilitation Process", In: JAFFRAY, D.A., ed. *World Congress on Medical Physics and Biomedical Engineering.* Springer International Publishing AG. 2015, p. 1107-1110. ISSN 1680-0737. ISBN 978-3-319-19387-8.

- Novotná, I., Tomanová, M. and Lhotská, L. "Statistical Evaluation of Rehabilitation Process Based on Objective Measurement", *Proceedings of BioDat 2014 - Conference on Advanced Methods of Biological Data and Signal Processing.* Czech Technical University in Prague. 2014. ISBN 978-80-01-05624-0.
- Novotná, I., Křemen, V., Holub, M., Čeřovský, Z., Tichý, M., Hrach, K., Jelinek, M. and Lhotská, L. "Case Study: Functional Verification of Multichannel Surface Electrode for Joint Patterns Investigation", *Proceedings of BioDat 2014 - Conference on Advanced Methods of Biological Data and Signal Processing.* Czech Technical University in Prague 2014. ISBN 978- 80-01-05624-0.
- Novotná, I., Křemen, V., Čeřovskýy, Z., Hrach, K., Jelínek, M., Tichý, M., and Lhotská, L. "Surface EMG Signal Processing for Evaluation of Isometric Voluntary Extension of the Knee Joint", *BioDat 2013 - Conference on Advanced Methods of Biological Data and Signal Processing.* Czech Technical University in Prague 2013. ISBN 978-80-01-05410-9
- Novotná, I., Holub, M., Křemen, V., Čeřovský, Z., Hrach, K., Jelínek, M. and Tichý, M. "Případová studie: Kloubní vzorce při využití povrchového EMG", *MEDSOFT 2014.* Creative Connections 2014. p. 173-183. ISSN 1803-8115. ISBN 978-80-86742-38-0.

Other Publications

- Volf, P., Kutílek, P., Hejda, J., Černý, R., Milerská, I. and Hána, K. "Methods evaluating upper arm and forearm movement during a quiet stance", *Lékař a technika - Clinician and Technology.* 2019, 49(2), p.58-65, ISSN 0301-5491.

Publications Unrelated to the Dissertation Topic

Peer-review Journals

- Macků, D. and Novotná, I. "Patients above the age of 70 face unjustified discrimination in heart transplants", *European Geriatric Medicine.* 2017, 8(5-6), 509-510. ISSN 1878-7649. DOI 10.1016/j.eurger.2017.07.020, IF 1.326.

Other Publications

- Macků, D. and Novotná, I. "The public's Acceptance of eHealth in the Czech Republic - Condition for success", *International Journal on Biomedicine and Healthcare.* 2016. ISSN 1805-8698.

Chapter 2

State of the Art

This chapter contains all needed prerequisites for further reading - short introduction to anatomy consequences, introducing basic approaches to measuring muscle response, characteristics of signals and their measurement and processing.

2.1 Functional Anatomy of the Muscle

The muscle system is responsible for movement of the human body, posture, movement of substances inside of body, and for generation of body heat. There are three main types of muscle in the human body: skeletal, smooth, and cardiac. Each skeletal muscle is an organ that consists of various tissues such as skeletal muscle fibers, blood vessels, nerve fibers, and connective tissue. Each muscle is wrapped in an epimysium (a sheath of dense, irregular connective tissue), which allows a muscle to contract and move powerfully while maintaining its structural integrity, separates muscle from other tissues, and allowing the muscle to move independently. Muscle fibers are organized into individual bundles (fascicle), by the perimysium (a middle layer of connective tissue). Inside each fascicle, each muscle fiber is encased in endomysium (a thin connective tissue layer of collagen and reticular fibers). The plasma membrane of muscle fibers is called the sarcolemma. The functional unit of the muscle fiber is a highly organized arrangement of the contractile myofilaments actin and myosin called sarcomere [12, 13, 3]. Structural hierarchy of skeletal muscle is shown in Fig. 2.1.

Functional and biomechanical units of muscles are motor units (MUs). A MU consists of the individual muscle fibers innervated by a single motor nerve cell, or motoneuron. The site where a motor neuron's terminal meets the muscle fiber is called the neuromuscular junction (NMJ) [12]. The essential role of the NMJ is to convert a temporal sequence of action potentials (APs) in motor neurons into muscle contractions [14]. The NMJ is composed of synaptic end bulbs, motor end plate and synaptic clef.

- Synaptic end bulb is a bulbous swelling at the end of each axon terminal, which contains many synaptic vesicles such as neurotransmitter called acetylcholine (ACh).

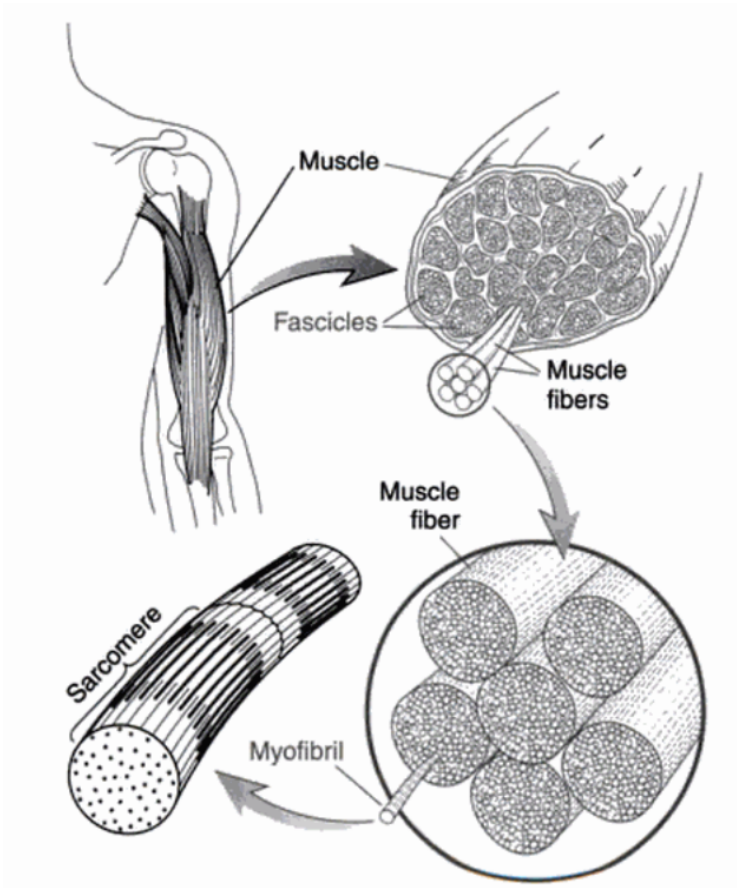

Figure 2.1: Structural hierarchy of skeletal muscle. Adopted from [3].

The ACh is responsible for transmission of impulse from axon to muscle fiber through the synapse.

- Motor end plate is the part of the sarcolemma, which is in the closest proximity to the synaptic end bulb.
- Synaptic cleft is the space between the presynaptic and postsynaptic membranes (the motor end plate and synaptic end bulb) [4, 15].

The terminal boutons of the motor nerve axon contain mitochondria and small spherical synaptic vesicles that store the ACh. Synaptic cleft contains an amorphous-looking basal lamina that, among many functions, anchors the enzyme acetylcholinesterase (AChE). The peaks of the postsynaptic folds are particularly electron dense because of their high concentration of acetylcholine receptors (AChRs). When the action potential (AP) reaches the motor nerve terminal, the depolarization opens voltage-gated calcium channels (VGCCs), resulting in the Ca^{2+-}dependent release of ACh into the synaptic space. ACh diffuses rapidly to the postsynaptic membrane and binds to the AChRs, leading to opening of

the ACh-gated ion channel and a local depolarization called the end plate potential (EPP). If the EPP exceeds a certain threshold, voltage-gated sodium channels that lie at the bottom of the postsynaptic folds are opened, which results in generation of the muscle action potential that propagates along the muscle fiber and activates muscle contraction. The action of ACh is terminated by its dissociation from the AChR by hydrolysis by AChE, and by diffusion from the synaptic cleft. Meanwhile, in the motor nerve terminal, the resting membrane potential is restored through the opening of voltage-gated potassium channels (VGKCs) [15].

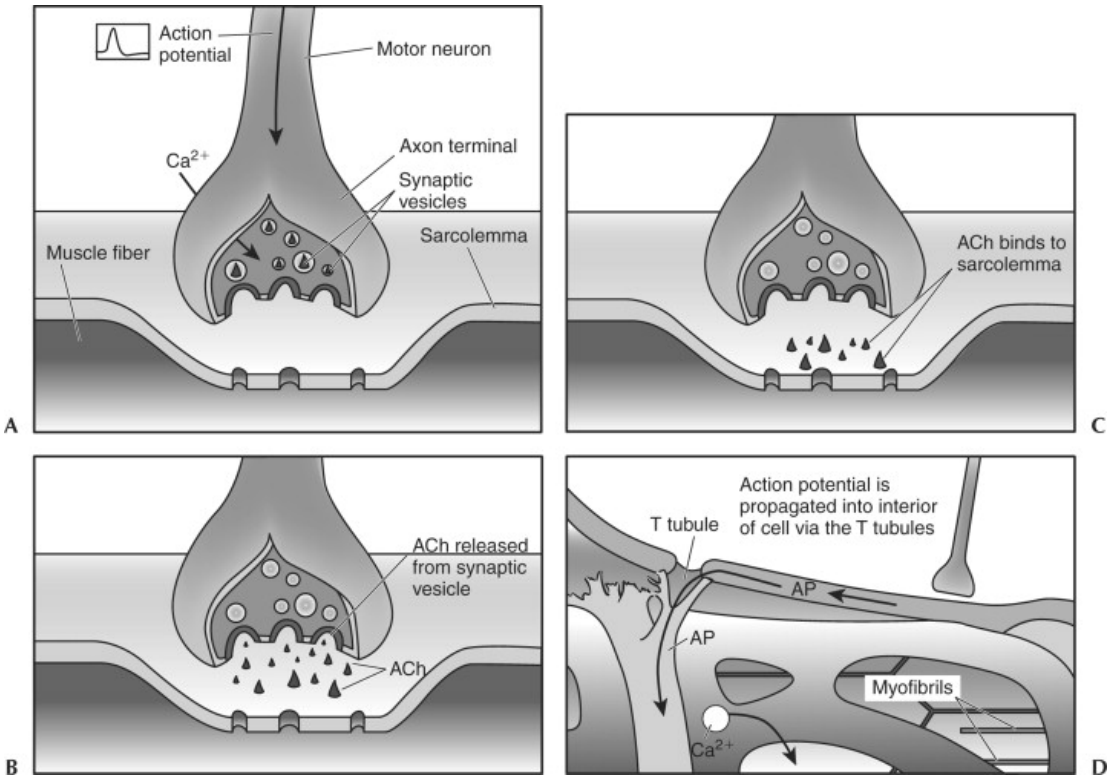

Figure 2.2: Events at the neuromuscular junction. A) An action potential in the axon terminal causes the uptake of Ca^{2+} into the axon terminal and the subsequent release of the neurotransmitter. B) The neurotransmitter (ACh) is released from the synaptic vesicles and diffuses across the synaptic cleft. C) Generation of action potential: The binding of the ACh to receptors of the sarcolemma causes a change in membrane permeability, causing the AP to be initiated in the sarcolemma. D) The AP is propagated into the interior of the cells via the T tubules. Adopted from [4].

Basically, there are two approaches to measuring skeletal muscle response (electrical and mechanical). Electrical methods include electromyography and mechanical represents myotonometry.

2.2 Electromyography

Electromyography (EMG) signals are generated by skeletal muscles, which are the motors allowing the movement of our bodies. This process supports central control strategies, signal transmission along nerve fibers and across neuromuscular junctions and electrical activation of the muscle fibres. Those fibers are organized in elementary MUs. MUs produce forces that result in movement of bones by a chain of complex biochemical events. The EMG signals provide a window on the actor as well as on its controller [5].

2.2.1 Electrodes

EMG signals can be measured directly from muscles by needle electrodes or from skin by surface electrodes. The signals are used for observation of the musculoskeletal system functions. Those are estimated by the rate of involvement of muscle fibers, monitoring local changes in EMG during muscle fatigue and by analysing intervals (i.e. during gate analysis or study movement trajectory). EMG amplitude of the bipolar measurement is used for monitoring muscle activation levels and forces produced during muscle contraction [16].

EMG electrodes can be divided in groups shown in Fig. 2.3.

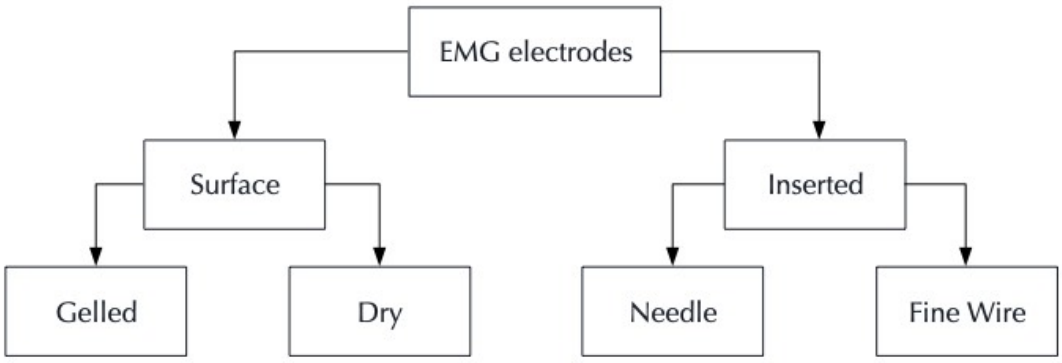

Figure 2.3: Types of electrodes

Application of surface EMG (SEMG) electrodes requires proper skin preparation beforehand. In order to obtain a good quality of SEMG signal, the skin and hair must be completely removed from the location where the SEMG electrodes are to be placed. It is advisable to use an abrasive gel to reduce amount of dry skin layer.

Gelled Electrodes

Gelled SEMG electrodes contain electrolytic gel as an interface between skin and electrodes. Solution of potassium chloride (KCl) is used as an electrolyte and silver-silver chloride (Ag-AgCl) is the most common composite for the metallic part of these electrodes. Their disadvantage is the possibility of their movement during measurements that

creates a motion artifact in measured SEMG signal [17]. The scheme of gelled electrodes is shown in Fig. 2.4 B).

Dry Electrodes

Advantage of dry electrodes is that they do not require gel interface between the skin and the electrode body. Bar electrodes and electrodes grids are examples of dry electrodes. Disadvantage is the possibility of formation of a half-cell potential due to perspiration. Another disadvantage is the variable area of the electrodes due to the changing pressure on the electrodes to the skin, which can cause a change in capacity [17]. The scheme of dry electrodes is shown in Fig. 2.4 A).

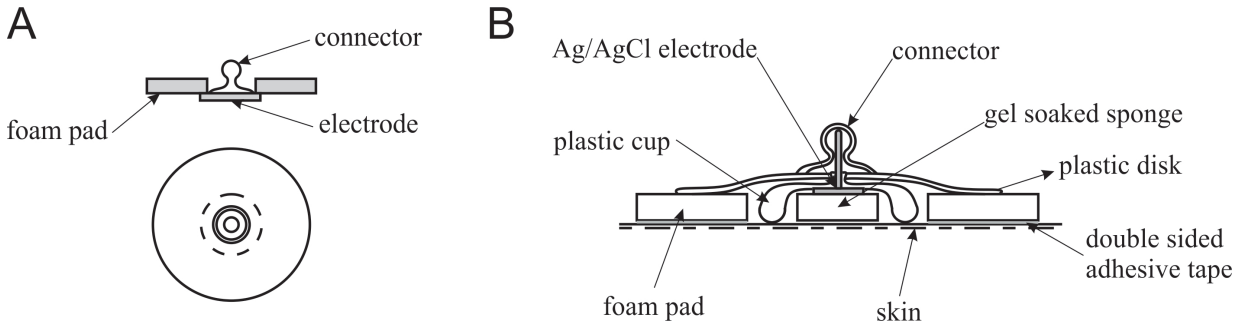

Figure 2.4: Scheme of A) dry electrodes and B) gelled electrodes.

Needle Electrodes

Small pickup area of needle electrodes enables to detect individual motor unit action potentials (MUAPs) during relatively low force contraction. Advantage is that the electrodes may be conveniently repositioned within the muscle (after insertion) so that new tissue territories may be explored. Nevertheless, their application is more complicated than the surface ones and may be uncomfortable for the patient [17]. Exact placement of these electrodes must be checked using an ultrasound device, which makes the procedure more demanding.

Fine Wire Electrodes

Wire electrodes are made from any small diameter, highly non-oxidizing, stiff wire with insulation. They are placed directly into the cell and measure potential difference across the cell membranes. In order not to destroy the function of the cell we must take into account the size of each electrode. Most common design is a metal film vapor-deposited on a thin glass fiber or micropipette [17].

2.2.2 Electrode Location

The paradoxical problem with SEMG is that it is one of the easiest electrophysiological signals to measure, but also one of the hardest to interpret quantitatively. The raw surface electromyography recordings contain the signal that originates in the muscle and various noise components that are unavoidable. There are many aspects that affect the purity of the recorded signals. The first question is where to actually place the electrodes on a muscle to reach the purest signal as possible and with the maximal amplitude.

Recommendations for the location of sensors (a bipolar electrode montage) for a number of often studied muscles are given by idea of SEMG for the Non-Invasive Assessment of Muscles (SENIAM) [18]. SENIAM works with sensors instead of electrodes, because there are more types of measuring devices than electrodes.

SENIAM recommendations are derived from several principles. The most important one is respect to the longitudinal (in fiber direction) location of the sensor on the muscle. It is recommended to place the sensor halfway the (most) distal motor endplate zone to the distal tendon. With respect to the transversal location of the sensor on the muscle, it is also recommended to locate the sensor on the surface away from the 'edge' of other subdivisions or other muscles so that the geometrical distance to other muscles is maximized [18, 19].

During last several years the importance of electrode configuration and location has been addressed in a number of methodological and clinical publications [5, 16, 20, 21]. The monopolar configuration contains the entire information available from the recorded signal but is used almost exclusively used in research applications because of its sensitivity to common mode signals. The single differential also referred to as bipolar differential is the most widely used configuration [5].

The single differential signal generated by a single fiber and detected with electrodes placed symmetrically with respect to the NMJ will theoretically be zero. Because of scatter of the NMJs neuromuscular junctions this electrode location corresponds to a minimum of signal amplitude. When electrodes are applied in spite of SENIAM (i.e. over the innervation zone (IZ) of a muscle) single differential electrode systems usually detect signals that are of low amplitude and contain lot of noise. Those configurations also carry little information because of the cancellation effect due to the bidirectional propagation, and are extremely sensitive to small displacements between electrodes and muscle [5]. Situation example can be seen in Fig. 2.5 that highlights the importance of a correct electrode placement.

2.2.3 Multichannel SEMG

In recent years, great effort has been performed to overcome the limitations of the classic bipolar SEMG recording technique. The major reason for increasing the number of electrodes in SEMG is to increase the number of recording positions placed over the muscle in order to obtain a map of the potential distribution over the skin rather than a single local observation [22, 23].

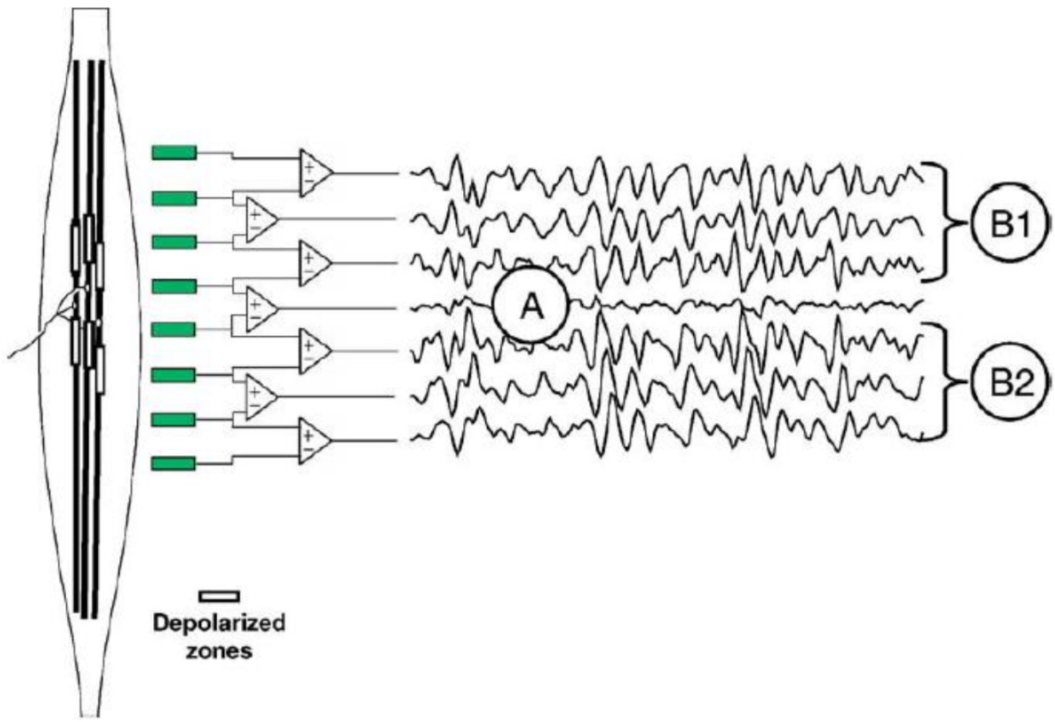

Figure 2.5: An example of SEMG signal recorded with linear electrode array in single differential mode during a strong contraction of a Vastus medialis muscle. The observed signal amplitude minimum over the IZ (A) and the phase reversal (B1 and B2) is the consequence of both the single differential recording mode and the movement of the depolarized zones toward tendon terminations in opposite direction. Adopted from [5].

Linear electrodes arrays and electrode grids are assumed for multichannel recordings.

2.2.3.1 Linear Electrode Arrays

The linear electrode arrays provide valuable information about muscle. It is used to find the locations of the IZ and tendons, and the fiber length. Another use is for estimation of muscle fiber conduction velocity or investigation of single MU control and conduction properties [24]. Measuring modalities are shown in Fig. 2.6.

2.2.3.2 Electrode Grids

An electrode grid makes the analog movie, which evolves in space and time under a 2 dimensional array. Each image of the movie is time specific and defines an area in the x and y directions. The distribution of SEMG amplitude provides a topographical representation of muscle activity [25].

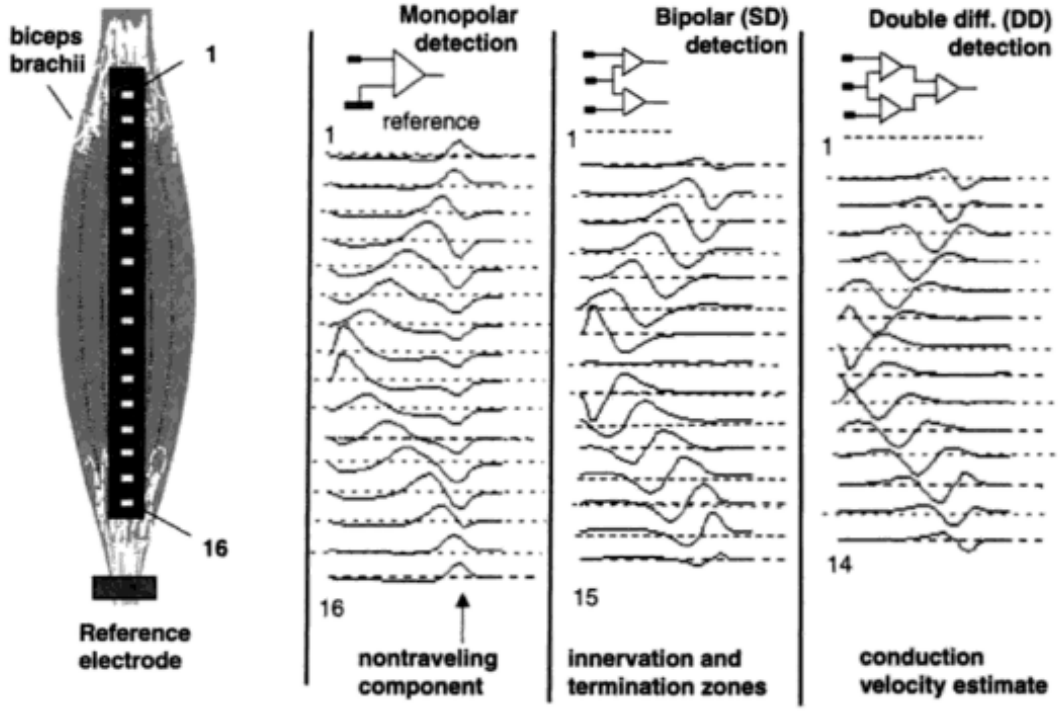

Figure 2.6: Modalities of detection of SEMG signals with linear electrode arrays. Adopted from [5].

2.2.4 Signal Processing

One unfortunate but unavoidable fact with regards to acquisition of biological electrical signals is that pure signals are very rarely, if ever, obtained. Elements contaminating pure SEMG signals are other biological signals (e.g. from the heart) and noise (generated by electrical equipment in proximity or from moving wires during data measuring). The process of removing this contamination is known as signal processing. It is in fact a series of mathematical steps which attempt to remove the additional elements and leave only the pure SEMG signal [26].

Type of Noise

- **Inherent Noise in the Electrode**

  The surface electrodes are widely used for SEMG recordings. It has been found that these silver electrodes give adequate signal-to-noise ratio and are electrically very steady [27, 28].

  When the electrode size enlarges, the impedance decreases. However, electrode size should not be very large. On the other hand, high electrode impedance effectively

reduces the signal quality and gives low signal-to-noise ratio. Therefore, both parameters should be taken into consideration. Researchers are allowed to use high electrode impedances for experiments in which statistical power is high or in which large numbers of electrodes are necessary, but tend to switch to low electrode impedances for experiments in which statistical power would otherwise be too low [28, 29].

- **Movement Artifacts**

  The most common disturbing signal is a motion artifact that is caused by movement of the cable connecting the electrode to the amplifier and the interface between the detection surface of the skin and the electrode [28]. The harmonics of this unwanted signal are usually in the 0-20 Hz frequency range. Information concerning the firing rates of the active motor units is unfortunately partially also contained in this spectrum range [29].

- **Electromagnetic/Power-line Noise Artifacts**

  Ambient noise is generated by electromagnetic devices such as computers, force plates, power lines etc. The dominant concern for the ambient noise arises from the 50 Hz (or 60 Hz) radiation from power sources, which is also called Power-Line Interference. This is caused by differences in the electrode impedances and in stray currents through the patient and the cables [30].

- **Electrocardiographic Artifacts**

  The most interfering component in SEMG signals is electrical activity of the heart. This physiological artifact is called an "electrocardiogram (ECG) artifact". In general the EMG recordings containing the ECG artifacts can often be determined by mere visual inspection. Nonetheless it is difficult to algorithmically remove the contamination because of the ECG's complicated waveform (broad-band spectral distribution). This distribution covers many higher harmonics characterizing the ECG but also reflects the transient nature of the heart rate, which causes peaks at harmonics to broaden substantially [31, 28].

- **Cross-talk Artifacts**

  Crosstalk is undesirable EMG signal from a muscle group that is not commonly monitored. It contaminates the signal and can cause an incorrect interpretation of the signal information. It can be minimized by choosing electrode size and inter-electrode distance. The mathematical relationship between the target muscle EMG and crosstalk is presented as [28]:

$$T_b^2 = Rb_c^2 + T_i^2 + Ob_c^2, \tag{2.1}$$

  where T_b is the background EMG activity recorded at the target muscle, T_i is the intrinsic activity of the target muscle itself, R_b is the crosstalk from the remote muscle and O_b is the crosstalk from other muscles.

Before any type of filtering to remove noise, the signal itself must be viewed and the frequency content of the signal must be considered. One approach to analyze the frequency of a signal is to use Fourier analysis. Fourier analysis is a process to determine the range of frequencies present in a signal. Typically fast Fourier transform is used to analyze frequency content of signals and as such is available in a wide variety of programming languages [26].

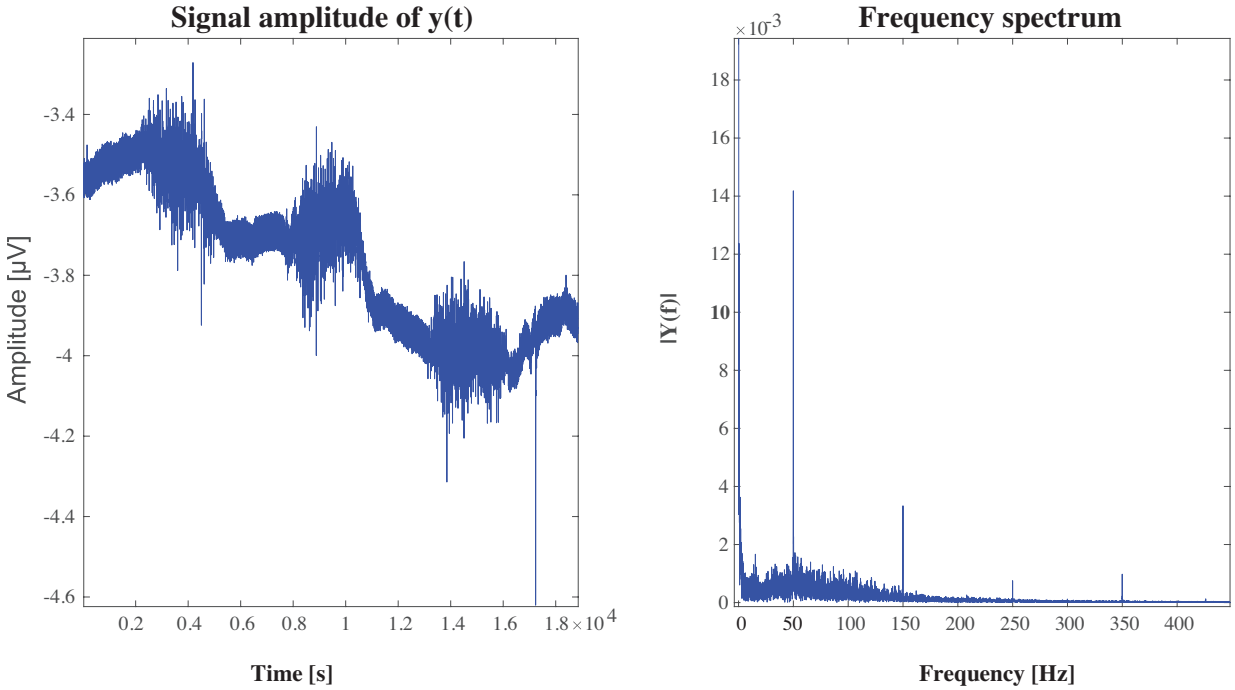

Figure 2.7: Example of original signal $y(t)$ amplitude before filtering and its spectrum based on frequency analysis using Fourier transform. Power line artifacts are manifest as spectral peaks at the power line frequency (here 50 Hz) and multiples.

Visible noise in raw signal

A primary characteristic of the raw myoelectric signal is that the signal is centered around zero. Zero offset is simply a graph which is not centered on the zero line, i.e. the middle of the graph is slightly above or below the zero line. The simplest way to check for zero offset, other than to view it on a graph is to calculate the average value for the signal. If the average of the signal is not zero the simplest correction is to subtract the average value from each data point in the signal [26].

The majority of the EMG signal frequency concentration is between 20-200 Hz, with minor contributions potentially extending up to 1000 Hz. Therefore, very low frequencies e.g. 1-5 Hz in the signal are likely to be noise, and as such they should be removed [26].

In Fig. 2.7 a 50 Hz electrical noise and its higher harmonic components are observed. These frequencies have to be removed.

2.2.5 Signal Denoising

There are two key groups for considering signal filters. The first one is low pass filters which retain signal frequencies below the filter cut-off frequency and attenuate frequencies above the filter cut off frequency. A low pass filter response is shown in the Fig. 2.8 A).

A low pass filter can be developed by using a resistor-capacitor (RC) circuit (Fig. 2.8 C)). This circuit is a first order low pass filter. It is the simplest low pass filter possible. The cut-off frequency f_c of the low pass filter is given in Eq. (2.2) [32].

$$f_c = \frac{1}{2\pi RC}, \tag{2.2}$$

The second group is high-pass filters which are filters that retain signal frequencies above the filter cut off frequency and attenuate frequencies below the filter cut off frequency. A high pass filter response is shown in Fig. 2.8 B) [26].

A RC circuit of high pass filter is in Fig. 2.8 D). The cut-off frequency equation is the same as that of Eq.(2.2).

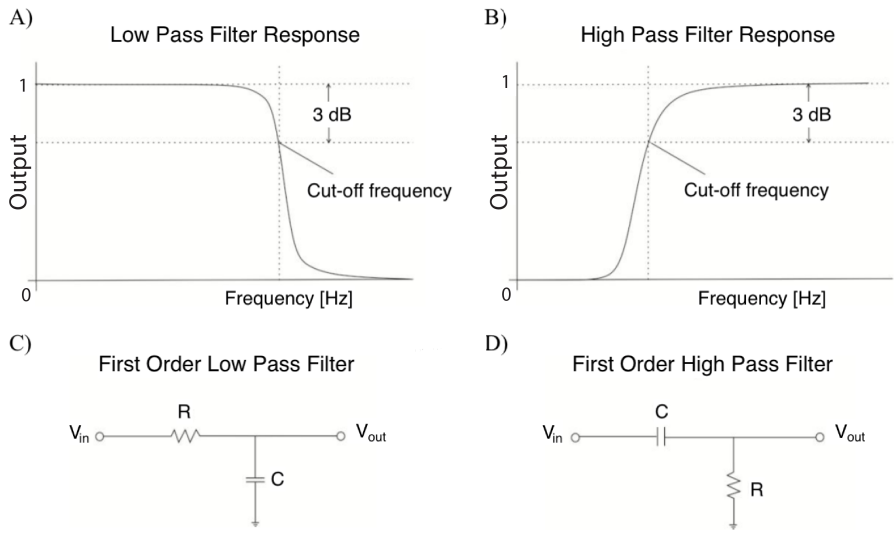

Figure 2.8: A) Low pass filter response. B) High pass filter response, C) RC circuit of low pass filter, D) RC circuit of high pass filter

To remove the unwanted frequency range 0-20 Hz the high-pass filter is therefore designed with a cutoff frequency in the 15 to 20 Hz (or in movement analysis in the 25 to 30 Hz) range [5].

With the exception of few cases, about 95% of SEMG power is accounted for by harmonics up to 400 Hz and most of the remaining percent by electrode and equipment noise. A low pass filter should be applied to the signal to further attenuate these unwanted components. The cut-off frequency is usually chosen near to 500 Hz and the sampling frequency must then be 1000 samples/second or higher (sampling theorem: sampling must be > 2 times the highest frequency in the signal) [18].

The simplest method of removing narrow bandwidth interference from a recorded signal is to use a notch filter. Digital notch filters come in a variety of different forms that can be used for various purposes and that achieve different results. An example of notch filter response is shown in Fig. 2.9. In general, this is not a good practice because it removes power from a frequency band where EMG shows high-power density and introduces phase rotation that extends to frequencies below and above the central frequency thereby dramatically changing the waveform of the EMG [5, 33].

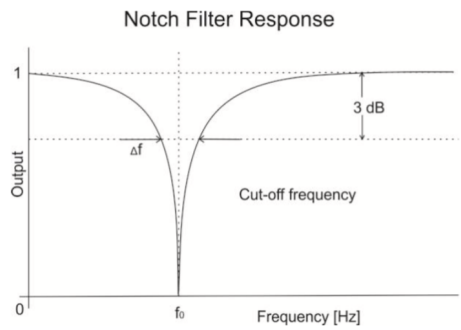

Figure 2.9: Notch Filter Response, f_0 denotes the center frequency and Δf denotes the frequency bandwidth

2.2.6 Signal Analysis

Two basic approaches are used to process signal from SEMG. The first one involves analyzing the characteristics of interference patterns, such as the number of times the SEMG signal changes direction, called turns. The second one is based on power spectral analysis. Analysis of interference patterns has one main advantage according to D. A. Gabriel et al. [34]: the SEMG signal does not need to be stationary. The only methodological control required is that they perform contractions that are standardized from session to session. Patients can either maintain a constant level of force or exert a maximum effort contraction [34].

2.2.6.1 Time domain signal analysis

This type of analysis of the measured SEMG signals is characterized by a signal waveform display.

Spike shape analysis

Spike shape analysis uses two major components of the SEMG signal: spikes and peaks (Fig. 2.10). A spike is composed of a single upward and downward deflection. A peak is defined as a pair of upward and downward deflections within a spike that do not together constitute a discrete spike [6].

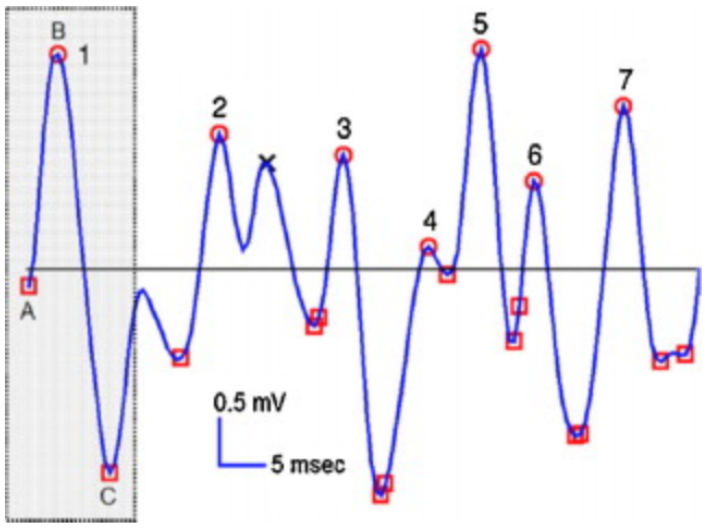

Figure 2.10: An illustration of SEMG spike shape analysis. Adopted from [6]

The variables computed to perform a spike shape analysis include mean spike amplitude (MSA), mean spike frequency (MSF), mean spike slope (MSS), mean spike duration (MSD) and mean number of peaks per spike ($MNPPS$). The MSA calculation is shown as

$$SA_y = \frac{(B_y - A_y) + (B_y - C_y)}{2}, \tag{2.3}$$

and

$$MSA = \sum_{i=1}^{NS} \frac{SA_y}{NS}, \tag{2.4}$$

where SA_y is spike amplitude, the x and y subscripts are the x- and y-coordinates of points A (the beginning of each spike), B (the highest peak in a spike) and C (the end of each spike) and NS is the number of spikes in a given sample of SEMG [6].

MSF is calculated by taking the NS seen in the data window and dividing by the total duration (TD) of that data analysis window. The MSF algorithm is shown as

$$MFS = \frac{NS}{TD}, \tag{2.5}$$

where NS is the number of spikes and TD is the total duration of a given sample of SEMG [6].

Individual spike slopes are calculated from the beginning of each spike (point A) to its peak (point B) simply based on the x- and y-coordinates of points A and B on the spike. Once the slope for each spike is calculated, the mean spike slope across the data window is determined as the sum of the spike slopes divided by the number of spikes (NS) seen within that data window. The MSS algorithm is shown in as

$$SS = \frac{B_y - A_y}{B_x - A_x}, \tag{2.6}$$

and

$$MSS = \sum_{i=1}^{NS} \frac{SS}{NS}, \tag{2.7}$$

where SS is the spike slope and NS is the number of spikes of a given sample of SEMG [6].

$MNPPS$ is calculated by determining the number of peaks (P) in the recording window and dividing it by the NS in the same window. The $MNPPS$ algorithm is shown as

$$MNPPS = \frac{P}{NS}. \tag{2.8}$$

MSD is calculated by determining the duration of each individual spike. The duration of all of the spikes within the data window are then summed and divided by the NS. The MSD algorithm is shown as

$$MSD = \sum_{i=1}^{NS} \frac{C_x - A_x}{NS}, \tag{2.9}$$

where NS is the number of spikes in a given window of SEMG [6].

As an additional parameter to evaluate the SEMG signal, the averaged rectified value (ARV) and the root mean squared value (RMS) are used.

$$ARV = \frac{1}{n} \sum_{n} |x_n|, \tag{2.10}$$

$$RMS = \sqrt{\frac{1}{n}\sum_{n} x_n^2}, \tag{2.11}$$

where x_n are the values of the SEMG signal, and n is the number of samples. Furthermore, the number of zero crossing (ZCR, that tracks the number of times the waveform crosses zero, switching from a positive signal to a negative one) is used. [35, 36].

2.2.6.2 Spectral analysis

Time domain analysis may not provide us with sufficient signal description. Frequency domain data processing is used for more advantageous analysis. The basic mathematical operation, which is used to transform most of the biological signals from time to frequency domain is Fourier transform. Thus, the Fourier transform tells us what frequencies are contained in a given signal.

Fourier transform

The Fourier Transform (FT) of input signal $x(t)$ is defined as the following notation:

$$F(\omega) = \int_{-\infty}^{+\infty} x(t)e^{-\mathrm{j}\omega t}dt, \tag{2.12}$$

where ω is the angular frequency and $\omega = 2\pi f$ with f as the input frequency, $x(t)$ is the time domain signal. Then $F(\omega)$ is its FT represented in frequency domain, which is the sum over all time of the signal $x(t)$ multiplied by complex exponential [37].

In digital signal processing, determining the frequency content of a signal by a technique called Discrete Fourier Transform (DFT) is one of the main aspects in feature extraction and understanding the characteristics of a digital signal. Fast Fourier Transform (FFT) is the practical application name used for the DFT that maps discrete-time sequences into discrete-frequency representation as in equation:

$$F(k) = \sum_{n=0}^{N-1} x[n]e^{-\mathrm{j}2\pi kt/N}, \tag{2.13}$$

where x is the input sequence, F is the DFT, $2\pi k$ is the angular frequency of input sequence frequency k and N is the number of samples in both discrete-time and the discrete-frequency domains [37].

Thanks to FFT we can display the frequency spectrum of the signal(Fig. 2.11). The power spectrum or power spectral density (PSD)(Fig. 2.12) gives us the signal power distrubution along the frequency axis. So we see which frequency is the most powerful.

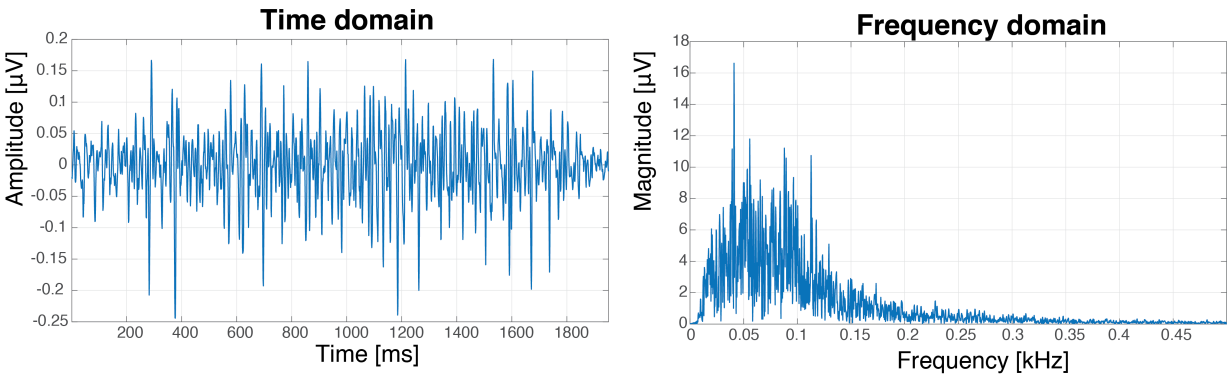

Figure 2.11: Example of SEMG signal and frequency spectrum.

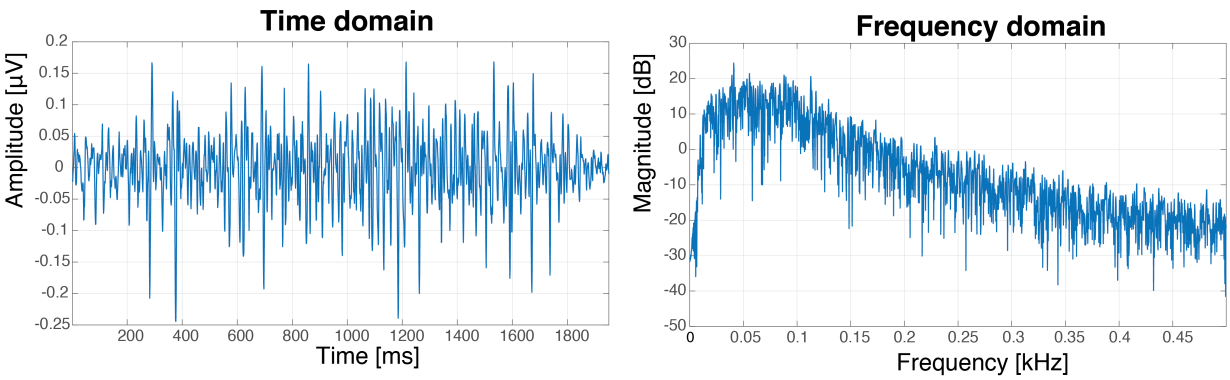

Figure 2.12: Example of SEMG signal and power spectral density (PSD[dB])

In PSD we are mostly interested in the most powerful component, i.e. the maximum of this spectrum and the mean or median power. The power density median frequency is the frequency at which the cumulative sum of the spectrum reaches 50% of the total value. Furthermore, the first spectral moment is used, which represents the center of energy distribution in the spectrum. It is therefore a weighted average of the spectral lines. The second spectral moment represents the spread of the spectrum and it is analogous to statistical variance and is an indicator of spectrum spreading. Generally, the spectral moment can be described by equation [38]:

$$m_n^{'} = \frac{1}{I} \sum_{l=c_1}^{c_2} S(l)(l/N\Delta t)^n, \tag{2.14}$$

where N is the power spectrum ($S(l)$) length, I is the frequency range from frequency c_1 to frequency c_2 and Δt is the sampling interval.

Wavelet transform

In the last decade, wavelet transform (WT) became an effective tool to extract useful information from the EMG signal [39, 40]. WT can essentially be divided into discrete and continuous forms. It efficiently transforms the signals with a flexible resolution [28].

This new tool differs from the Fourier transform in the way in which it localizes the information in the time-frequency plane. It is capable of trading one type of resolution for the other. This makes it especially suitable for the analysis of non-stationary signals [41].

The basic idea in wavelet theory is to reject the concept of fixed size windows. WT decomposes a signal into several multiresolution components according to a basis function called the wavelet function (WF). The WF is both dilated and translated in time undertaking a two-dimensional cross correlation with the time domain SEMG signal [42, 43].

WT consists of two stages. The first is analysis (decomposition) and the second is synthesis (reconstruction). Analysis is the calculation of approximations and details of signal using wavelet filters. Generating an original signal of these values is called synthesis. If we denote approximations on the p level as a_p and details on the p level as d_p, wavelet transformation on the p level we can represent by the Fig. 2.13.

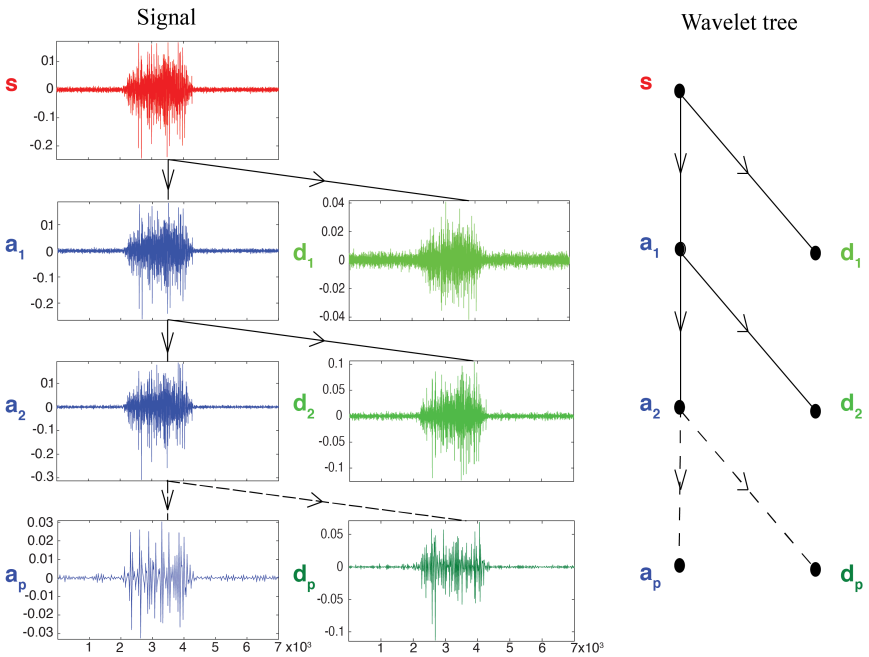

Figure 2.13: Example of signals (s) wavelet transform (type coif1) and wavelet tree where a_1, ..., a_p is space of approximations and d_1, ..., d_p is space of details.

The signal s can be imagined as a vector which can be expressed as the directive sum:

$$s = a_p \oplus d_p \oplus d_{p-1} \oplus \cdots \oplus d_1, \tag{2.15}$$

2.3 Myotonometry

The optimal concentration of blood plasma salts and ions and the protein composition is necessary for the normal activities of biological tissue and it depends on the tone and biomechanical properties [44]. Skeletal muscle never completely relaxes. Some fibers are always slightly contracted so they are in an active state and ready for further contraction. This slight contraction is called muscle tone [45].

Objective measurement of myotonometric parameters would greatly enhance detection of risk of injury and monitoring the effects of interventions, such as treatment [46]. The principal difference between myotonometry and traditional measurement of muscle parameter is that it can measure the tone, elasticity and stiffness simultaneously.

2.3.1 Measurement Equipment

The probe at the end of myometer (Fig. 2.14) has to be placed perpendicularly to the surface of the skin. Constant pre-pressure (pre-load force of 0.18 N) is applied between the probe and the surface of the skin for compressing subcutaneous tissues which allows for the registration of the damping natural oscillation of the muscle through the skin and subcutaneous tissues. A short mechanical impulses (duration 15 ms, 0.58 N) are delivered to the tissue under the probe. The mechanical impulses generate damped oscillations within the muscle, which are recorded by an accelerometer in the form of an acceleration curve (shown in Fig. 2.15) from which five parameters are calculated [47, 48].

- **Oscillation frequency**

  Oscillation frequency $F[Hz]$ characterizes the tone (intrinsic tension on the cellular level) of a muscle in its passive or resting state without any voluntary contraction and is defined as the maximum frequency (Eq. (2.16)) computed from the signal spectrum by FFT [49, 7].

$$F = f_{max}. \tag{2.16}$$

  The higher the natural oscillation frequency, the higher is the tone. F is known to increase with contraction (state of tension) and stretch [7].

- **Dynamic stiffness**

  Dynamic stiffness $S[Nm^{-1}]$ characterizes the resistance of a muscle to a contraction or to an external force that deforms its shape and is calculated as [7]:

$$S = m_{probe}\frac{a_{max}}{\Delta l}, \tag{2.17}$$

  where m_{probe} is a mass of the measurement mechanism and Δl is a maximum displacement of the tissue [7].

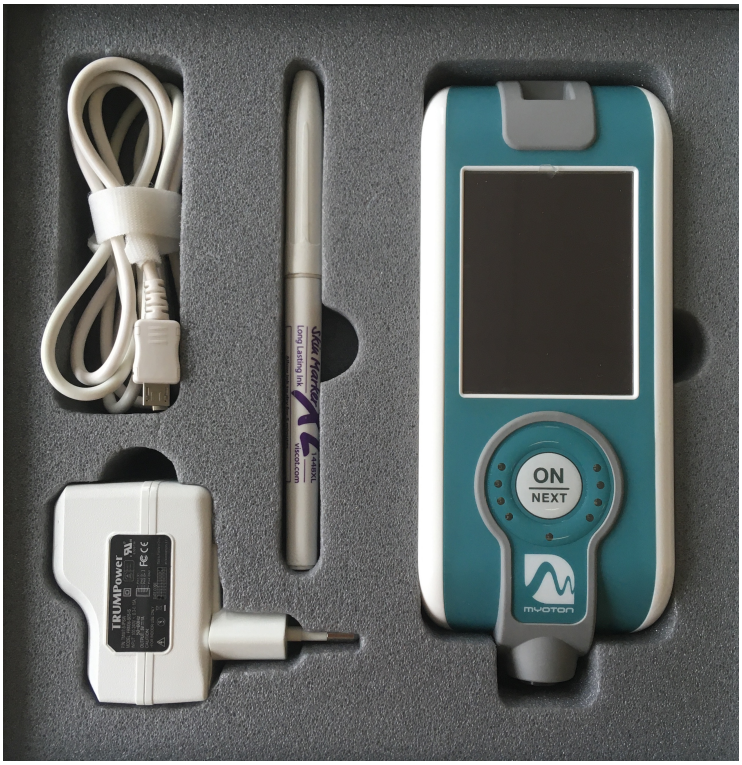

Figure 2.14: MyotonPro Device. `www.myoton.com`

- **Logarithmic decrement**

  Logarithmic decrement D represents muscle elasticity and indicates how much mechanical energy is lost in the tissue during an oscillation cycle. D is expressed in arbitrary units [7]:

$$D = \ln\left(\frac{a_1}{a_3}\right), \tag{2.18}$$

  where a_1 is a maximum tissue resistance and a_3 is a maximum displacement of the second period of oscillation which takes place due to the recuperation of stored residual mechanical energy in the tissue. The smaller the decrement value, the smaller will be the dissipation of mechanical energy and higher will be the elasticity of tissue. Decrement of zero would represent absolute elasticity and zero dissipation of mechanical energy [7].

- **Mechanical stress relaxation time**

  Mechanical stress relaxation time $R[ms]$ is the time for a muscle to recover its shape from deformation after a voluntary contraction or a removal of an external force. It is calculated as:

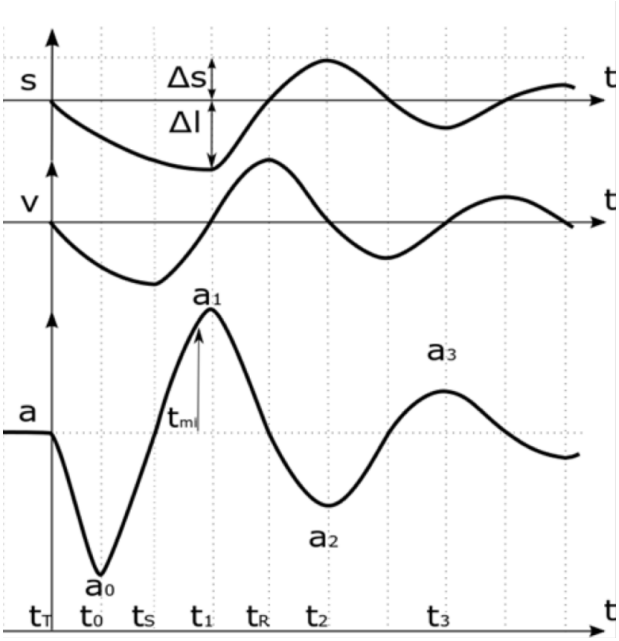

Figure 2.15: Oscillation curve. a: acceleration of the damped oscillation, a_0: maximum acceleration, a_1: maximum displacement, a_2: maximum opposite displacement due to the residual inertia of the tissue oscillation, a_3: maximum displacement of the second period of oscillation which takes place due to the recuperation of stored residual mechanical energy, ΔS: precompression of subcutaneous tissues above the muscle being measured, Δl: maximum displacement of the tissue, S: displacement (tissue oscillation), t: time, t_{mi}: the end of mechanical impulse, t_0: the time when maximum acceleration was reached, t_T: start of the mechanical impulse, t_r: the time when tissue returns to its initial shape, t_s: zero acceleration and maximum velocity due to the force of deformation, V: oscillation velocity. Adopted from [7]

$$R = t_R - t_1, \tag{2.19}$$

where t_R is the time when tissue returns to its initial shape and t_1 is the time when maximum displacement was reached [50].

- **Creep (Deborah number)**

  Creep C is the gradual elongation of a tissue over time when placed under a constant tensile stress. This is the ratio of the relaxation and deformation time of the muscle [50]. Creep can be described by equation:

$$C = \frac{R}{(t_1 - t_T)}, \tag{2.20}$$

where R is the mechanical stress relaxation time, t_1 is the time when maximum displacement was reached and t_T is the start of the mechanical impulse. The smaller the difference of relaxation and deformation time, the higher the value of the C parameter indicating the creep. Younger and healthier muscles have a smaller value of the C parameter [50].

2.4 Conclusion

This chapter provides basic information about anatomical consequences. There are described basic principles of measuring muscle response by electromyography and myotonometry. Further information is always given in the introduction to each chapter.

The following text is divided into three main chapters that focus on three main themes (and sub-goals) of the thesis. The first one deals with the measurement of joint patterns using electromyography. Based on the charged information, a separate topic of semiautomatic detector development was created. The third topic is measuring muscle parameters using myotonometry.

Chapter 3

Representation of Joint Patterns

3.1 Introduction

Investigation of joint patterns is one of many ways to detect soft tissue pathology. It is examination of the joint mobility of a given joint. Limiting this momentum indicates damage to structures that affect the performance of isolated motion in the joint. For identification, passive and active motion range tests performed by a physiotherapist are used. So-called articular blockages can result in reactive changes in skeletal muscle tension.

Functional blockage of the joint is a common clinical term that expresses one of the most common functional disorders in the musculoskeletal system. It can be defined as a malfunction that is not accompanied by a structural disruption of the joint. The total range of motion does not change with the functional joint block, but there is a relative change in the magnitude of the partial movements that make up the total motion around one joint axis [51]. According to Velé [52], joint motion is a small movement in the joint in other direction than those typical of its function. Loss of joint clearance is manifested by stiffness in the joint and deterioration of joint mobility. The articular clearance is defined by the elasticity of the articular capsule and the pull of the short muscles that clamp around the joint and act parallel to the axis of the movable segment [52].

Lewit [53] divides joint blocking symptoms to limit joint movement, loss of joint clearance, and reactive changes in skeletal muscle tension that cross the blocked joint and perform active movement there. Joint blockades have a high tendency to chaining. In this way, the flexion or extension chains of joint dysfunctions arise in the limbs. On the lower limb, these chains are caused by many causes, such as defective pelvis position, and traumatic conditions of the hip, knee and ankle.

The examination of the articular barriers according to Rychlíková [54] consists in delaying the bones that form the joint and subsequently in shifting the bones to one another. It is therefore an examination in non-physiological ways, when movements are performed passively. The examination of the joint in physiological directions, i.e. in flexion or extension, is dealt with by Tichý [51]. In this examination, skeletal muscles are much more pronounced, and in addition to them other soft tissues that cover the joint (fascia, subcutis, skin). Hy-

pertonus or skeletal muscle spasm will most likely affect the position of the physiological joint barrier and the size of its joint will based on the assumption that skeletal muscle tension changes in joint blockages. This change could be detected by SEMG.

This chapter is divided into three parts and based on my conference articles [8, 55, 56, 1]. The first section deals with the measurement of joint paterns using bipolar electrodes on the muscles vastus lateralis and vastus medialis. One set of bipolar electrodes was used on each muscle. The findings of this experiment are followed by the second section, which extends the measurement to multichannel one, using up to ten sets of bipolar electrodes. There was designed and built a special multi-channel electrode, due to the large size of the electrodes used in the previous experiment. The last third section describes the solution.

3.2 Surface Electromyography

3.2.1 Experiment Introduction

This section explains the preliminary results of the study of muscle activity in knee extension by using bipolar electrodes. The quadriceps femoris muscle is the great extensor of the knee. This muscle consists of four parts: rectus femoris, vastus lateralis, vastus medialis, and vastus intermedius. Rectus femoris is located in the middle, while vastus lateralis forms the bulk of the lateral thigh, vastus medialis is in the medial thigh, and vastus intermedius lies deep to the rectus femoris between vastus lateralis and medialis. Rectus femoris is a particular muscle (it is also a flexor muscle at the hip joint) while the other components are monoarticular muscles [57]. It is expected that the different morphological and dynamic behavior of the quadriceps components would cause these muscles respond differently to artificially induces joint blockages by a reflective heel pad.

3.2.2 Materials and Methods

3.2.2.1 Subjects

19 subjects, 15 females (23.5 ± 4.0 years) and 4 males (32.8 ± 11.8 years) participated voluntarily in this study. First, they were informed about the entire study procedure. Then they were examined by a physiotherapist. Anamnesis included the determination of the dominant limb and functional examination whether the patient does not suffer from bacterial inflammation and does not show neurological changes conducting reflex activity in the lower dominant limb.

3.2.2.2 Electrodes Localization

Bipolar electrodes (40.8 x 34 mm) with scanning area 13.2 mm^2 (Ambu Blue Sensor P) were placed on two heads of quadriceps femoris muscle - vastus medialis (VM) and vastus lateralis (VL). According to the study A. Reinoldi [58] was the IZ VL localized at a distance 94±13.2 mm on the line from lateral patella to the anterior upper of the hip bone and

the VM muscle was located at a distance 51.7±13.0 mm below fifty degrees from the patellar line and the upper pin hip bone (Fig. 3.2).

3.2.2.3 Measurement Procedure

The measurement was carried out on a special measuring chair (Fig. 3.1) for using the equipment Biomonitor ME6000. The angle in the knee joint was set to 70° flexion and hip at 120° between pelvis and femur which corresponds to relaxed sitting. Each patient did three isometric maximum voluntary contraction (MVC) at knee extension before the experiment.

Figure 3.1: The special designed measuring chair with adjustable angles in the knee and hip. Adopted from [8]

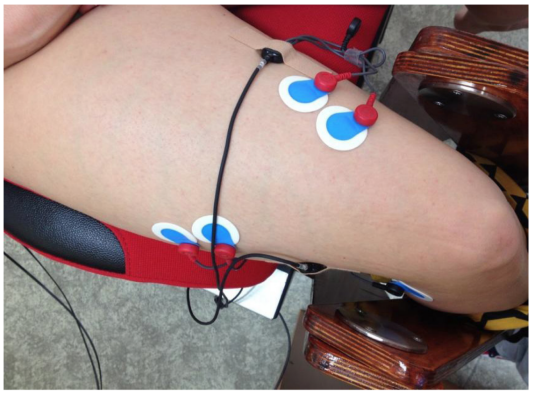

Figure 3.2: The electrode location on the muscle vastus medialis and vastus lateralis. Adopted from [8].

The contraction always lasted 2s with a rest period of 30 s. During these contractions, a force sensor value was recorded, which was then used to calculate a submaximal (60%) MVC value. After a two-minute rest period, three submaximal 60% contractions were measured with 2min rest between contractions. The measurement was carried out without heel pad (WHP) and with the use of a pronation heel pad (PHP) and supination heel pad (SHP)(Fig. 3.3). At the end of the experiment there was performed MVC measurement for investigation of the muscle fatigue again.

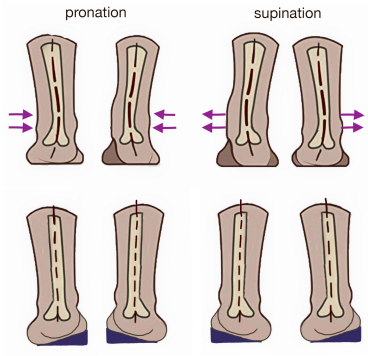

Figure 3.3: Pronation and supination of the ankle and the example how to use the heel pad. Adopted from [1].

3.2.2.4 Signal Preprocessing

Recorded raw SEMG signals contained several contaminating elements (e.g. power grid frequency, offset and baseline wander). Interference frequency alternating current was eliminated by measuring device and grounding. The signal offset was dealt with by subtraction of the signal median from the raw SEMG. Obvious baseline wander presented in the raw SEMG was removed by nonlinear filtering aiming to find and subtract isoline from the signal.

Individual steps of isoline subtraction were based on the triple decimation of the original signal, its filtration (low pass - 4th order Butterworth filter with normalized cutoff frequency 0.4) and triple backward interpolation to the original sampling frequency of 1 kHz.

3.2.2.5 Contraction Detector

Before own SEMG analysis of isometric contractions it was necessary to detect these contractions and to choose 2s segments where subject maintained the value of submaximal contraction slightly fluctuating around 60% of MVC (shown in Fig. 3.4 D). To do so a smoothed Hilbert envelope of the signal was calculated. Value of 3 standard deviations (SD) of recorded SEMG was used as the threshold for detection of single contractions (spindles) (shown in Fig. 3.4 B). SEMG 60% MVC segments where subjects maintained a constant force were located at the end of each found spindle. Value corresponding to the median amplitude calculated from spindle amplitudes was used as the threshold to find the start of 60% MVC segment coming from the end of found spindles. From that point backward 2s SEMG record was considered as 60% MVC segment (Fig. 3.4 D).

3.2.2.6 Contraction Analysis

Nineteen parameters were calculated on the extracted 2s parts of SEMG based on Spike shape analysis and frequency and time domain analysis. Parameters include calculation of the spike amplitude, mean spike amplitude, mean spike frequency, mean spike slope,

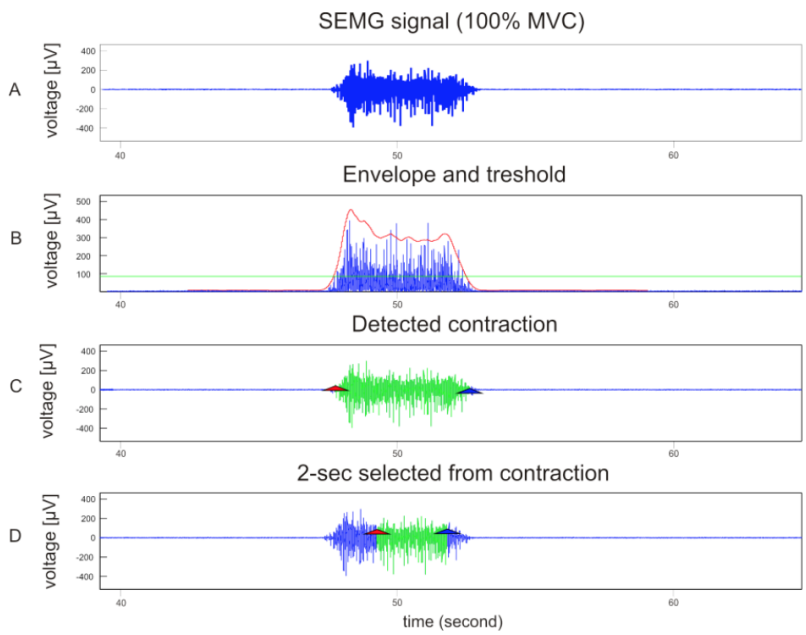

Figure 3.4: Illustration of 2s segment of the SEMG signal and the process of extraction useful part of the signal for further analysis. A) One out of three isometric contractions is shown to present the process of next steps of signal selection. B) The original signal rectified. A setup threshold level 3 SD of the signal – marked in green and envelope of the signal (red). C) A detected contraction (green) is shown. D) 2s of useful signal for further analysis (green). Selection is made from the end of contraction showed in C and tracked from the back end of the signal forward (right to left). 2s of signal from the point where envelope of the signal is higher than 3 SD are taken into account. Adopted from [8]

mean number of peaks per spike, number of spikes, mean spike duration, zero-crossing rate, most powerful frequency in the spectrum, median of PSD, the first spectral moment, the second spectral moment, average rectified filtered SEMG signal, median, maxima, minima, standard deviation and power of the signal after rectification. (Detailed description of parameters can be found in 2.2.6).

3.2.3 Experiment Results

A two-way analysis of variance (ANOVA) was performed on the 19 computed parameters. The factors were application of the heel pad and the subject. Significance was set to $p<0.05$. Pair-wise comparisons were performed with post hoc Tukey method. Significance was set to $p<0.05$. Two statistically significant ($p<0.05$) effects of changes in heel pad have been proved for parameters median for the VM muscle and first spectral moment for the VL muscle. It was shown, that there are statistically significant differences in muscle activity in measurements without reflex heel pad vs. supine reflex heel pad (parameter

Median SEMG, absolute value of the differences between means: 1.07 μV, p<0.05) and also in measurements without reflex heel pad vs. pronation reflex heel pad (parameter first spectral moment of SEMG, absolute value of the difference between means: 1.15 Hz, p<0.05) (Fig. 3.5).

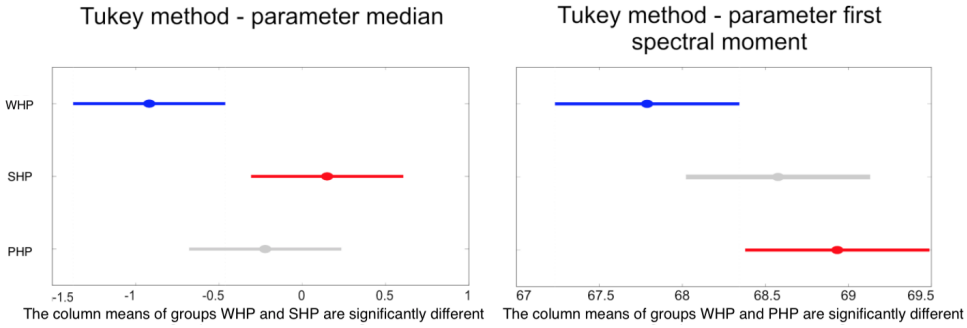

Figure 3.5: Tukey method for parameter madian and first spectral moment. WHP means measurement without heel pad, SHP - supine heel pad, PHP - pronation heel pad.

3.2.4 Discussion and Conclusion

This study investigates changes in SEMG parameters based on spike shape analysis and frequency and time domain analyzes. It shows that there are statistically significant changes in the muscle patterns in a situation where the subject is exposed to artificially triggered flexion or extension reflex chains. The question is whether these changes will be reflected in muscle timing analysis. Based on the results, another measurement was designed using a higher number of bipolar electrodes to determine whether the joint pattern paths chain differently using reflective heel pads.

3.3 High Density Surface Electromyography

3.3.1 Experiment Introduction

Based on the results of the previous experiment 3.2, another measurement using high density SEMG (HD SEMG) was proposed. HD SEMG is a technique to measure electrical muscle activity with multiple (more then two) closely spaced electrodes. A major reason for increasing the number of electrodes is to increase the number of recording position, leading to topographical information concerning the distribution of the EMG activity over a muscle or the timing relationships between different muscles [59]. We hypothesize that a reflective heel pad artificially induces joint blockages and thus results in topographical SEMG signals changes caused by flexors and extensors in the leg. The muscles rectus femoris and vastus medialis were selected for this purpouse by using HD SEMG.

3.3.2 Materials and Methods

3.3.2.1 Subject

One healthy proband (male, 46 years) was randomly selected to conduct this experiment. Information to this study was provided before examination by a physiotherapist. Medical history provided information about the dominant lower limb and functional examination. No bacterial inflammation or neurological rewiring reflex activity in the dominant lower limb was recorded.

3.3.2.2 Measurement Procedure

The measurement was set as in the previous study described in 3.2. Eight electrodes were placed on the proband's dominant lower limb on VMs (channels Ch1-Ch4) and twelve on rectus femoris (RF) (channels Ch5-Ch10) with bipolar electrode connection (shown in Fig. 3.6). Selected SEMG signals were recorded during three isometric MVC of the knee extensors with two minutes rest between contractions. First one consisted of extension without heel pad. The second and third one used pronation and supination heel pad respectively.

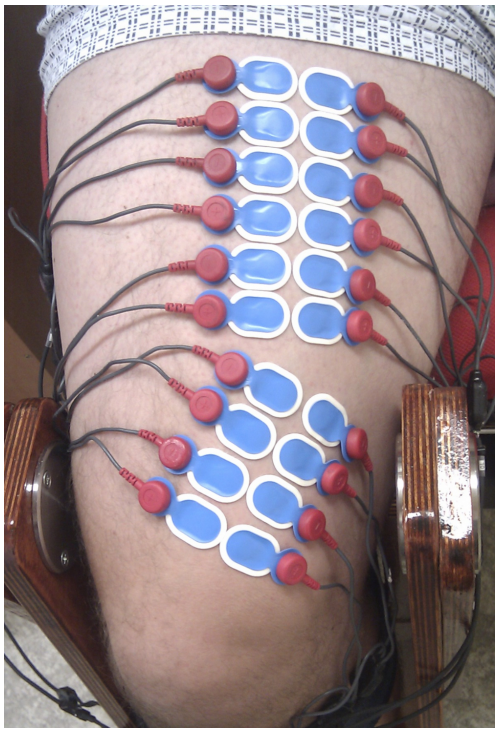

Figure 3.6: Bipolar connection of electrodes and its placement on the muscle vastus medialis and rectus femoris. Adopted from [1].

3.3.2.3 Signal Processing

Signals from all channels were processed by our designed algorithms successively implemented in Matlab environment. First, each signal was filtered by using Butterworth bandpass filter of second order with cutoff frequency 20 Hz and 350 Hz respectively. The envelope after rectification was calculated using a moving average method with 0.4 s window. The threshold used to get the contractions is one SD of the whole signal. Because the start depends on the threshold size and is different for each signal, we used the method similar to the study [60]. We created a slope line from the point where the threshold crosses the envelope (it is the position where the signal falls below the threshold) to 1 s before this point and looked for the maximum difference between the slope line and the signal envelope for detection of the contraction start. Fig. 3.7 shows an example of how the measurement is performed to assess the start of the contraction.

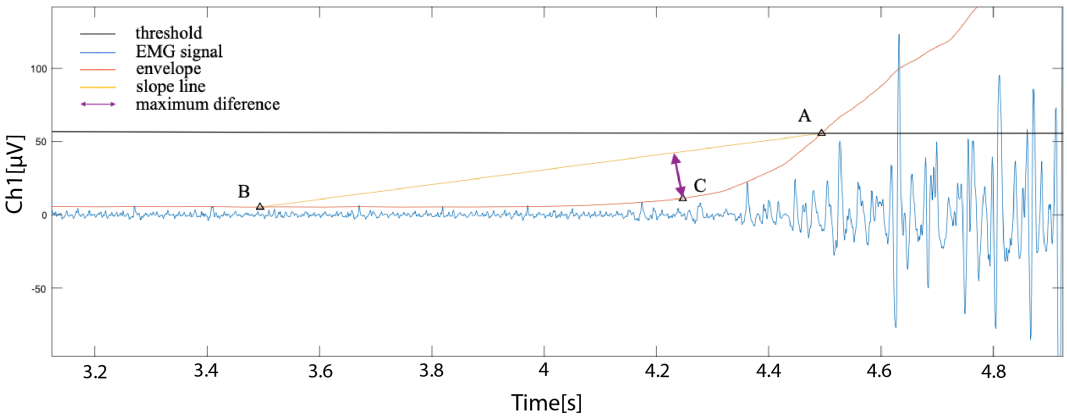

Figure 3.7: Method for estimation of contraction start (point C). After selecting the peak where the threshold crosses the envelope (point A) and a line from this point to the position 1s before (point B) is created. Then the differences between the line and the signal envelope are calculated and the position where the difference has its maximum is the start of contraction. Adopted from [1].

This method was applied to all channels (Ch1-Ch4 VM, CH5-Ch10 RF) and all contractions. The starts of contraction are linked for better visual evaluation. An example of it is shown in Fig. 3.8.

3.3.2.4 Data Analysis

Because the specific topic in this study was to investigate the joint pattern and the muscle timing, it was necessary to find out the way how to explain the result.

Muscle activation pattern is represented by contraction starts in all channels. The first order polynomial model was chosen to investigate these patterns. For each contraction we

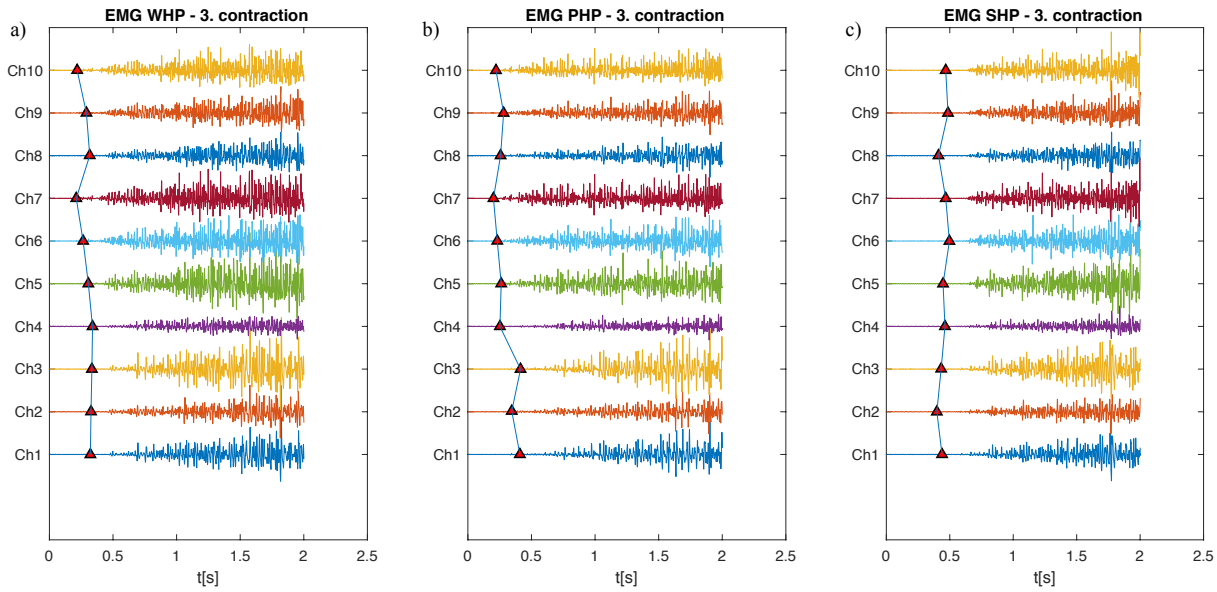

Figure 3.8: Example of start position of third contraction on the channel (Ch1-Ch4 vastus medialis, Ch5-Ch10 rectus femoris). (**a**) Start of contraction without using heel pad (WHP), (**b**) start of contraction with pronation heel pad (PHP), (**c**) start of contraction with supination heel pad (SHP). Red triangles represent the start of contraction. These point are linked by blue line for better visual evaluation. Adopted from [1].

fit this model in the least-squares sense. Then the mean approximation curve was calculated for each type of measurement (WHP, PHP and SHP). Since the data was measured on one proband only, it is not possible to prove statistically significant changes. Based on these results, contraction starts were sorted from the fastest channel to the slowest one and represented in Tab. 3.1.

3.3.3 Experiment Results

The positions of contraction start on all channels were interleaved with a straight line using the least squares approximation (the example is shown in the Fig. 3.9).

The mean approximation curve was calculated for contraction without using heel pad, with pronation and supination heel pad. Mean approximation curve is shown in the Fig. 3.10.

The slope of the mean approximation curves without using heel pad and with pronation heel pad is similar. The mean approximation curve with supination heel pad has a reverse slope. These results indicate that the muscle rectus femoris starts the contraction in the cases WHP and PHP and vastus medialis starts contraction with SHP.

The start positions of contraction were sorted from the fastest channel for better understanding of the result. The results are more clearly interpreted in the table (Tab. 3.1). Muscle rectus femoris is faster in all three contractions and the SEMG signal spreads in

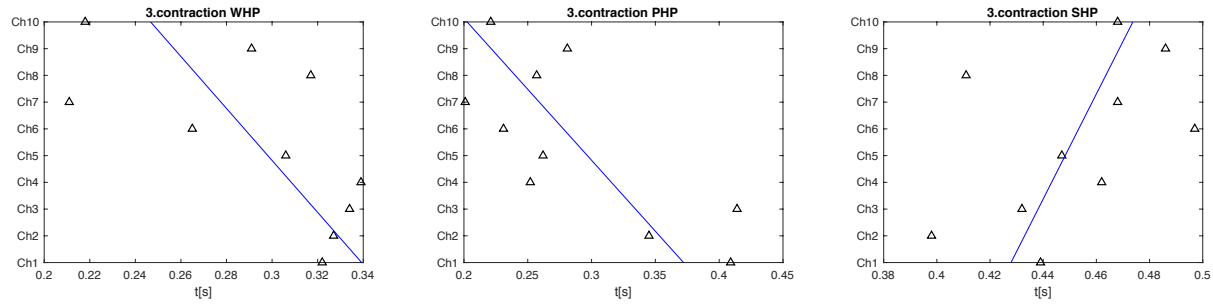

Figure 3.9: Example of start position of third contraction on the channel (Ch1-Ch10) and approximation curve. (**a**) Start of contraction without using heel pad (WHP), (**b**) start of contraction with pronation heel pad (PHP), (**c**) start of contraction with supination heel pad (SHP). Adopted from [1].

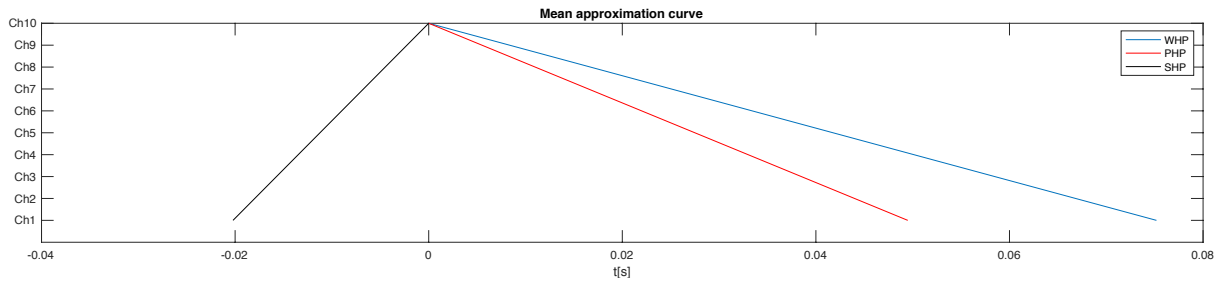

Figure 3.10: Mean approximation curve without using heel pad (WHP, blue line), with pronation heel pad (PHP, red line) and supination heel pad (SHP, black line). Adopted from [1].

the same way. Muscle vastus medialis is slower than rectus femoris. A signal propagation is more complicated in the cases with using pronation and supination heel pad and the muscles mutually cooperate.

3.3.4 Discussion and Conclusion

This study deals with timing analysis and HD SEMG signal propagation on the muscle vastus medialis and rectus femoris.

Three measurements were carried out (without heel pad, with using pronation and supination heel pad) on the previously designed chair. The angle of the knee joint was fixed at 70° flexion and hip at 120° between the pelvis and the femur. The electrodes were placed on the muscle vastus medialis and rectus femoris. HD-SEMG signals were recorded during three isometric voluntary contractions of the knee. Desired three muscle contraction on all ten channels were apparent after filtration without evidence of greater interference.

Firstly, one standard deviation was used as the threshold for the detection of con-

Table 3.1: The positions of contraction (con) starts sorted from the fastest channel. WHP- without using heel pad, PHP- pronation heel pad, SHP- supination heel pad. Adopted from [1].

	WHP			**PHP**			**SHP**	
1.con	**2.con**	**3.con**	**1.con**	**2.con**	**3.con**	**1.con**	**2.con**	**3.con**
4.134^{7}	10.591^{7}	16.811^{7}	1.475^{4}	7.748^{4}	14.701^{7}	1.773^{4}	6.992^{8}	12.598^{2}
4.135^{10}	10.595^{10}	16.818^{10}	1.486^{8}	7.804^{8}	14.721^{10}	1.834^{2}	6.993^{2}	12.611^{8}
4.178^{6}	10.608^{6}	16.865^{6}	1.497^{2}	7.807^{7}	14.731^{6}	1.834^{7}	7.022^{5}	12.632^{3}
4.195^{9}	10.626^{9}	16.891^{9}	1.515^{7}	7.810^{10}	14.752^{4}	1.834^{10}	7.041^{7}	12.639^{1}
4.208^{5}	10.637^{1}	16.906^{5}	1.516^{1}	7.812^{1}	14.757^{8}	1.842^{9}	7.043^{10}	12.647^{5}
4.212^{8}	10.642^{3}	16.917^{8}	1.520^{10}	7.823^{2}	14.762^{5}	1.846^{1}	7.054^{4}	12.662^{4}
4.216^{4}	10.648^{2}	16.922^{1}	1.527^{3}	7.828^{6}	14.781^{9}	1.846^{3}	7.063^{3}	12.668^{7}
4.235^{2}	10.652^{4}	16.927^{2}	1.546^{6}	7.831^{3}	14.845^{2}	1.859^{6}	7.063^{9}	12.668^{10}
4.247^{1}	10.661^{5}	16.934^{3}	1.546^{9}	7.839^{9}	14.909^{1}	1.871^{5}	7.070^{1}	12.686^{9}
4.255^{3}	10.664^{8}	16.939^{4}	1.550^{5}	$7.86^{5}7$	14.914^{3}	1.895^{8}	7.077^{6}	12.697^{6}

^{1,2,3,4} Number of the channel on the muscle vastus medialis

^{5,6,7,8,9,10} Number of the channel on the muscle rectus femoris

traction starts. Then a slope line was calculated from the point where threshold crosses the signal envelope to the point 1 s before. The new position of contraction was calculated as the maximum difference between the slope line and the signal envelope.

Muscle quadriceps femoris (with patella and ligament patellae) is the only knee extensor. Muscles vastus medialis and vastus lateralis have an extension and stabilization function. Muscles vastus intermedius and rectus femoris have only extension function.

The need for knee stabilization is eliminated by fixing the leg in the chair in a position corresponding to the relaxed sitting position and without using heel pad. Thus, at the beginning, it is not necessary to stabilize the knee and the vastus medialis muscle will engage the extension function to assist the muscle rectus femoris in contraction. When using the heel pad, the knee is artificially destabilized and the vastus medialis muscle performs both stabilizing and extension functions, which our results match (Tab. 3.1).

The described research was a pilot study that had as its main aim to prove the feasibility of the proposed experiment and successive data analysis. Although the tests were performed on one subject they are promising. Based on these results, a multichannel electrode with 10 mm symmetric distances around 5 mm centre gab was designed and developed.

3.4 Multi-channel Surface Electrode

3.4.1 Experiment Introduction

Based on the results of a previous study (3.3), it was found that the use of standard electrodes is not sufficient because of their size. It is not possible to accurately determine the location of innervation zone and it is very difficult to detect the propagation of the signal across the muscle. Therefore, a new multi-channel electrode was designed. Unfortunately this electrode encounters problems with standard equipment for the measurement of SEMG signals. New measuring equipment had to be designed. This study aims to determinate functionality and suitability of these novel designs for evaluation of joint patterns.

3.4.2 Materials and Methods

3.4.2.1 Measurement Equipment

The initial prototype of our electrode was based on Merletti's multi-channel electrodes [5]. It results in dry uninsulated multi-channel electrode with twenty silver contact surfaces. Size of each contact area is 12 mm^2. Its design is symmetric with 10 mm distances around 5 mm center gap (shown at Fig. 3.11).

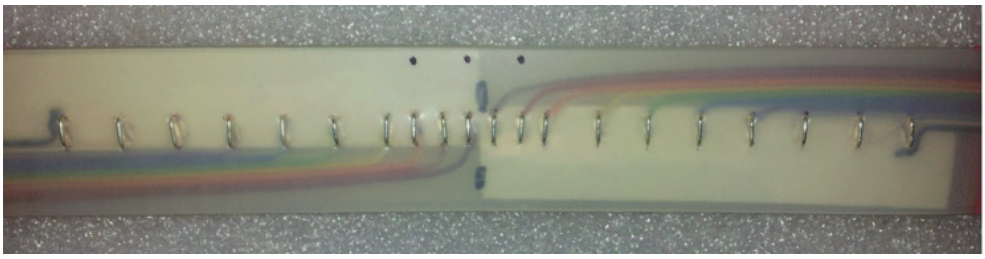

Figure 3.11: Multi-channel electrode with 10 mm symmetric distances around 5 mm center gab. Adopted from [8].

We have created a prototype of new measurement equipment (Fig. 3.12). This device is delta-sigma analog to digital multi-channel converter with matching input impedance of operational amplifier.

Theoretical number of quantization levels is equal to 24 bits. It has a programmable sampling rate (500 up to 32,000 samples per second), which fully suits the measurement of SEMG signals. Modular involvement allows measurement up to 256 channels in the bipolar multi-electrode array. This device is able to record signals from used electrodes together with measurement parameters. Resulted stored record allows for later detailed analysis and evaluation. Extensive work on corresponding software has been conducted.

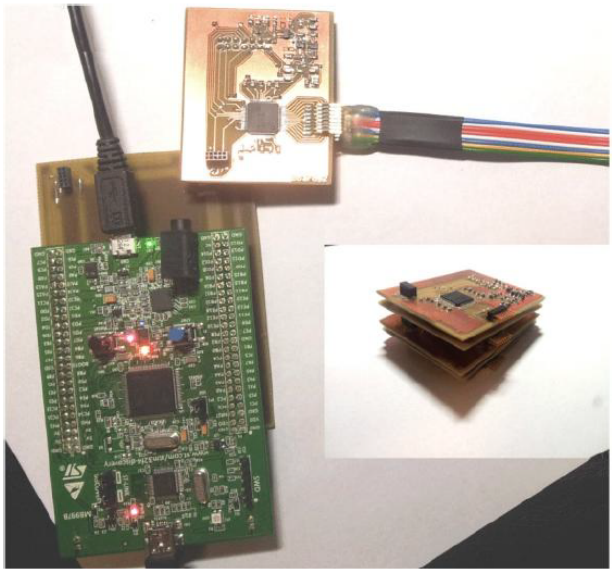

Figure 3.12: Prototype of the new measurement equipment. Adopted from [8].

3.4.2.2 Subjects

One healthy proband (male, 46 years) was randomly selected to conduct this experiment. Information to this study was provided before examination by a physiotherapist. Medical history provided information about the dominant lower limb and functional examination. No bacterial inflammation or neurological rewiring reflex activity in the dominant lower limb was recorded.

3.4.2.3 Measurement Procedure

The measurement was set as in the previous study described in 3.2.2.3. Multi-channel electrode was placed on the proband's dominant lower limb on vastus medialis. Selected SEMG signals were recorded during three isometric maximum voluntary contractions of the knee extensors. First one consisted of extension without heel pad (WHP). The second and third one used supination (SHP) and pronation heel pad (PHP) respectively.

3.4.2.4 Signal Processing

Sixteen out of twenty available channels were connected to check the function of the electrode. All 16 channels were processed by our designed algorithms in Matlab environment. First, the frequency spectrum (Fig. 3.13) was calculated by frequency analysis based on Fourier transform.

Interferences caused by main hums were removed by IIR notch filter (notch located at 50 Hz, or 0.1 π radians per sample). Low frequencies (offset null output signal and

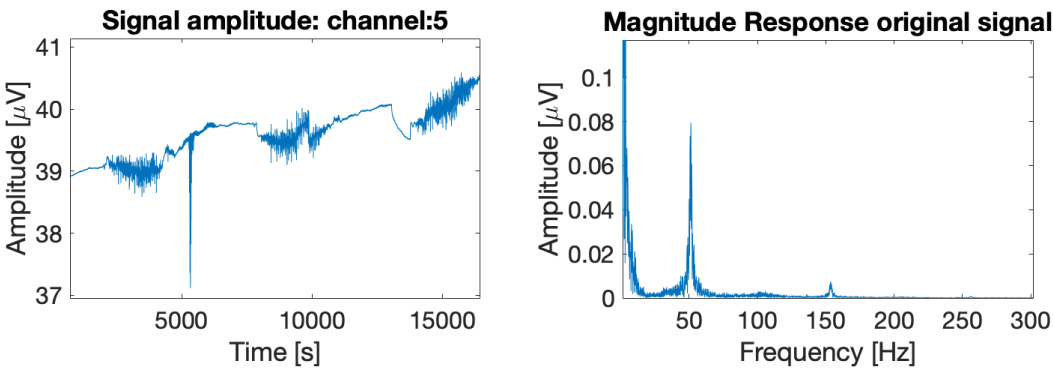

Figure 3.13: Example of original signal amplitude from channel five before filtering and its spectrum based on frequency analysis using Fourier transform. Adopted from [2].

motion artifacts) were removed by high-pass filter (Butterworth filter, 4th order with normalized frequency 0.02). Suppression of ratio interferences were removed by IIR filter (Butterworth filter, 8th order, type low-pass with normalized frequency 0.25).

3.4.3 Experiment Results

Three measurements were carried out (without heel pad, using pronation and supination heel pad). Desired three muscle contractions on all channels were apparent after filtration without evidence of greater interference. Examples of ten filtered signals are shown in Fig. 3.14. Such modified signals are suitable for subsequent processing and parametrization to determine the effect of using reflective heel pad to knee joint patterns.

For simple comparison there were calculated the most powerful frequency and the first spectral moment (weighted average of spectral lines) of two second long segments. Results of the parameters for channels 7-16 are shown in Tab. 3.2 and in Tab. 3.3.

As we can see at Tab. 3.4, the parameter the most powerful frequency is increased in one channel and decreased in eight channels when using supination heel pad. There was further observed increase in three cases and decrease in seven cases when using pronation heel pad. The parameter first spectral moment increased in seven channels and decreased in three channels when using the supination heel pad and increased in five cases and decrease in five cases when using the pronation heel pad.

3.4.4 Discussion and Conclusion

Based on conducted measurements we conclude that introduced electrode can be used to subsequent analysis of joint patterns. At this time, the measuring device is further developed. Signal processing and parametrization are simultaneously in progress. Preliminary results anticipate sufficient potential for new clinical discoveries.

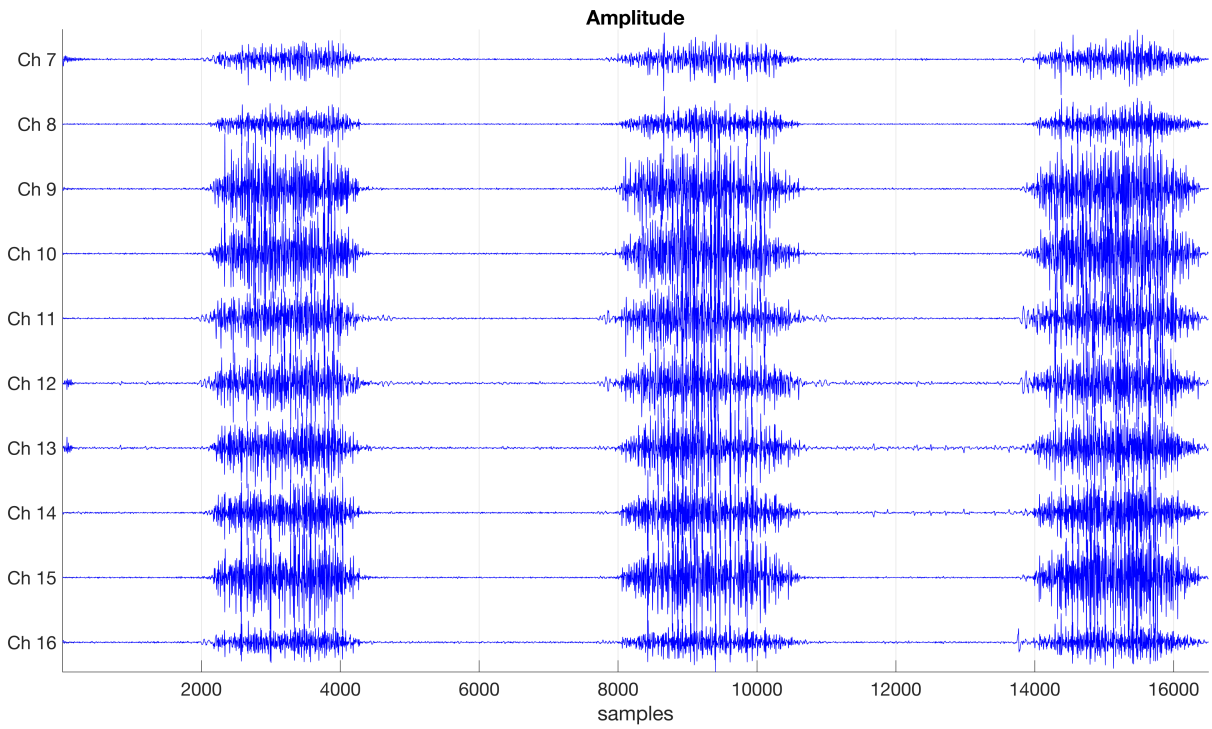

Figure 3.14: Example of signal amplitude from channels number 7-16 after filtration. Adopted from [2].

3.5 Conclusion

This chapter has discussed investigation of joint patterns using different measurement SEMG methods. The first part was focused on signal analysis using spike shape analysis and analysis with frequency and time domain. Only two bipolar electrodes were placed on the muscles of vastus medialis and vastus lateralis. 19 probands participated in the study. Each first performed three maximum voluntary contractions from which the 60% MVC was calculated. Patients maintained this value three times in succession without the use of a heel pad, with supination and pronation heel pad. From these contractions, the 2s segment was selected, with the submaximal contraction value fluctuating around 60% MVC. 19 parameters were then calculated on these segments. Two-way ANOVA and post-hoc Tukey method were used. Statistically significant changes were detected in the parameter Median (non-heel pad versus supination-heel pad measurements) and the first spectral moment (non-heel pad versus pronation-heel pad measurements). The basic thresholding method was used to detect contractions. A value of 3 standard deviations was used as a threshold.

The second part deals with HD SEMG measurements using eight bipolar electrodes on the muscle vastus medialis and twelve on the muscle rectus femoris. The SEMG signal

Table 3.2: Comparison of the parameter most powerful frequency (mean value ± standard deviation SD) without heel pad (WHP), with pronation heel pad (PHP), with supination heel pad (SHP). Adopted from [2].

	Most powerful frequency [Hz] mean ± SD		
channel	**WHP**	**PHP**	**SHP**
Ch7	31.00 ± 8.04	25.33 ± 4.64	25.67 ± 5.44
Ch8	33.67 ± 11.03	33.33 ± 1.70	28.00 ± 7.79
Ch9	33.33 ± 4.11	39.67 ± 6.34	23.67 ± 7.36
Ch10	26.00 ± 5.10	34.00 ± 12.03	20.00 ± 7.48
Ch11	29.00 ± 11.05	35.60 ± 12.81	25.33 ± 4.50
Ch12	31.00 ± 11.22	28.00 ± 9.80	36.00 ± 2.94
Ch13	37.33 ± 4.92	31.33 ± 9.57	37.33 ± 2.62
Ch14	41.33 ± 10.66	35.67 ± 5.25	35.33 ± 8.73
Ch15	34.67 ± 5.25	31.00 ± 10.71	31.33 ± 2.87
Ch16	35.00 ± 0.82	33.67 ± 11.15	34.33 ± 5.56

was recorded during the three maximum voluntary contractions without heel pad, with pronation and supination heel pad. In this study, we focused on examining muscle timing. A contraction detector that combines several methods has been proposed for this purpose. It is a combination of thresholding and Philips QT Interval Measurement Technique [60], which is used in ECG signal processing. The value of one standard deviation is used as the threshold. The point where the signal envelope exceeds the set threshold is connected to the point by 1s earlier. The maximum distance from the signal envelope is sought from this line. This point is intended as the beginning of contraction. However, the use of 20 standard electrodes is not sufficient due to their size. It is not possible to accurately determine the location of the innervation zone and it is very difficult to detect the spread of the signal through the muscle.

Therefore, the third part of this chapter deals with the design and examination of the functionality of a new multi-channel electrode. The initial prototype of the electrode was based on Merletti's multi-channel electrodes [5]. It is dry uninsulated multi-channel electrode with twenty silver contact surfaces. Size of each contact area is 12mm^2. Its design is symmetric with 10 mm distances around 5 mm center gap. A control measurement was made with this electrode to determine its usability and functionality. Measured signals do not show any sign of greater interference. Preliminary results anticipate sufficient potential for new clinical discoveries.

Thanks to the acquired knowledge from these measurements the research described in the next chapter was performed that let to the development of a new semi-automatic detector for polysomnography REM sleep without atonia in REM sleep behavior disorder.

Table 3.3: Comparison of the parameter first spectral moment (mean value ± standard deviation SD) without heel pad (WHP), with pronation heel pad (PHP), with supination heel pad (SHP). Adopted from [2].

	First spectral moment [Hz] mean ± SD		
channel	**WHP**	**PHP**	**SHP**
Ch7	80.57 ± 11.87	79.35 ± 7.79	78.27 ± 9.28
Ch8	83.42 ± 10.81	80.46 ± 7.47	87.35 ± 7.09
Ch9	76.69 ± 4.90	93.85 ± 9.92	78.28 ± 9.77
Ch10	85.91 ± 6.88	85.54 ± 7.19	73.76 ± 6.03
Ch11	71.36 ± 1.36	70.75 ± 3.01	73.03 ± 4.36
Ch12	65.18 ± 1.78	71.90 ± 7.37	71.91 ± 8.41
Ch13	75.04 ± 3.37	85.22 ± 2.82	83.27 ± 9.84
Ch14	76.79 ± 0.61	79.15 ± 3.22	82.61 ± 14.69
Ch15	69.12 ± 3.57	76.60 ± 6.31	81.01 ± 5.89
Ch16	79.59 ± 3.47	71.81 ± 3.90	74.94 ± 1.18

Table 3.4: General overview of increasing or decreasing parameters most powerful frequency and first spectral moment.

	increase		**decrease**	
parameter	**SHP**	**PHP**	**SHP**	**PHP**
Most powerful frequency	1	3	8	7
First spectral moment	7	5	3	5

Chapter 4

Polysomnography REM Sleep without Atonia in REM Sleep Behavior Disorder

4.1 Introduction

Sleep is essential for optimal human health and brain function. Polysomnography (PSG) is used to display and characterize the architecture of human sleep for clinical and research purposes [61]. PSG records human bioelectrical signals including electroencephalography (EEG), electrooculography (EOG), and electromyography (EMG) to determine non-rapid eye movement (NREM) and rapid eye movement (REM) sleep stages, and cardiorespiratory polygraphy to detect sleep disordered breathing. REM sleep was described by the eminent French neurophysiologist Michel Jouvet as somneil paradoxique (paradoxical sleep), since EEG (brain wave activity) resembles the awake state, while the EMG channels demonstrate skeletal muscle paralysis [62, 63].

Parasomnias are undesirable, potentially injurious complex behaviors arising from either NREM or REM sleep. REM sleep behavior disorder (RBD) is increasingly recognized as a common human parasomnia,occurring in approximately 1-7 % of the elderly adult population, and is diagnosed when there are vocalizations or complex motor behaviors such as screaming, shouting, punching, arm flailing, or kicking movements that parallel nightmares and represent dream enactment, accompanied by the loss of normal REM sleep atonia [63]. REM sleep atonia loss, also known as REM sleep without atonia (RSWA), results from dysregulation of normal REM sleep atonia (paralysis). Quantifying RSWA relies on expert visual scoring by a sleep neurologist or somnologist, which is labor intensive, time consuming, and variable between laboratories [64, 65, 66]. A variety of automated RSWA scoring methods have also been developed, but to date have not been widely applied in the field since they typically either require expensive commercial software or expert computer programming resources [67, 68, 69, 70, 65].

SEMG recordings of the submentalis and anterior tibialis muscles are used for standard RSWA scoring [71]. RSWA identified by EMG recordings are of three types which are defined by both amplitude and duration criteria. Phasic muscle activity bursts have

an amplitude four times larger than the background EMG voltage amplitude, with a duration lasting at least 0.1 seconds up to an upper limit of either 4.9 or 14.9 seconds (with a mean duration of less than approximately 0.5 seconds in normal people, although most patients with REM sleep behavior disorder have longer phasic burst duration than 0.5 seconds). Tonic muscle activity has an amplitude that is at least twice the lowest REM background voltage and lasting 15 or more seconds in duration. Any muscle activity meets the standards for either phasic or tonic muscle activity and occurs within 3 second miniepochs of time, within a standard 30 second PSG epoch used for sleep stage scoring. Any muscle activity meets the standards for either phasic or tonic muscle activity, and is scored positively when either muscle activity type occurs. Current conventions derive the quantity of these REM sleep muscle activity metrics by counting the amount of positively scored phasic or tonic muscle activity and dividing by total REM sleep time, yielding percentages of abnormal muscle activity during REM sleep. Investigators have defined various levels or thresholds of REM sleep muscle activity that distinguish RBD patients from controls without RBD [64, 66, 68].

In this chapter, we present fully automated or semi-automated detection of electrophysiological signature of RSWA implemented in Matlab programming environment. Several options of parameters and settings can be used within the system such as filters, ECG detectors, methods for envelope calculations and settings for clinical rules and thresholds. An expert clinical neurologist scorer has an opportunity to change a score suggested by automated analysis based on a further visual, manual review of the data. We plan to utilize the methods described to create a framework and a graphical user interface for clinical practice. This chapter based on article [9].

4.2 Semi-automated detection of PSG RSWA in RBD

4.2.1 Experiment Introduction

Various methods exist for automated extraction of muscle activity in PSG recordings (for both phasic and tonic muscle activity). One method is to compare the signal's envelope to a set threshold. The threshold is most often derived from baseline signal amplitude characteristic (mean and SD). Different thresholds are used in the literature, for example 2 SD (this value includes 95 % of noise amplitude) [72, 73] and 3 SD (includes 99.7 % of noise amplitude) [74, 75]. A signal envelope that crosses above a defined threshold value is considered as an onset of EMG activity. The offset of muscle activity is the point where the envelope falls under a defined threshold [72]. Raw or rectified data are used most often for visual, manual evaluations [76]. On the other hand, automatic methods require a calculated envelope to its function [77].

There are several methods for creating signal envelopes, but for biosignals only a subset is relevant. The most widely used is linear envelope [78]. Another widely used method applies a Savitzky-Golay filter, which is basically a specialized FIR filter [79, 80]. The last

method we consider is based on another approach. Peaks of rectified/powered signals are connected, thus creating a peaks interpolated envelope instead of filtration.

SEMG signal validity for automated analysis depends on excellent technical recordings which are not overly contaminated by environmental noise or biological artifacts such as sweat, excessive muscle or movement artifact, or especially cardiac electrical activity [81]. Electrical activity of the heart muscle (ECG) has a similar electrophysiological signature as phasic muscle activity in EMG leads, and the ECG activity is ubiquitous in many clinical recordings which utilize yoked or combined limb recordings due to amplification of ECG QRS cycle artifact by long interelectrode distances [81]. It is difficult to remove ECG contamination of SEMG correctly by signal de-noising because of the ECG's complicated waveform (broadband spectral distribution) that lies in a frequency range that is similar and partially overlapping with that of muscle activity [82]. One example of the methods for ECG artifact removal can be wavelet de-noising [83]. Wavelets commonly used for de-noising biomedical signals include the Daubechies (db2, db4, db8 and db6) wavelets that are chosen because of having shapes similar to the biomedical signals [83, 84].

4.2.2 Materials and Methods

The design of the presented detector is modular. The modular diagram is shown in Fig. 4.1. Each module can be turned on or off. Optimal function of each module is obtained by tuning particular parameters used within the module.

Default settings of each module were set by using Precision-Recall (P-R) analysis on training datasets (see in 4.2.2.3). The examination here is focused on testing and comparing results of automated methods using several types of envelope creation, ECG detection method, and filtering approaches. These methods are optimized using training datasets and tested using validation on an out-of-sample dataset. An expert neurologist scorer can also correct the automated results of the detector in the graphical interface, where he/she simply clicks on the desired detection and chooses to delete it. This detection is then cleared not only from the graphical interface but also from the stored automatic detection. Our results are focused on comparison of three different types of envelope calculations while maintaining other optimized parameters.

4.2.2.1 Dataset

PSG recordings were conducted on 16-channel Nicolet NicVue digital system, according to previously published general acquisition method [85, 86]. Since all PSG data were completely deidentified, the Mayo Clinic IRB considered this research project as meeting exempt status for Human Subjects research review. EMG recordings included submentalis, bipolar linked (yoked) anterior tibialis muscles, which are commonly sampled in clinical sleep laboratories, and the extensor digitorum communis (arm) muscle, since arm muscles may be more specific for RBD diagnosis [87, 88]. 30-second PSG epochs were used for standard sleep stage scoring [89]. The presence of RSWA in RBD may invalidate application of standard sleep scoring rules, so similar to previous well established methods,

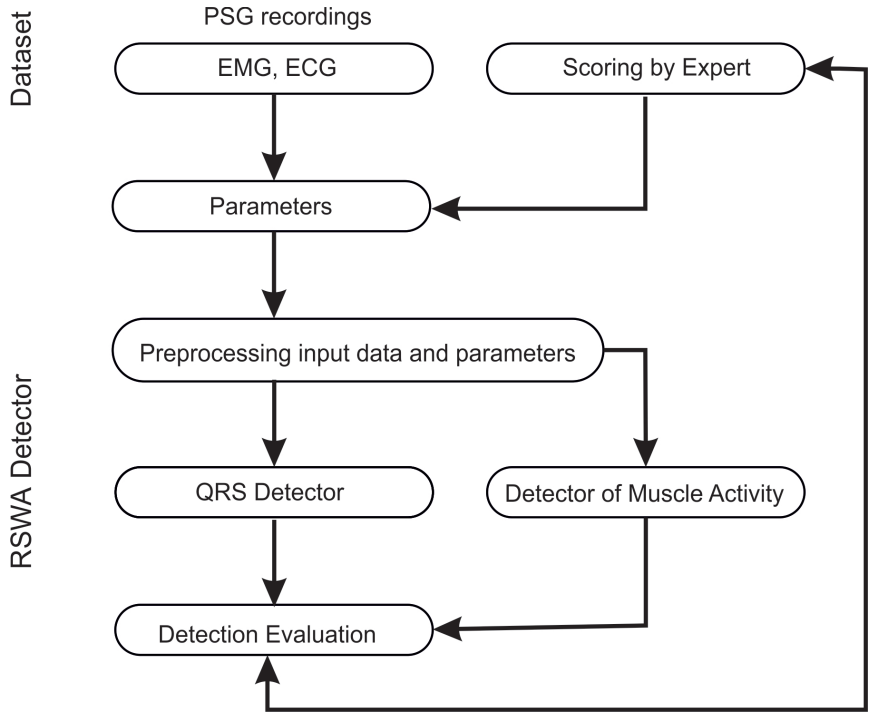

Figure 4.1: RSWA detection workflow module diagram. Dataset consists of EMG and ECG signals and scoring of contractions by an expert. Several options of parameters and setting can be used (filters, ECG detectors, methods for envelope calculations, settings of clinical rules and thresholds). Preprocessing input data and parameters are used for creating the new folder for saving of settings and results of each individual patient. The QRS detector is used to find QRS complexes and their subsequent representation in the EMG signal. The detector of muscle activity shows RSWA. RSWA detections are evaluated based on the results of an automatic detector. QRS complexes and visual, manual review and scoring by an expert can then suggest the possibility of changing parameters and detections. The expert role in semi-automated processing is called "expert-in-the-loop". Adopted from [9].

we considered the occurrence of the first rapid eye movement in the EOG channel for determination of REM sleep onset, and the end of REM sleep by absence of rapid eye movements for 3 consecutive minutes, or when EEG features of awakening or NREM sleep (i.e. K complexes or sleep spindles) were observed [64, 90, 85, 86]. EMG channels were set with a sensitivity of 5 μV/mm with low frequency filter of 10 Hz, high frequency filter of 70 Hz, and a sampling rate of 500 Hz, similar to previously published method [85, 86]. ECG signal was preprocessed as EEG data. Interference frequency alternating current (f = 60 Hz) was eliminated from all signals by use of a notch filter.

All datasets were manually scored by a neurologist (EKS) who was board-certified in sleep medicine, by 30 sec epochs according to guidelines [89, 91]. For detector purposes

overnight SEMG from the left leg was used as SEMG channel for REM sleep muscle activity detection and ECG II lead signal was used for detection of QRS.

4.2.2.2 Semi-Automated RSWA Detector – Expert-in-the-loop Approach

The core of RSWA detector is composed of four main parts. The first part is responsible for preprocessing of input data and parameters. The second part consists of detection of QRS complexes in the anterior tibialis muscle. Automatically detected heartbeat events are further used to decrease false positive rate of muscle activity detection (the third part). The final processing step is the overall evaluation of detected muscle activity events. Expert neurologist scorers can also repeat the process with changes of optional parameters.

QRS Detector

We used ECG lead II channel of PSG (sampling frequency 500 Hz) to obtain detection and precise timing where ECG artifacts can occur in SEMG. The ECG signal is often corrupted by noise from power line interference (50/60 Hz), motion artefacts and changes in the electrode-skin interface. Large and wide P and T waves can also act as sources of interference.

In current state of the art literature, standard frequency band for detecting QRS complexes of ECG is from 2-40 Hz [92, 93, 94, 95, 96]. However, this depends on the used filtering method and the magnitude and phase response of the filters.

The methodology used to detect QRS complexes involves several stages. The first stage is filtration of baseline wander (frequency range up to 2 Hz) using band pass filter with frequency band 2-40 Hz [92]. In our case, the Butterworth filter (5th order, type band pass with lower cutoff frequency 0.02 and higher cutoff frequency 0.16 which corresponds to the frequency band 2-40 Hz according to Nyquist theorem, Magnitude and Phase Response is shown in Figure 4.2) is used by zero-phase digital filtering.

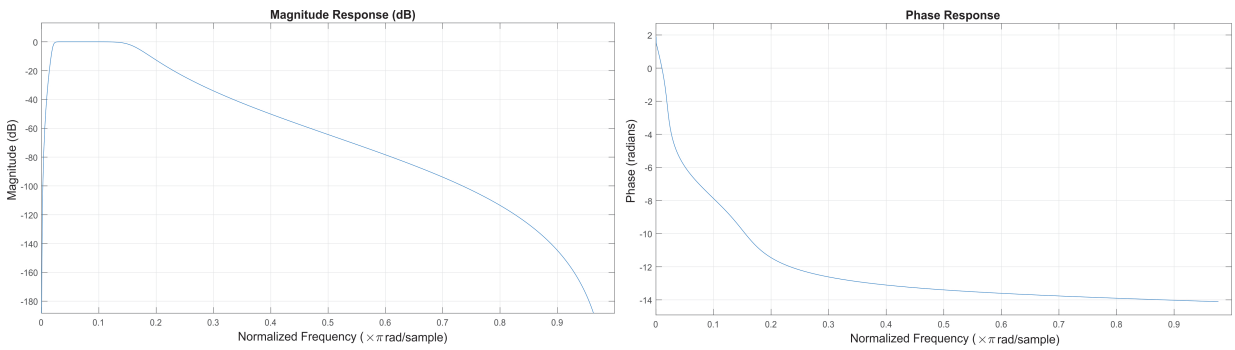

Figure 4.2: Magnitude and Phase response of the Butterworth filter, 5. order, type band pass with cutoff frequency [0.02 0.16]. Adopted from [9]

Zero-phase filtering uses the information in the signal at points before and after the current point. The input signal is filtered once in the forward direction, then the filtered se-

quence is reversed and run back through the filter (the block diagram of filtering is shown in Figure 4.3). The result has zero phase frequency characteristic [97].

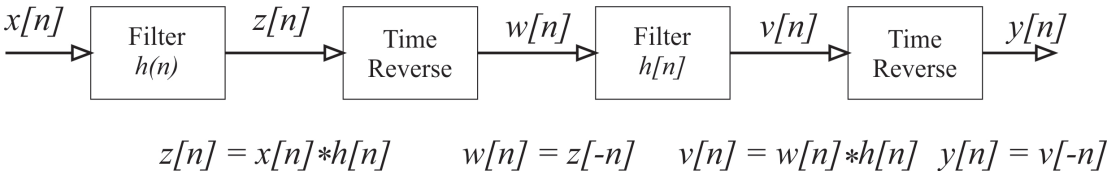

Figure 4.3: Block diagram of zero-phase filtering. Adopted from [9].

If $x[n]$ is the input sequence and $h[n]$ is the filter's impulse response, then the result of the first filter pass *z[n]* is:

$$Z(e^{j\omega}) = H(e^{j\omega})X(e^{j\omega}), \tag{4.1}$$

where $Z(e^{j\omega})$, $X(e^{j\omega})$ and $H(e^{j\omega})$ are the Fourier transforms of $z[n]$, $x[n]$ and $h[n]$, respectively. Time reversal corresponds to replacing ω by $-\omega$ in the frequency domain, so after time-reversal we get $W(e^{j\omega})$(the Fourier transforms of $w[n]$):

$$W(e^{j\omega}) = H(e^{-j\omega})X(e^{-j\omega}). \tag{4.2}$$

The second filter pass $v[n]$ ($V(e^{j\omega})$, respectively) corresponds to another multiplication with $H(e^{j\omega})$:

$$V(e^{j\omega}) = H(e^{j\omega})W(e^{j\omega}) = H(e^{j\omega})H(e^{-j\omega})X(e^{-j\omega}), \tag{4.3}$$

which after time-reversal finally gives for the spectrum of the output signal $y[n](Y(e^{j\omega})$, respectively):

$$Y(e^{j\omega}) = V(e^{-j\omega}) = H(e^{j\omega})H(e^{-j\omega})X(e^{j\omega}) = \left|H(e^{j\omega})\right|^2 X(e^{j\omega}), \tag{4.4}$$

because for real-valued filter coefficients we have $H(e^{-j\omega}) = H^*(e^{j\omega})$. Equation (4.4) shows that the output spectrum is obtained by filtering with a filter with frequency response $|H(e^{j\omega})|^2$, which is purely real-valued [98, 99].

The second stage is highlighting QRS complexes by the energy of samples (equation 4.5) from voltage amplitude.

$$E(t) = y(t)^2, \tag{4.5}$$

where $y(t)$ is the signal $y[n]$ after filtering in the time domain[100].

The energy of signal is smoothed by zero-phase filtration (using FIR filter, numerator length 32, and denominator length 1).

The floating mean average interpolation is used for the suppression of the amplitude drifting. The window is set to the 15 s with 50 % overlap for calculation of the mean value. After dividing the signal energy by this estimate, we get the signal without the amplitude drifting (shown in Figure 4.4).

Maximal amplitudes above the set threshold (mean of signal + 2|SD|) [72, 101] are detected as positions of QRS complexes. The whole process is shown in Figure 4.5.

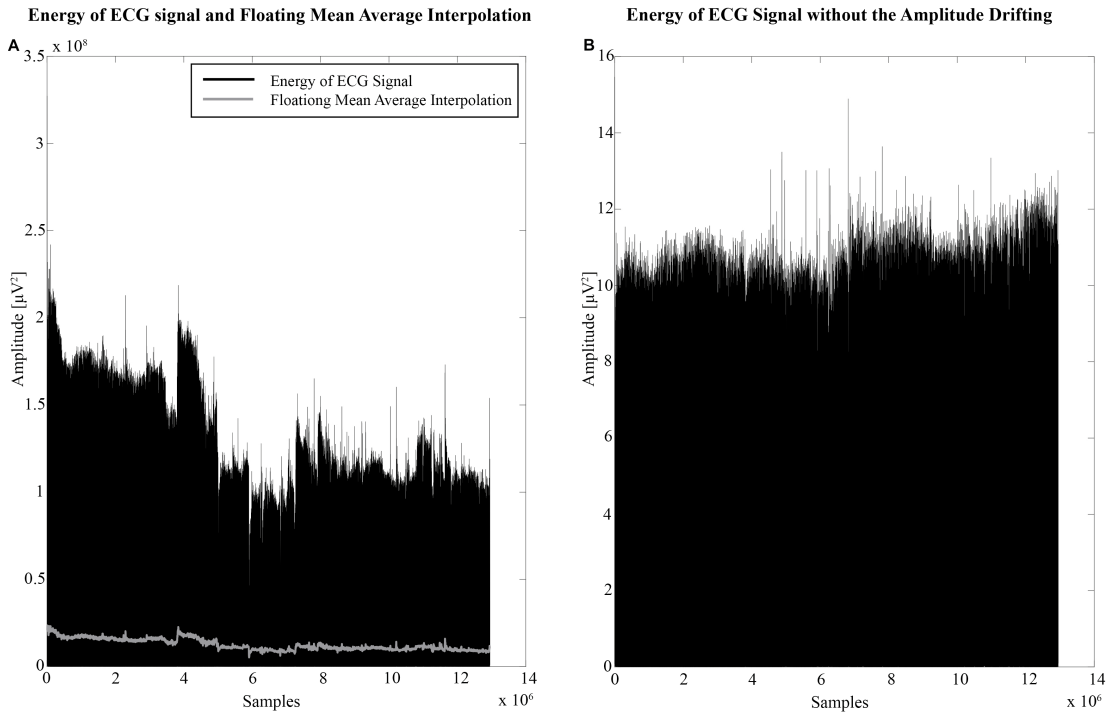

Figure 4.4: The suppression of the amplitude drifting. A) Energy of the ECG signal and floatind mean average interpolation, B) Energy of the ECG signal without the amplitude drifting. Adopted from [9].

Detector of Muscle Activity

Discrete wavelet transformation (DWT) and inverse discrete wavelet transformation (IDWT) are used for SEMG filtration to diminish ECG contamination. In DWT, the signal $x(t)$ is decomposed on different scales as follows:

$$x(t) = \sum_{i=1}^{K} \sum_{k=-\infty}^{\infty} d_i(k)\psi_{i,k}(t) + \sum_{k=-\infty}^{\infty} a_K(k)\phi_{K,k}(t), \tag{4.6}$$

where $\psi_{i,k}(t)$ are discrete analysis wavelets and $\phi_{K,k}(t)$ are discrete scaling functions, $d_i(k)$ are detailed signals (wavelet coefficients) at scale 2^K, and $a_K(k)$ is the approximated signal (scaling coefficients) at scale 2^K.

DWT can be implemented by the scaling and wavelet filters:

$$h(n) = \frac{1}{\sqrt{2}} \langle \phi(t), \phi(2t-n) \rangle \tag{4.7}$$

$$g(n) = \frac{1}{\sqrt{2}} \langle \psi(t), \psi(2t-n) \rangle = (-1)^n h(1-n). \tag{4.8}$$

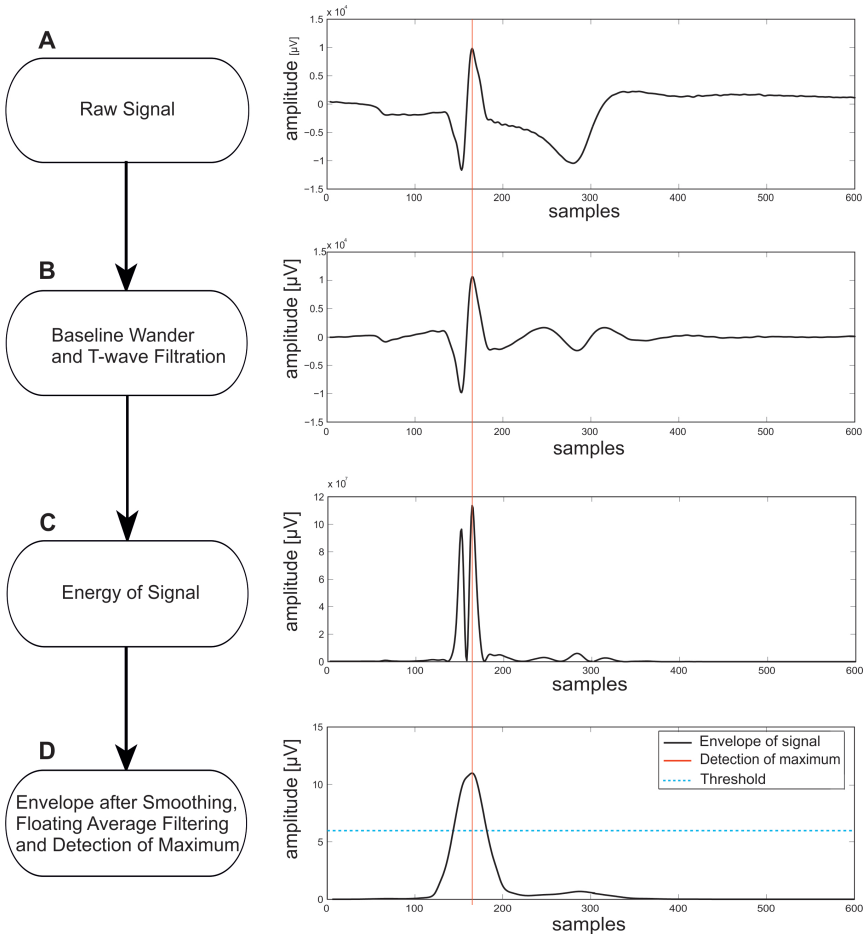

Figure 4.5: Process of R-waves detection. A) Raw ECG signal; B) ECG signal after filtration of baseline wander and T-wave interference; C) Highlighting of QRS complex by the energy of the signal; D) The envelope of the energy of ECG signal after smoothing and floating mean average interpolation and detection of the maximum. Adopted from [9].

The estimation of the detail signal at level j will be done by convolving the approximate signal at level $j-1$ with the coefficients $g(n)$. Convolving the approximate signal at level $j-1$ with the coefficients $h(n)$ gives an estimate for the approximate signal at level j [102]. The discrete scaling function plays a key role. As this function Daubechies wavelets are commonly used for denoising biomedical signals. Wavelets are generally chosen whose shapes are similar to those of the QRS complexes [39, 103]. Daubechies wavelet transformation of the 4th order (db4) is used in our case (Daubechies function and db4 Wavelet are shown in Figure 4.6). Decomposition low-pass filter (cutoff frequency 144.4 Hz) and decomposition high-pass filter (cutoff frequency 105.5 Hz) are applied for computing wavelet decomposition by DWT. Single-level reconstructed detail coefficients vector is used for removing ECG artifact by IDWT. The whole process is shown in Figure 4.7.

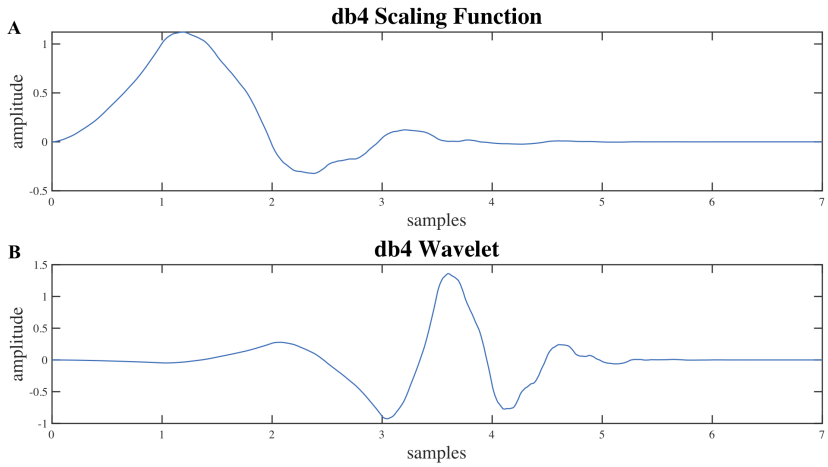

Figure 4.6: A) db4 wavelet scaling function, B) db4 wavelet. Adopted from [9].

The filtered SEMG signal was first rectified to create the selected envelope. The first tested option how to create the envelope was a linear envelope created by moving average (MA) filter (length 26 based on sampling frequency 500 Hz - 0.1 s). The second option is a peak interpolation (PKS) method (peaks of rectified/powered signals are connected thus creating peaks interpolated envelope instead of filtration), and the third option to create the envelope used a Savitzky-Golay (SavGol) filter (5th order, window size 0.3 s). The visual description can be found in Figure 4.8.

Then the filtered signal and its envelope was entered a thresholding procedure to detect the onset and the offset of muscle activity based on an iterative method. Three standard deviations of data from all REM periods for a given whole night PSG recording were used as the default threshold. In the first iteration, the submitted signal was used. Other iterations did not take the whole signal, but only parts without previously detected muscle activity. Iteration process ended while the difference between the lengths of detected EMG activity was not less than 0.008 seconds, which corresponded to accuracy of 4 samples (8 % of minimal length of contraction). This was optimized by data driven optimization procedure with fitness function F1 score. We run the optimization procedure on training data only. An example of onset detection using iterative method is shown in Figure 4.9.

Since this detector is running by default in REM sleep phases to detect RSWA, all other parts of the data are skipped for detection analysis (taken from sleep stage scoring done manually). If the automated detector runs without ECG suppression or filtering, and because of overlapping SEMG and ECG spectrum, far fields of ECG QRS complexes in SEMG channel creates an unwanted artifactual signal that is prone to false positive detections of the detector. The occurrence of these false positive detections can be suppressed if chosen by using the information from QRS detector.

The last step of the detector is to connect detections that are close to each other. That is based on predefined clinical rules [104]. RSWA detections that are longer than the predefined length (15s – according to clinical standards) are removed and are not

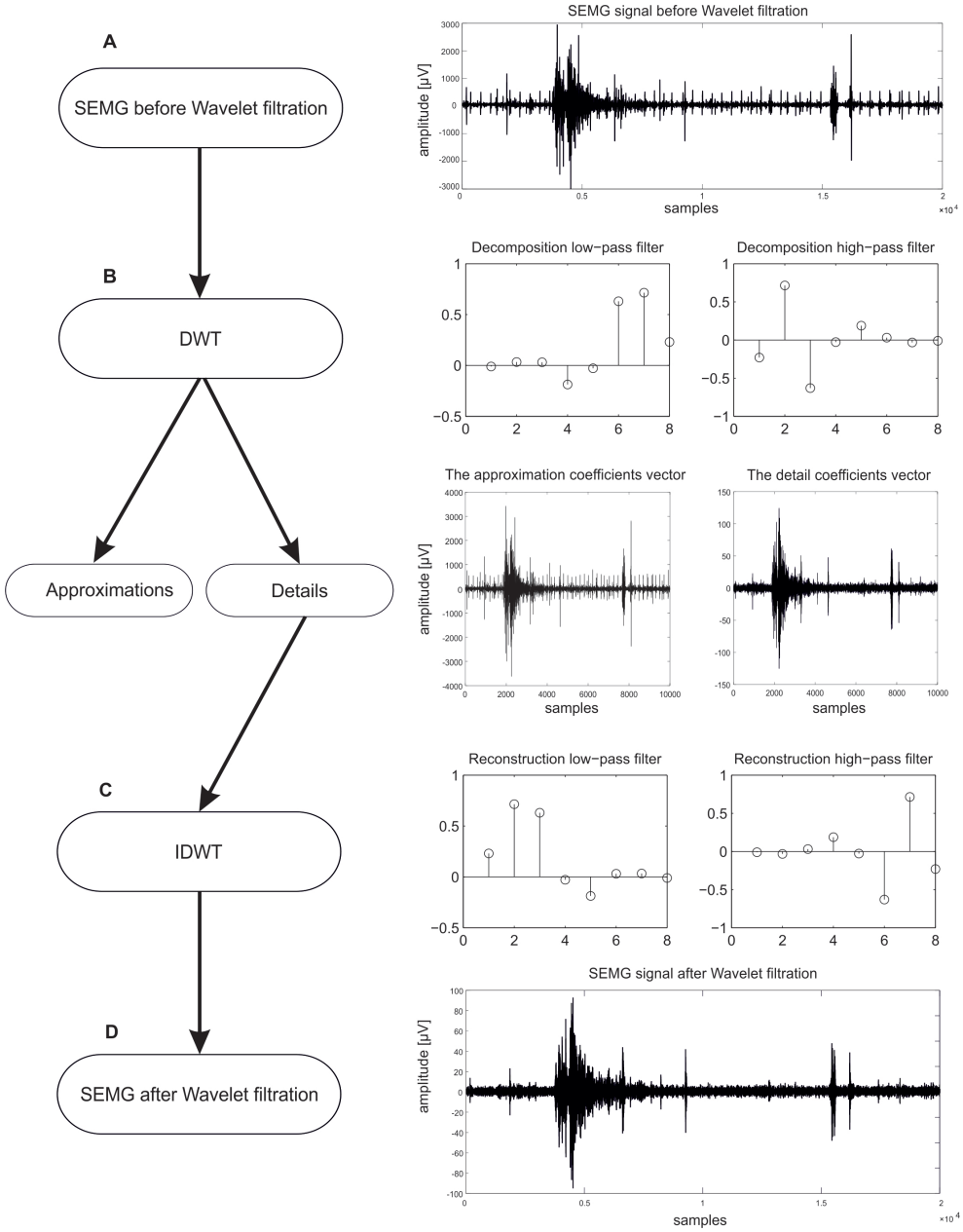

Figure 4.7: Wavelet filtration of SEMG signal. A) SEMG signal before filtration; B) The DWT performs a single level one-dimensional decomposition with respect to a particular wavelet decomposition filters (low-pass and high-pass filter by db4 wavelet); C) The IDWT performs a reconstruction with respect to reconstruction filters (low-pass and high-pass filter by db4 wavelet); D) SEMG signal after wavelet filtration using single-level reconstructed detail coefficients vector. Adopted from [9].

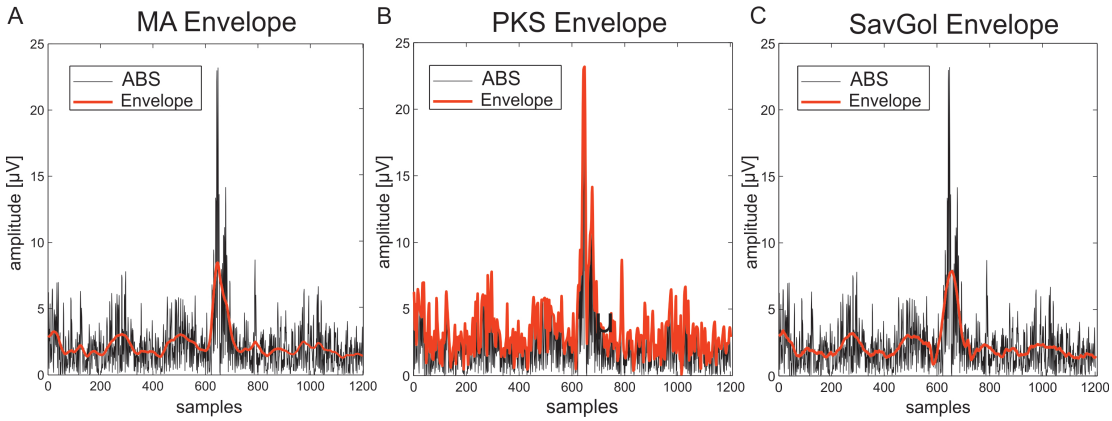

Figure 4.8: A) Absolute value of the signal (ABS) and envelope by moving average filter; B) Absolute value of the signal (ABS) and envelope by peaks interpolation; C) Absolute value of the signal (ABS) and Savitzky-Golay envelope. Adopted from [9].

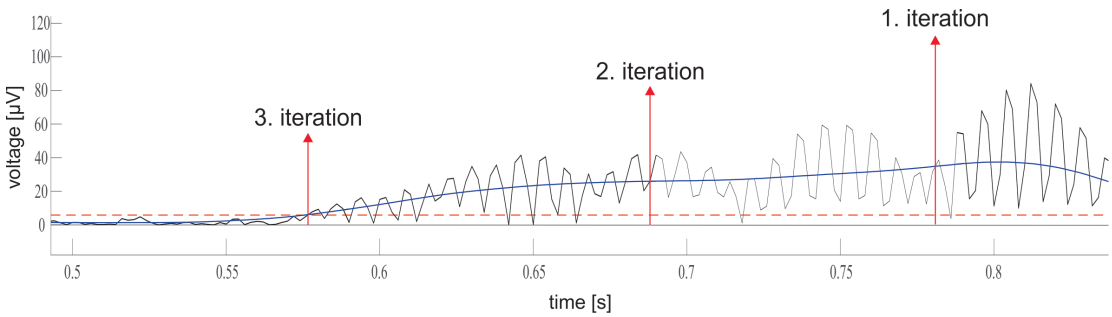

Figure 4.9: The iterative method to find optimal onsets detection. The threshold (dashed red line) is calculated as 3 SD from the entire filtered signal (black line) in the first iteration. Then detected muscle activities (signal envelope (blue line) above the threshold) are removed from the signal, and the threshold is calculated again (iteration 2). Iteration end is while the difference between two consecutive found onsets of EMG activity is less than 0.008 second. Onsets of the muscle contraction are marked by the red arrow for each iteration. Adopted from [9].

considered as part of phasic RSWA muscle activity. Minimal length of contractions (0.1 s) and join cluster of RSWA if gap is less than set time (0.2 s) adhere to standard approaches for visual, manual scoring [85, 86].

4.2.2.3 Statistical Analysis and Optimization of Automated Classifier

Original dataset was randomly split to training (data of 2 patients) and validation data set (data of 5 patients). The binary classification class imbalance problem was solved by using

relevance measures P-R to assess precision (P, equation 4.9) and recall (R, equation 4.10), and F1 measure (harmonic mean of P-R, equation 4.11).

$$P = \frac{TP}{TP + FP}, \tag{4.9}$$

$$R = \frac{TP}{TP + FN}, \tag{4.10}$$

$$F1 = 2 \cdot \frac{P \cdot R}{P + R}, \tag{4.11}$$

where TP are true positives, FP false positives and FN false negatives RSWA detections. P-R analysis on training data set was used to set up optimal parameters (Table 4.1).

Table 4.1: Default setting of parameters based on the best result using optimization procedure on training data.

Use Wavelet transformation for filtering of SEMG signal	✓
Use absolute value of the SEMG signal for muscle activity detection	✓
Use the energy of the SEMG signal for highlighting muscle activity	x
Number of standard deviations used for detection	3
Minimal difference of selected time for contractions between iterations [s]	0.008
Window size for MA filter [s]	0.1
Window size for SavGol filter [s]	0.3

Setup of the classifier that maximized the area under the curve (AUC) [105, 106] on training data was then used to be tested on the out-of-sample dataset. Results are presented as those P, R, and F1 using out-of-sample validation dataset (Table 4.2).

4.2.3 Experiment Results

The original dataset consisted of 7 individual PSG recordings of individual adult RBD subjects. The average time of PSG signals was 6.4 ± 2.03 hours. (1.05 ± 0.47 hours containing REM stages). Detection was performed with three different envelope methods. Table 4.2 summarizes the final results for all considered events. By the wide margin, the worst results were achieved by the PKS envelope. Thus no further in-depth results for this method are shown. Best performance of automated classifier was achieved by MA method (recall 0.908 ± 0.083. precision 0.617 ± 0.111 and F1 0.726 ± 0.077).

Further in-depth results of our analysis for MA envelope compared to manual detections are shown in Table 4.3. Mean recall of the validation data set was 0.9163 ± 0.1007 with precision 0.6424 ± 0.1234. The lowest recall was 0.7557 with precision 0.7433. The lowest precision was 0.4286 with one hundred percent recall.

Table 4.4 shows results of detection for SavGol envelope. Mean recall was 0.8821 ± 0.1292 and precision 0.6673 ± 0.1537 for validation data set. The lowest recall was 0.6694 with precision 0.8223. The lowest precision was 0.4175 with 100 % recall.

Table 4.2: Statistical results summary across all processed datasets. The average recall, precision, and F1 score are shown. MA: moving average filter, SavGol: Savitzky-Golay filter, PKS: peaks interpolation

	MA	**SavGol**	**PKS**
recall	0.908 ± 0.083	0.874 ± 0.106	1.000 ± 0.000
precision	0.617 ± 0.111	0.642 ± 0.135	0.065 ± 0.040
F1	0.726 ± 0.077	0.726 ± 0.083	0.121 ± 0.069

Table 4.3: Results of analysis for individual RBD subjects in the study by using MA envelope. The number of true positive events (TP), false positive events (FP), false negative events (FN), recall, precision and F1 score are shown.

Subjects P3 and P7 (set used for training)

	TP	**FP**	**FN**	**recall**	**precision**	**F1**
P3	234	214	32	0.8797	0.5223	0.6555
P7	104	73	12	0.8966	0.5876	0.7099

Subjects P1, P2, P4, P5, P6 (validation set)

	TP	**FP**	**FN**	**recall**	**precision**	**F1**
P1	178	78	13	0.9319	0.6953	0.7964
P2	362	125	117	0.7557	0.7433	0.7495
P4	42	56	0	1	0.4286	0.6
P5	22	10	0	1	0.6875	0.8148
P6	253	132	30	0.894	0.6571	0.7575

4.2.3.1 Detection Evaluation

An example of the performance of individual detection algorithms in SEMG analysis by using MA envelope is shown in Figure 4.10. The figure displays process of the particular algorithm from raw data to the RSWA signal. QRS detection in ECG data is also shown in the figure because of their reflection of the SEMG signal.

4.2.4 Discussion and Conclusion

In the past it was believed that the evaluation of the SEMG background is difficult because of mixture of multiple motor units firing at various period [107]. A short abstract [108] reported a very preliminary study of an automatic quantification of the chin SEMG activity by criteria of duration and amplitude. During the previous years, some authors have used computer automated techniques to analyze RSWA [109, 110, 111], but most of them were using chin SEMG for analyzing. According to the study [112], highest rates of phasic

Table 4.4: Results of analysis for individual subjects in the study by using SavGol envelope. The number of true positive events (TP), false positive events (FP), false negative events (FN), recall, precision and F1 score are shown.

Subjects P3 and P7 (set used for training)

	TP	**FP**	**FN**	**recall**	**precision**	**F1**
P3	225	194	37	0.8588	0.5370	0.6608
P7	98	59	17	0.8522	0.6242	0.7206

Subjects P1, P2, P4, P5, P6 (validation set)

	TP	**FP**	**FN**	**recall**	**precision**	**F1**
P1	177	77	16	0.9171	0.6969	0.7920
P2	324	70	160	0.6694	0.8223	0.7380
P4	43	60	0	1.0000	0.4175	0.5890
P5	24	8	1	0.9600	0.7500	0.8421
P6	241	130	38	0.8638	0.6496	0.7415

EMG activity were found in the mentalis muscle, the flexor digitorum superficialis muscle in the upper limb muscles, and the extensor digitorum brevis muscle in the lower limb muscles.

In current literature, the semi-automated scoring algorithm was compared with the visual observation of two human raters in the study by Jeppesen [111]. Agreements of human and computer scoring on single epoch level were high for all activity types ('tonic' activity both raters 97 %, 'phasic' activity 95 % & 93 %, 'any' activity both raters 95 %). Nevertheless, authors discarded 17 % of 30 second epochs and 12 % of 3 seconds mini-epochs for the elimination of flow events, arousal, and artifacts. Motor activity during REM sleep was quantified manually and computer assisted in the study by Hackner [113]. Computer-derived indices (with and without artifact correlation) for the SEMG activity correlated well with the manually derived indices (all Spearman rhos 0.66-0.98).

Because of the subjective nature of visual, manual scoring, even by expert raters, the reliability of this gold standard remains somewhat uncertain. During our evaluation phase, we encountered many detected RSWA events that were selected by visual, manual expert scorer differently than by the detector that were inconsistent with previously selected/discarded events of the same nature (length, amplitude of envelope, frequency characteristic and even visual evaluation).

It is commonly accepted that only about 10 % of information that is hidden in recorded signal is obtainable by visual observation. Even if this is not true, there remains a level of skepticism in the internal reliability of expert evaluation that is not supported by machine pre-evaluation. Since expert scorers interested in or capable of validly visually scoring RSWA are extremely limited in number, making the routine scoring of PSG for RBD

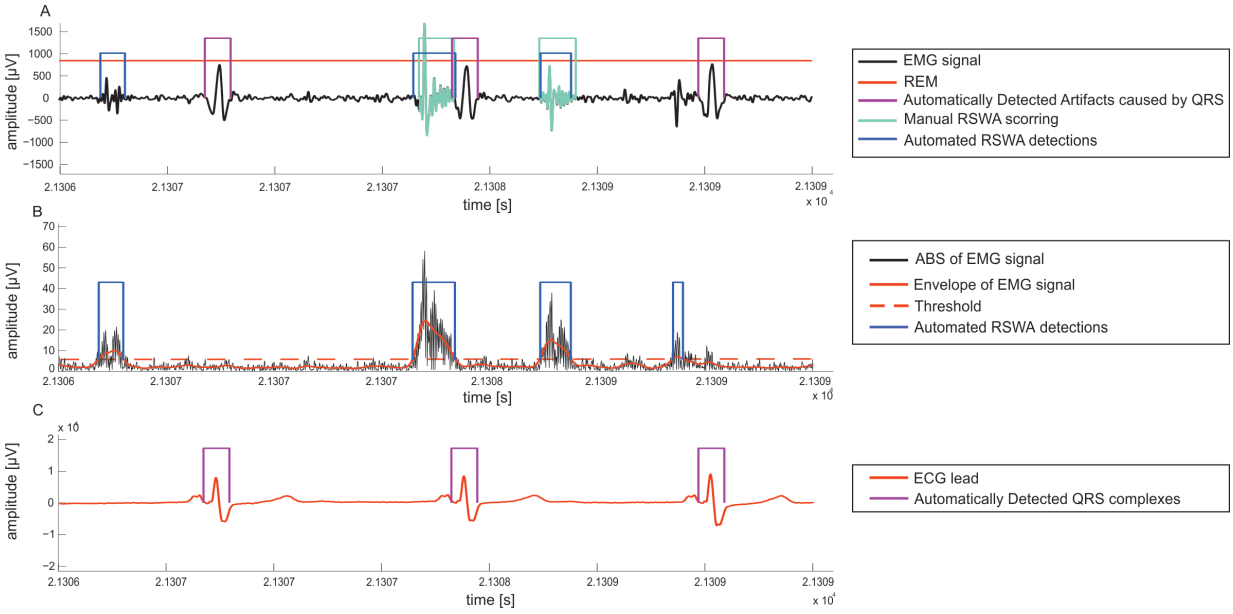

Figure 4.10: An example of SEMG data with RSWA detection. From top to bottom: A) EMG data with automated QRS detection (purple) by using ECG lead data (plot C), manual RSWA scoring performed by visual, manual scoring by an expert scorer (light green), automated RSWA detections by suggested method (blue); B) plot shows principle and threshold of RSWA detection on filtered SEMG envelope. Bottom plot C) shows ECG signal with QRS detection. Adopted from [9]

patients a very resource intensive and scarce resource, automated techniques that are reliable for RSWA detection are greatly needed in the field for both further research and future clinical application in diagnosis. Every module has been primarily selected to help expert evaluation. The automatic detection part is only the natural evaluation thus our main focus is on recall. Based on the results this approach seems to be working because of globally increasing recall with decreasing precision.

However, results of automatic detections are very likely to be both more accurate and consistent than human visual detections. In our preliminary studies, it appears highly likely that our detector was optimized on a training dataset that contained more difficult to evaluate RSWA signals than in the validation set, in which performance of our detector appeared significantly better.

The worst performance was observed using the peaks interpolation envelope methods, which is therefore of limited use in automatic detection for RSWA, although it may still be useful as an advisory tool with adjustment of advanced settings to detect subtle or difficult to discern RSWA muscle activity.

4.3 Conclusion

In this chapter, a supervised automated classifier is described. It was built on a combination of methods to detect RSWA of SEMG signals automatically. It was developed, implemented and tested in this chapter. The method was tested on data from 7 individual PSG recordings of individual human adult subjects with RBD, and all parts of our designed framework appeared reliable. For detection three methods were used for creating envelopes. Best detection was achieved using the mean envelope (average precision of 64.24 ± 12.34 %, recall 91.63 ± 10.07 %, and F1 score 74.36 ± 8.47 %). These results indicate that automated detector of RSWA can provide useful information to the physician and followed by expert additional overscoring and correction by visual, manual review, can be used within our framework for fast semi-automated RSWA quantification.

The degree of freedom in relation to selectable parameters of our framework are likely to assist in decreasing human error during visual manual evaluation, and inform the visual RSWA scoring process. Future studies analyzing blinded visual scoring with and without consideration of automated scoring detections may be useful to determine the influence of automated RSWA detection for research and clinical applications.

The next chapter deals with measuring myotonometric muscle parameters.

Chapter 5

Biomechanical Parameters of Muscles

5.1 Introduction

Human movements are composed of muscle-tendon complexes which perform contractions of muscle fibres linked by tendons. Many research groups focused on the analysis of individual movements, called rapid aimed movements or target-directed movements. Based on the understanding of these simpler activities, the understanding of the more complex ones is expected [114].

Objective measurement of myotonometric parameters would greatly enhance detection of risk of injury and monitoring of the effects of interventions, such as treatment [46]. It also helps top athletes and their coaches to set the right workload to achieve maximum performance and avoid injury from an over-training. The principal difference between myotonometry and traditional measurement of muscle parameter is that it can measure the tone, elasticity and stiffness simultaneously and non-invasively. MyotonPro device is based on the responses of soft tissue induced by a mechanical impulse and the subsequent simultaneous computation of the parameters such as oscillation frequency $F[Hz]$(representing the muscle tone), dynamic stiffness $S[Nm^{-1}]$, logarithmic decrement D (muscle elasticity), mechanical stress relaxation time $R[ms]$ and creep C [47, 48]. More information and parameter calculations are provided in the section 2.3.

This chapter is divided into three parts. The first section deals with an investigation of muscle parameters using MyotonPro device in two groups: active sportsmen and inactive individuals during physical exercise demonstrating by the squats and based on [10]. The second part is focused on differences in values of myotonometric parameters before and after rehabilitation process using INFINITY® method. Based on these studies, a third experiment was developed that deals with muscle imbalance before and after rehabilitation exercises aimed at strengthening the deep stabilization system. In this section there is also described graphical user interface created on the basis of cooperation with physiotherapists.

5.2 Objective Assessment Using MyotonPro

5.2.1 Experiment Introduction

In this study, we used the MyotonPRO device to determine muscle parameters during physical exercise (demonstrating by squats) in the group of active sportsmen (SA) and in the group of people who do not do any sport (SI) on the desired muscle: gluteus maximus left (GML), gluteus maximus right (GMR), vastus lateralis left (VLL), vastus lateralis right (VLR), vastus medialis left (VML) and vastus medialis right (VMR). The main aim was to compare muscle parameters in both groups (SA and SI).

5.2.2 Materials and Methods

5.2.2.1 Subjects

Twenty healthy male volunteered to participate in this study. Group 1 included 10 subjects (mean age: 23.5±3.2 years) which are active in the sports. Group 2 included 10 sport inactive subjects (mean age: 25.1±5.4 years). All subjects met the inclusion criteria (no chronic diseases affecting the musculoskeletal system such as diabetes mellitus, osteoporosis or rheumatism; no surgery or injuries of the lower limb and the foot; no intake of anabolic or other drugs affecting the musculoskeletal system).

5.2.2.2 Experimental Procedure

The site of measurement was located by visual observation and palpation of the largest area of muscle bulk during contraction of each muscle. A physical marker was positioned to ensure the same location of the sensor throughout the whole experiment.

The MyotonPRO device (version 5.0.0.203) was positioned at the measurement location and held while the device performed the predefined series of measurements: a multi-scan mode of five mechanical impulses.

The entire measurement process was divided into three phases. The first phase included the measurement of muscle parameters in a relaxed lying position. The second phase contained four sets of exercises. The proband had to make five squats in each set. Muscle parameters were measured in the relaxed lying position after each set. The third relaxation phase contained measurements in a relaxed lying position after 2, 4, 6, 8 and 10 minutes. The measurement process is summarized in Fig. 5.1).

5.2.2.3 Numerical and statistical analysis

Data were downloaded from the MyotonPRO device in the form of .CSV file and processed using Matlab 2018a software. The raw dataset contains values of all five mechanical impulses. The mean value with SD was first calculated for each subject, each muscle and each parameter. The data should be split into two parts for comparison of SA and inactive sportsmen (SI) groups. The first part contains the data from the squat phase (SP).

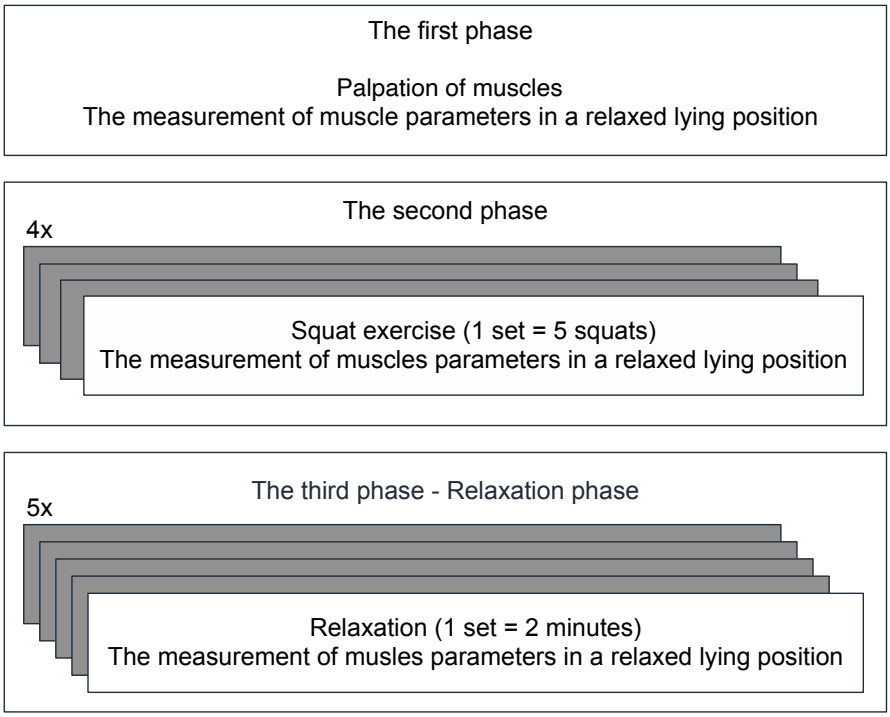

Figure 5.1: Diagram of whole measuring process. Adopted from [10].

The second part contains data from the relaxation phase (RP). The area under the curve representing the values of these two parts was calculated as the integration of function using the trapezoidal method. An unpaired t-test with 5% significance level was used for statistical analysis. To reject or confirm the null hypothesis (that the area value of SA and SI group comes from independent random samples from normal distributions with equal means and equal but unknown variances), a p-value must be calculated.

5.2.3 Experiment Results

A total of 20 healthy subjects (split into two groups: SA and SI group) were measured. The example of the mean value and SD for parameter Frequency and Creep is shown in Tab. 5.1 (Subject number: 1, group: SA, muscle: GML) and in Tab. 5.2 (Subject number: 1, group: SI, muscle: GML).

The area under the value representing squads (SP) and relaxation (RP) phase for each subject, each muscle and each parameter was calculated. Example of the area (subject: S1, group: SA, muscle: GML, parameter: Frequency) is shown in Fig. 5.2. Comparison of Frequency and Creep area (mean value±SD from SA and SI group) is shown in Tab. 5.3.

Table 5.1: Mean value±SD of parameter Frequency and Creep for Subject 1, SA group, muscle: GML

	Mode	Frequency [Hz]	Creep
SA	Before Squat	12.58±0.48	1.436±0.051
	05 Squats	12.14±0.06	1.160±0.190
	10 Squats	12.28±0.08	1.260±0.242
	15 Squats	11.62±0.11	1.220±0.219
	20 Squats	12.42±0.54	1.386±0.125
	02 minutes	11.46±0.06	1.260±0.072
	04 minutes	12.82±0.08	1.396±0.011
	06 minutes	11.38±0.13	1.218±0.027
	08 minutes	11.30±0.07	1.290±0.086
	10 minutes	11.42±0.05	1.352±0.010

Table 5.2: Mean value±SD of parameter Frequency and Creep for Subject 1, SI group, muscle: GML

	Mode	Frequency [Hz]	Creep
SI	Before Squat	10.86±0.09	1.804±0.016
	05 Squats	11.38±0.27	1.690±0.113
	10 Squats	11.68±0.05	1.712±0.013
	15 Squats	10.62±0.15	1.984±0.020
	20 Squats	11.30±0.29	1.824±0.024
	02 minutes	11.38±0.13	1.526±0.247
	04 minutes	11.20±0.19	1.736±0.175
	06 minutes	10.84±0.21	1.720±0.169
	08 minutes	10.68±0.08	1.784±0.055
	10 minutes	11.54±0.18	1.588±0.223

5.2.3.1 Gluteus Maximus

If the p-value is smaller than the significant level set to 5%, we reject the null hypothesis that mean values of the area are equal. Due to the result, the area of parameter Oscillation frequency was significantly smaller for the SI group than the SA group on the right side in the relaxation phase. The parameter Mechanical stress relaxation time was significantly higher for the SI group than for the SA group in the relaxation phase on both sides of muscle. A similar result was achieved with the Creep parameter, where the area value was larger for the SI group than for the SA group on both sides of the body in the relaxation phase and on the right side in the squat phase (Example of mean value of parameter Creep

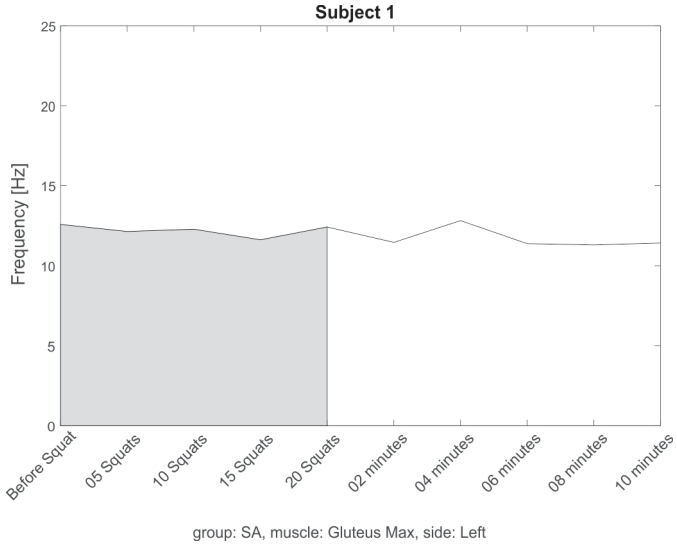

Figure 5.2: Area under the curve representing parameter Frequency. Subject 1, SA group, Muscle: gluteus maximus, left. Grey part represent area for SP and white part for RP. Adopted from [10].

for left side is shown at Fig. 5.3).

5.2.3.2 Vastus Lateralis

The area of Stiffness parameter was significantly smaller for the SI group than for the SA group on the left side of the body in the relaxation phase of the experiment. In the squat phase, there was significantly higher area for the SI group than SA group in both sides of the body for Decrement parameter.

5.2.3.3 Vastus Medialis

In the relaxation phase, there was a significantly smaller area value for the SI group than for the SA group for both sides of parameter Oscillation frequency and Stiffness. In the squat phase, there was calculated smaller area value for the SI group than for SA group on the right side for Oscillation frequency and Stiffness parameter and higher for the SI group than for the SA group for parameter Mechanical stress relaxation time.

5.2.4 Discussion and Conclusion

Because MyotonPro software has a very limited evaluation of results, we have decided to process the results by evaluating the area of each measurement phase using Matlab.

The parameter Oscillation Frequency characterises the muscle tone. Low tone is experienced as "floppy, mushy, dead weight" and high tone is experienced as "light, tight, and strong". Muscles with high tone are not necessarily strong and muscles with low tone are

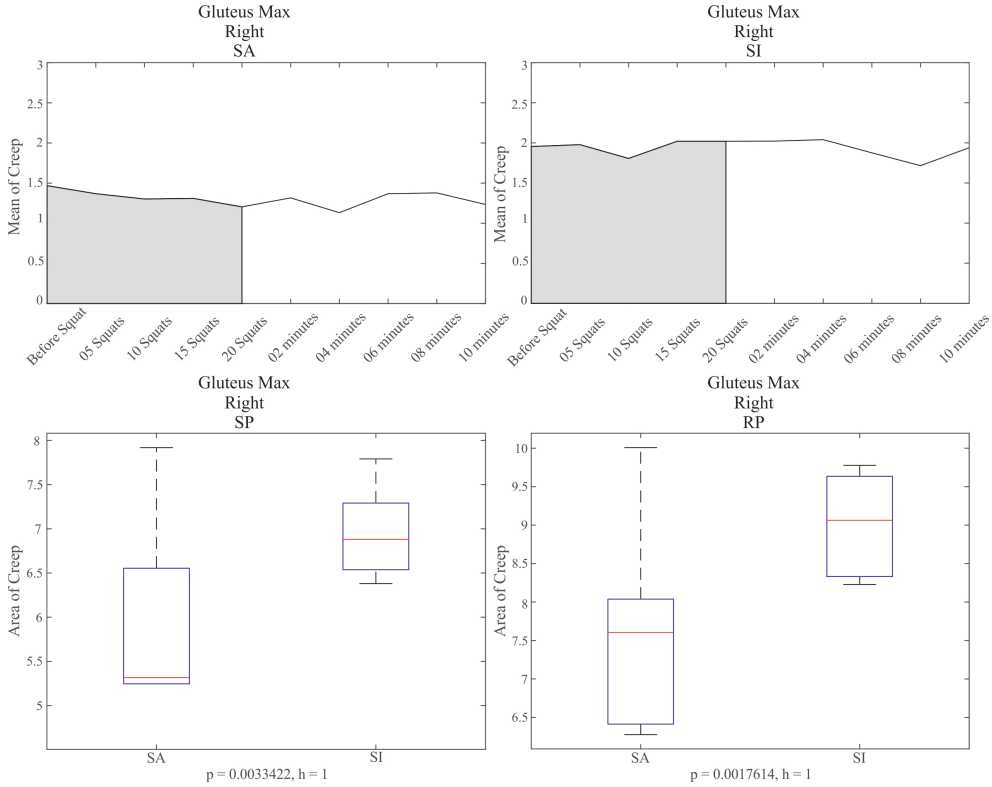

Figure 5.3: Value of mean area for parameter Creep. Muscle GM. Adopted from [10].

not necessarily weak. In general, low tone does increase flexibility and decrease strength and high tone does decrease flexibility and increase strength [115]. It can, therefore, be assumed that subjects in the SA group will have a higher muscle tone due to stronger but less flexible muscles. This was confirmed in the vastus medialis muscle and gluteus maximus.

The parameter Logarithmic decrement characterizes muscle's elasticity. Elasticity is inversely proportional to the decrement. A lower level of decrement reveals a better muscle elasticity and the ability of contraction [116]. Due to the result, the difference between area value is proved only on the muscle vastus lateralis on both sides of the body. Thus, we cannot say with certainty that in the SA group, the muscles are more elastic than in the SI group.

Stiffness is the biomechanical property of a muscle that characterises the resistance to a contraction or to an external force that deforms its initial shape [117]. Nevertheless, it does not imply that athletes have higher muscle stiffness. In case of abnormally high stiffness, a greater effort is required from the agonist muscle to stretch a stiff antagonist which leads to an inefficient economy of movement [118]. Our study only shows that in the SI group in the vastus medialis and vastus lateralis muscles, this value was significantly lower in the relaxation phase.

Mechanical Stress Relaxation Time is the time that the muscle needs to recover its shape

Table 5.3: Mean area±SD for the parameter Oscillation Frequency and Creep, SP-area of squat phase, RP-area of relaxation phase, SA-sport active group, SI-sport inactive group, GML-gluteus maximus left, GMR-gluteus maximus right, VLL-vastus lateralis left, VLR-vastus lateralis right, VML-vastus medialis left, VMR-vastus medialis right.

	O. frequency [Hz]			
	SP		RP	
	SA Mean±SD	SI Mean±SD	SA Mean±SD	SI Mean±SD
GML	47.64±2.95	45.99±2.20	58.68±2.61	56.26±3.16
GMR	49.01±4.37	46.05±3.43	59.13±3.93	55.27±2.94
VLL	76.73±5.31	70.40±11.98	90.82±7.71	87.56±14.87
VLR	75.81±8.09	71.66±9.77	94.85±12.19	86.24±10.44
VML	55.66±4.12	51.73±4.96	70.65±4.74	64.76±5.94
VMR	56.80±3.42	50.89±4.73	72.64±7.69	64.41±6.62
	Creep			
	SP		RP	
	SA Mean±SD	SI Mean±SD	SA Mean±SD	SI Mean±SD
GML	5.99±0.87	6.60±0.57	7.51±0.83	8.47±0.74
GMR	5.84±0.92	6.96±0.51	7.55±1.12	9.02±0.60
VLL	3.69±0.42	4.27±1.03	4.93±0.66	5.35±1.31
VLR	3.64±0.54	4.08±0.92	4.63±0.73	5.28±1.16
VML	5.10±0.60	5.57±0.77	6.33±0.66	6.90±0.86
VMR	4.98±0.53	5.62±0.83	6.15±0.84	6.94±1.17

from deformation after a voluntary contraction. As a result, in the SA group, the gluteus maximus muscle is recovered more rapidly than in the SI group.

The following section is focused on the evaluation of muscle parameters before and after the rehabilitation process using the INFINITY® method. The method is briefly described. The analysis also includes the symmetry index, which indicates the degree of symmetry of the parameters on the right and left sides of the body.

5.3 Objective Assessment of INFINITY® Rehabilitation Process

5.3.1 Experiment Introduction

Musculoskeletal problems are widespread throughout the world [119]. The most common musculoskeletal problem is low back pain (LBP). It is the fifth most common reason for

all physician visits [120].

From many studies and practice, it is clear that not only prevention but also follow-up care for a patient with LBP must include regular physical activity along with an appropriate method indicated rehabilitation that does not interfere with the musculoskeletal system [121].

The special rehabilitation method called INFINITY® has been developed at the Rehabilitation Clinic Brandys nad Orlici, and is used to rehabilitate patients with musculoskeletal problems. This method uses movement in the shape of infinity sign in part of exercises and is focused on the stabilization and strengthening of trunk muscles, dorsal and abdominal muscles, including the deep stabilization system. Rehabilitation is based on relaxation, extension, and mobilization of the soft tissues of the motor system [121].

The purpose of this section is to verify the presence of differences between the measured myotonometric parameters before and after the rehabilitation process using INFINITY® method by the MyotonPro device.

5.3.2 Materials and Methods

5.3.2.1 Subjects

Five healthy females (age: 27.2 $\pm$ 4.3 years) and five males (age: 23.6 $\pm$ 1.7 years) volunteered to participate in this study. All subjects met the inclusion criteria (no chronic diseases affecting the musculoskeletal system such as diabetes mellitus, osteoporosis or rheumatism, no intake of anabolic or other drugs affecting the musculoskeletal system).

5.3.2.2 Measures

Upper trapezius (TU), middle trapezius (TM), lower trapezius (TL), erector spinea (ES), external oblique (EO) and rectus abdominis (RA) muscles were selected for measurement on both sides of the body. The site of measurement was located by visual observation and palpation of the largest area of muscle bulk during contraction of each muscle. A physical marker was positioned to ensure the same location of the sensor throughout the whole experiment. The example of using MyotonPro device is shown in Fig. 5.4.

Oscillation frequency, dynamic stiffness, logarithmic decrement, mechanical stress relaxation time, creep and symmetry index were quantified using the damped oscillation method of the MyotonPro device.

The probe at the end of device was placed perpendicularly to the surface of the skin overlying all the selected muscles. Slight pressure (pre-compression force of 0.18 N) was applied between the probe and the surface of the skin, and a short mechanical impulses (5 single measurement with interval of 0.8 second with 0.4 N for 15 ms) were delivered to the tissue under the probe. The mechanical impulses generate damped oscillations within the muscle, which are recorded by an accelerometer. The device provides the resultant oscillation curve from which all parameters are calculated.

Figure 5.4: Example of using MyotonPro device.

5.3.2.3 Design and Procedure

All outcomes were obtained with the participant lying in a prone position (muscles: TU, TM, TL, ES) and in a supine position (muscles: EO, RA), with the upper extremities placed along the trunk. Myotonometric measurements were performed at one day before and immediately after the INFINITY® rehabilitation process.

INFINITY® rehabilitation process

There exist two principal types of Infinity motion: the macro-movement (amplitudes in a range of centimeters) and the micro-movement (amplitudes in a range of millimeters)[121].

Macro-movements were selected for our experiment. In upright standing a patient actively moves the center of gravity of the upper body along a specified infinity shape curve with ten repetitions (shown in Fig. 5.5).

5.3.2.4 Numerical and Statistical Analysis

Data were downloaded from the MyotonPRO device in the form of .CSV file and processed using Matlab 2018a software. Raw data set contains values of all five mechanical impulses. The mean value with the standard deviation (SD) was first calculated for each subject, each muscle and each parameter. Symmetry index was calculated by the formula:

$$(y - x)/((y + x)/2) * 100, \tag{5.1}$$

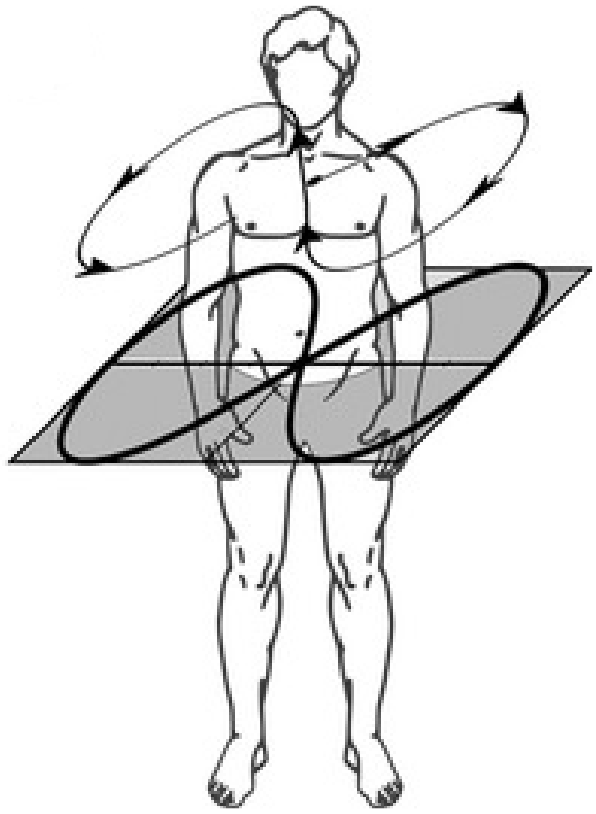

Figure 5.5: Trajectories of upper body center of gravity and its ∞ projection into the transversal plane. [11]

where y is value of parameter on the right side and x on the left side of the body.

Data were examined for normality using the one-sample Kolmogorov-Smirnov test with the 5% significance level and two-sided t-test.

5.3.3 Experiment Results

A total of 10 healthy subjects were measured. The example of the mean value and SD for one participant, two muscles and two parameters are shown in Tab. 5.4

The example of p-value of a two-sided t-test is shown in Tab. 5.5.

Statistically significant difference ($p<0.05$) was found in symmetry index of parameter Creep on the muscle upper trapezius and parameter Stiffness on the muscle rectus abdominis.

5.3.4 Discussion and Conclusion

According to the results of this experiment, the symmetry index of upper trapezius and rectus abdominis muscle creep and stiffness were improved after moving by the center of

Table 5.4: Example of mean value and SD for one participant, Creep (C) and Stiffness (S) parameters, erector spinae (ES) and rectus abdominis (RA) muscles, before and after infinity process.

	Muscle (side)	C Mean±SD	S [N/m] Mean±SD
Before	ES (left)	1.16±0.02	278.40±3.44
	ES (right)	0.94±0.03	351.40±14.08
	RA (left)	1.19±0.03	259.60±5.50
	RA (right)	1.48±0.17	231.40±25.12
After	ES (left)	0.98±0.03	341.80±12.34
	ES (right)	0.83±0.10	385.00±24.57
	RA (left)	1.45±0.06	223.80±6.98
	RA (right)	1.18±0.04	288.00±9.92

Table 5.5: Example of p-value of symmetry index (SI) for muscle upper trapezius (TU), erector spinea (ES), external oblique (EO), rectus abdominis (RA) and parameter Creep (C) and Stiffness (S).

Muscle	p SI for C	p SI for S
TU	0.024	0.967
ES	0.200	0.338
EO	0.383	0.532
RA	0.627	0.024

gravity along a specified Infinity shape curve. Results showed that MyotonPro device has good interrater reliability in measuring.

However, we have faced several difficulties in this experiment. The biggest problem is the representation of the results supplied software for this device, which are exported to tables or austere charts and are not entirely suitable for the work of physiotherapists. For this reason, the following experiment was designed, which aims, among other things, to design a graphical user interface tailored to the needs of physiotherapists.

5.4 Investigation of Muscle Imbalance

5.4.1 Experiment Introduction

Sedentary occupation and lack of exercise lead to the gradual muscle wasting and its shortening of the whole body and the development of muscle imbalance. This imbalance and closely related poor posture lead to back pain. At the beginning of greatest number of problems is the weakening of the deepest layers of muscles that fix the spine and allow us to upright standing (the so-called deep muscle system (DMS)). Insufficient functioning of the DMS leads to excessive strain on the joints and segments of the spine. The function of deep spine stabilizers is partially taken over by the superficial muscles and muscle imbalance occurs [122].

There are more and more professions characterized by sitting. Muscle imbalance involves a weakening of muscles, shortening of muscles and impaired spine statics and dynamics in a long-term sitting position. Sooner or later, unpleasant complications in the locomotor system will occur. This can be a muscle block, a neck or chest pain, a headache or a shoulder pain. There is a typical increased muscle tension in the neck, back and neck area. Muscle stiffness of the lumbar and sacral spine may be manifested as hip or knee pain. There is also a shortening of the calf muscles and thus less resistance of the Achilles tendon [123].

Prevention of muscle imbalance should be aimed at eliminating their causes, ie. stretching the shortened and strengthening weakened muscles (so-called compensatory exercise).

In this experiment, we focused on examining muscle myotonometric parameters before and after a physiotherapeutic exercise aimed at strengthening and stretching the deep muscular system by MyotonPro device. A graphical user interface (GUI) was designed for this purpose.

5.4.2 Materials and Methods

5.4.2.1 Measures

Eight females (age: 56.9±8.4 years) volunteered to participate in this study.

The experiment settings and used methods were the same as in the previous study 5.3. Upper trapezius (TU), middle trapezius (TM), erector spinea (ES), rectus abdominis (RA), pectoral major (PM) and gluteus maximus (GM) were selected after consultation with a physiotherapist. All muscles were measured before and after an exercise lasting an hour and a half in an upright posture. The symmetry index was calculated by the formula 5.1.

5.4.2.2 Graphical User Interface

Because Myoton software does not allow graphical display of results, a graphical user interface was designed using Matlab2019a. After starting the application, the user selects

which patient and which parameter wants to display using the Validate button. After that the measured muscles were figured (example for two patients is shown in Fig. 5.6).

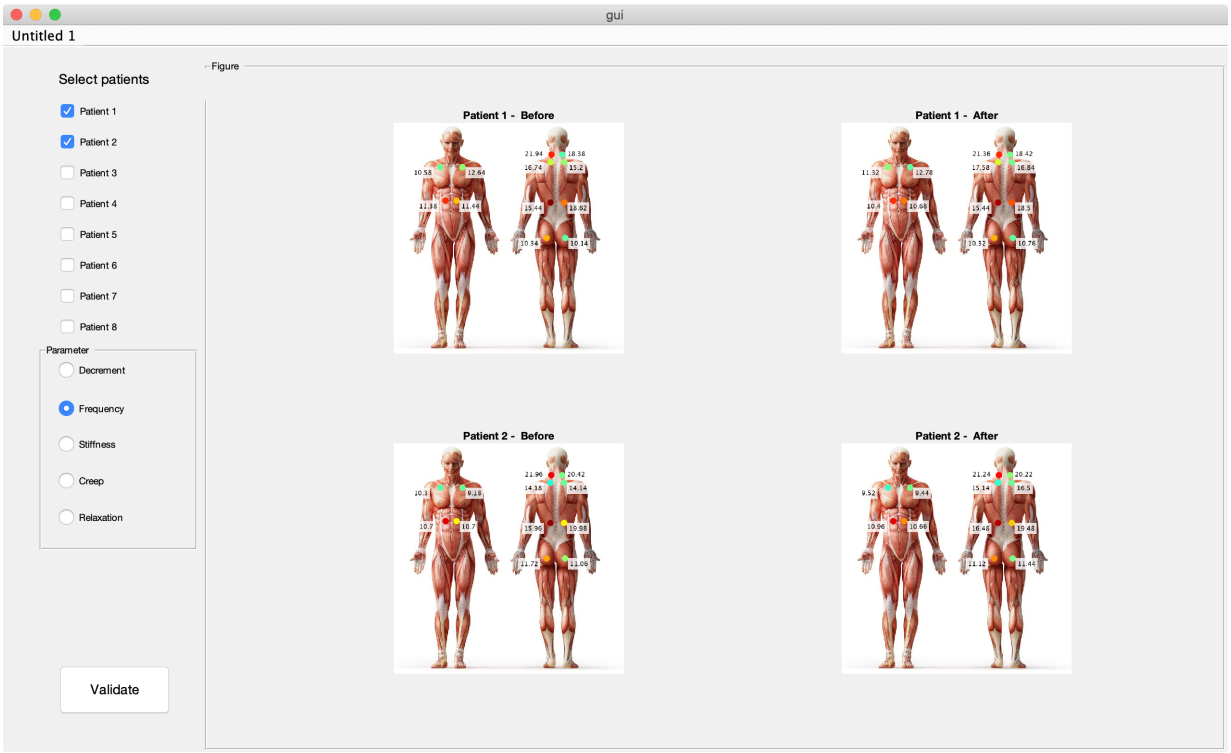

Figure 5.6: Graphical user interface. User can choose which patient and which parameters want to display in the left side. Measured muscles were displayed after pressing the Validate button.

The results of each parameter are displayed in a simple table along with a graph of pre- and post-treatment values and a symmetry index calculation (shown in Fig. 5.7).

5.4.3 Experiment Results

Symmetry index was calculated for all five parameter. The negative values indicate left-sided symmetry. It means, that the value of calculated parameter is higher on the left side. The results of symmetry index for parameter Decrement and Oscillation Frequency are shown in the Tab. 5.6 and the Tab. 5.7 respectively. Graphical interpretations of symmetry index for parameter Oscilation Frequency is shown in the Fig. 5.8.

The overall results for the symmetry index are summarized in the Table 5.8.

5.4.4 Discussion and Conclusion

Overall, symmetry improved in 119 cases out of 240. In 55 cases the right-left symmetry changed to left-right or vice versa. Evaluating the effectiveness of collective physiotherapy

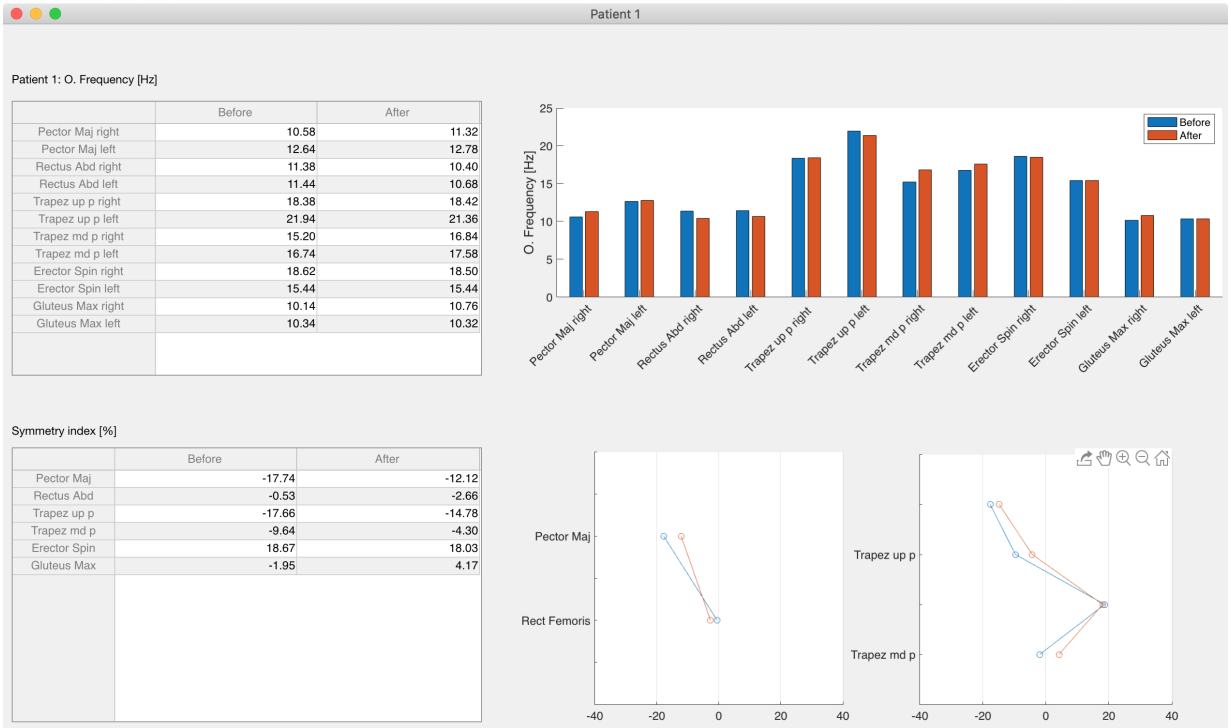

Figure 5.7: Results for patient P1 with graphical interpretation for parameter Oscillation Frequency.

exercise is quite complicated. The group is inhomogeneous. Each proband does a different job. Some probands have other sports activities. Some go to this physiotherapy exercise only. However, they all have a common factor - sedentary occupation, suggesting the similar nature of musculoskeletal problems caused by muscle wasting and the development of poor posture leading to back pain. This study was designed as a feasibility study performed with the aim to answer the question whether this type of measurement can show objectively effect of special rehabilitation exercises focused on deep muscle system that is difficult to measure in general. The main conclusion is that the values of symmetry and other parameters indicate improvement in a very transparent way. Our future research is aimed at longitudinal measurement of the volunteers' group. For better and easier understanding of the results, a graphical user interface has been designed. The physiotherapist can choose an individual proband and compare the results before and after exercise. Based on the results of symmetry index in the next exercise he/she can focus on individual muscle parts where the symmetry was not achieved. This enables better efficiency of physiotherapy exercises.

5.5 Conclusion

This chapter has discussed investigation of biomechanical muscle parameters using Myoton-Pro device. The first part was focused on finding differences of muscle parameters in the

Table 5.6: Symmetry index [%] for parameter Decrement for patients P1-P8 before and after treatment. The negative values indicate left-sided symmetry and the positive values indicate right-sided symmetry.

	Muscle	P1	P2	P3	P4	P5	P6	P7	P8
Before	PM	6.15	-16.17	-18.18	-10.03	0.82	-2.33	1.84	21.51
	RA	-1.77	-10.00	14.50	10.74	-5.94	12.26	0.39	-8.67
	TU	1.55	8.00	11.82	-3.04	0.00	11.25	-18.79	24.36
	TM	-11.17	-10.10	4.43	-6.75	-26.87	-1.91	19.23	20.25
	ES	11.68	16.42	-3.93	8.99	-33.40	-17.19	24.15	20.31
	GM	25.26	9.73	-4.96	16.97	-4.65	-10.21	-37.37	0.70
After	PM	-8.71	-2.91	-25.35	0.45	14.26	-1.29	-5.31	10.09
	RA	-7.19	-5.85	4.37	4.67	-10.46	-9.21	-15.11	-7.09
	TU	-6.13	5.66	14.91	8.79	-0.76	-0.95	-10.04	9.31
	TM	-16.49	-11.13	12.62	-2.43	19.50	-8.52	0.93	17.90
	ES	18.17	14.86	-7.61	10.49	-30.24	2.57	0.47	16.67
	GM	-10.69	8.20	-27.36	19.84	4.18	7.38	-17.12	-3.96

group of active sportsmen and inactive individuals. The measurement was performed during physical exercise (demonstrated by squats). The entire measurement process was divided into three parts: measurement before exercise, measurement during squats sets and during relaxation phase. Although some differences were statistically significant in this experiment, MyotonPro is not an entirely suitable tool for continuous measurement. Representing the results is not easy to grasp. For this reason, a second experiment was created in which we focused on the evaluation of muscle parameters before and after the rehabilitation process using the INFINITY® method. The symmetry parameter was used for the analysis, which is always calculated from the left and right muscle parameters. The physiotherapists reported this parameter as crucial. Based on the physiotherapists' requirements, a third experiment was created, which is focused primarily on the symmetry index. A beta version of the graphical user interface was created as a by-product of this study.

Table 5.7: Symmetry index [%] for parameter Oscillation Frequency for patients P1-P8 before and after treatment.The negative values indicate left-sided symmetry and the positive values indicate right-sided symmetry.

	Muscle	P1	P2	P3	P4	P5	P6	P7	P8
Before	PM	-17.74	11.50	-6.85	0.84	-1.43	12.92	-2.09	2.82
	RA	-0.53	0.00	-2.08	-2.77	-3.47	1.42	-2.59	-2.56
	TU	-17.66	-7.27	-10.18	-10.96	11.90	-6.58	3.93	-12.73
	TM	-9.64	-0.28	9.31	7.07	15.17	4.66	8.67	-3.17
	ES	18.67	22.37	-8.82	11.13	16.83	12.35	3.92	0.63
	GM	-1.95	-5.79	4.58	-4.67	1.22	9.05	-7.80	6.28
After	PM	-12.12	0.84	18.66	-6.12	-4.51	4.59	-5.22	15.69
	RA	-2.66	2.78	0.73	-4.25	-5.55	-0.85	-2.87	-6.80
	TU	-14.78	-4.92	-11.94	-12.36	6.65	0.86	19.86	-14.75
	TM	-4.30	8.60	14.39	0.82	8.42	13.18	8.26	14.07
	ES	18.03	16.69	-4.94	13.35	25.32	15.32	9.43	-2.38
	GM	4.17	2.84	-1.35	1.09	2.44	7.22	-7.61	0.00

Table 5.8: Summary results for the symmetry index expressed as the number of patients who improved symmetry and a change from left-right to right-left or vice versa for parameter oscillation frequency (F), mechanical stress relaxation time (R), logarithmic decrement (D), dynamic stiffness (S), creep (C).

	Improvement					Change				
Muscle	F	R	D	S	C	F	R	D	S	C
PM	3	4	4	4	4	2	1	3	1	1
RA	2	3	5	5	3	2	3	2	5	2
TU	4	5	4	5	5	1	0	4	0	0
TM	4	4	4	4	4	2	1	1	1	2
ES	3	2	5	4	3	1	0	1	0	0
GM	6	3	5	4	4	4	6	4	1	4

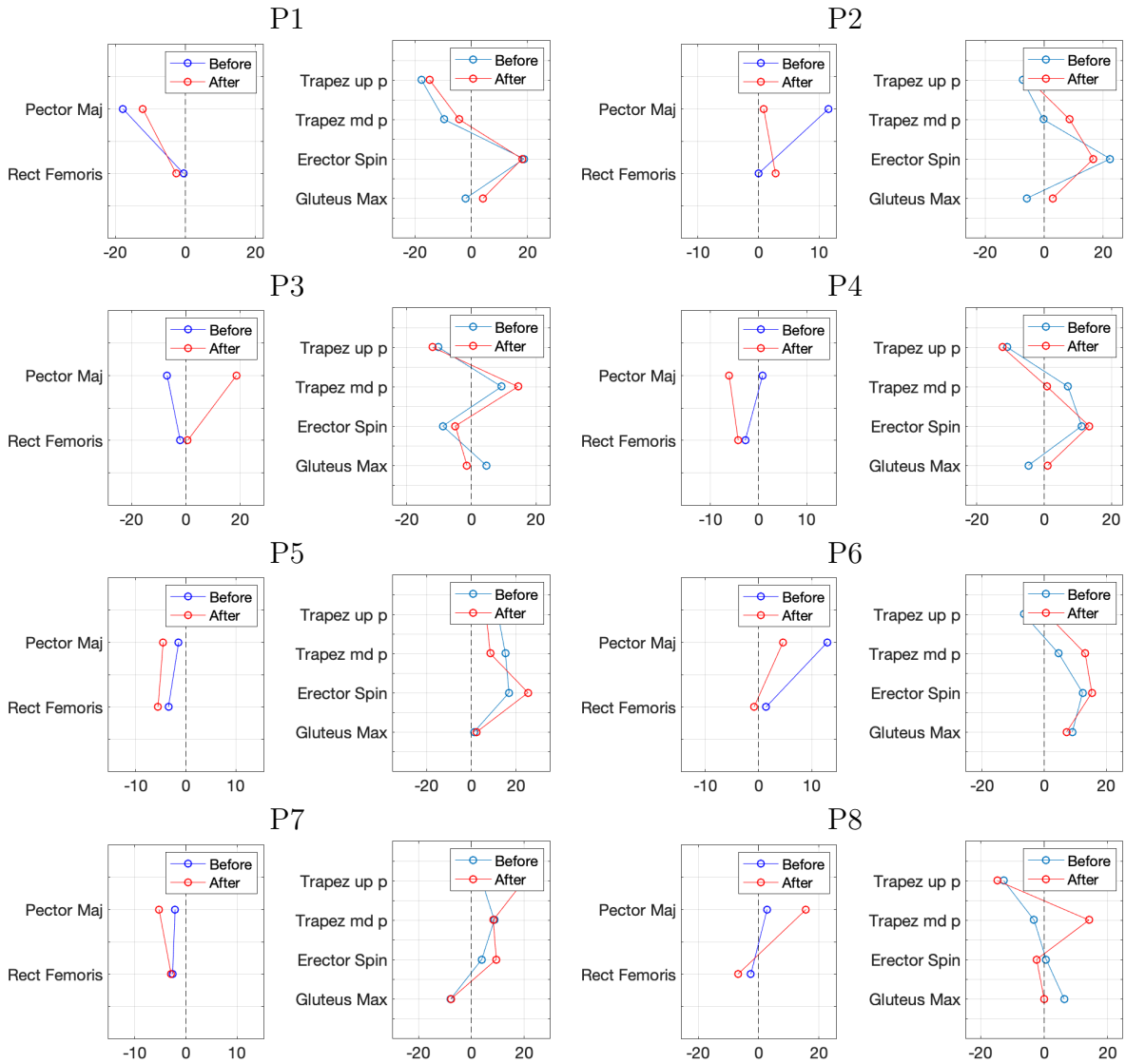

Figure 5.8: Graphical interpretations of symmetry index [%] for parameter Oscillation Frequency for patients P1-P8 before (blue line) and after (red line) treatment. The negative values indicate left-sided symmetry and the positive values indicate right-sided symmetry.

Chapter 6

Summary and Perspective

This thesis deals with complex evaluation of muscle parameters. We did not focus only on the analysis of SEMG signals, but we also expanded the work with myotonometric measurement, which deepens the knowledge of the overall state of muscle. While SEMG measurements are more suitable for continuous measurements in a laboratory environment, myotonometrics provide us with knowledge of muscle stiffness at a particular time. Thanks to its handy use, MyotonPro device can be used, for example, directly on the sport grounds to adjust the athlete's weight to minimize injury from excessive training.

Based on cooperation with physiotherapists, doctors and coaches, three main topics of this thesis were proposed. Using recent advances in SEMG signal analysis, detection of muscle contraction and other fields we have designed reliable methods and applications that will help research and diagnostics both in the laboratory and can serve trainers and athletes directly in the sport field. To achieve the objectives of this work we used both expertise and practical experience. In addition to the theoretical description of each experiment, we also describe implementation methods, which allows for repeated experiments.

6.1 Thesis Achievement

The main research aims set in Section 1.2 have been described in detail in Chapters 3, 4, 5 and accomplished as follows:

- Investigation of joint patterns is one of many ways to detect soft tissue pathology. Currently, the examination is performed manually and the passive and the active motion range test performed by a physiotherapist is used for identification. Our aim was to design a measurement using SEMG that would facilitate this examination. At first it was necessary to get acquainted with the whole issue of joint patterns. We know from practice that if we use pronation heel pads, the joint range in the knee joint will change. However, the question was whether changes in joint patterns would also occur when measured using SEMG. The largest extensor of the knee joint is the quadriceps femoris. Therefore, the muscles vastus medialis and vastus lateralis

were selected for the first experiment (Section 3.2). Two bipolar electrodes were localized according to the study A. Reinoldi [58]. Nineteen probands participated in our study and nineteen parameters were calculated for SEMG signal analysis. Statistically significant changes were only confirmed for two parameters where subjects were exposed to artificially triggered flexion or extension chains. The question is whether these changes will be reflected in muscle timming analysis, when twenty electrodes in bipolar connection is used (Section 3.3). Detector that combines many methods of signal analysis has been designed for muscle timming analysis. Due to the large electrode size, it is not possible to accurately locate the inertial zone and it is very difficult to detect the spread of the signal through the muscle. For this reason, we proceeded to develop our own multi-channel electrode (Section 3.4), which would be better suited to this analysis. The basic prototype is inspired by Merletti's multi-channel electrode [22]. Basic measurements to determine its functionality and usability was made with this electrode. Sub results of muscle timming by developed detector for finding muscle contraction starts anticipate sufficient potential for new clinical discoveries.

Joint patterns were examined. Based on a study of muscle contraction detection, experiments were designed and a detector was developed to detect the beginning of muscle contractions for muscle timming analysis.

- Sleep is essential for optimal human health and brain function. REM sleep was described as paradoxical sleep, when the skeletal muscles are paralyzed. REM sleep behavior disorder is accompanied by the loss of normal REM sleep atonia. Quantifying RSWA relies on expert visual scoring by a sleep neurologist or somnologist. Variety of automated RSWA scoring method have also been developed but to date have not been widely applied in the field since they typically either require expensive commercial software or expert computer programming resources [67, 68, 69, 70, 65]. In this part of the thesis we used acquired knowledge and we proceeded from the previous muscle contraction detector, which we designed before. The beta version of the graphical user interface (Section 4.2) that allows to detect the loss of normal REM sleep atonia was developed. The functionality of the detector was tested on real PSG data from 7 subjects suffering from sleep disorder. Our detector reached average precision of 64.24 ± 12.34 %, recall 91.63 ± 10.07 %, and F1 score 74.36 ± 8.47 % on validation dataset (Section 4.2.3). These results indicate that automated detector of RSWA can provide useful information to the physician and followed by expert additional overscoring and correction by visual, manual review, can be used within our framework for fast semi-automated RSWA quantification 4.3.

- The principal difference between traditional SEMG measuring of muscle parameters and myotonometry is that myotonometry can measure the tone, elasticity and stiffness simultaneously. This allows us to expand our knowledge of muscle state. Objective measurement of myotonometric parameters would greatly enhance detection of risk of injury and monitoring of the effects of interventions, such as treatment.

Therefore, we do not need to use time-consuming and expensive SEMG measurements to determine the effectiveness of treatment. However, it cannot be argued that in any situation SEMG measurements can be replaced. Three experiments were made for this purpose. The first experiment (Section 5.2)was focused on examination of muscle parameters during physical exercise (demonstrated squats). Ten active athletes and ten non-athletes participated in the study. A three-part measurement was proposed. Muscle parameters had been measured before squatting in the first phase. The second phase consisted of four consecutive series of five squats where muscle parameters were measured after each series. The measurement in the third relaxation phase was made five times at two minutes interval. MyotonPro software has a very limited evaluation of results, so we have decided to process the results by evaluating the area of each measurement phase. The results of the study show some statistically significant differences in muscle parameters in the group of athletes and non-athletes (Section 5.2.3). However, their representation is not easy to grasp and SEMG analysis would be useful for this experiment. For this reason, another experiment was created to help us deepen the knowledge of myotonometric analysis and its usefulness (Section 5.3). The study is focused on comparison of muscle parameters before and after the rehabilitation process, when the index of symmetry was used for the analysis. The major problem is that the representation of the results exported to tables or austere charts are not entirely suitable for the work of physiotherapists. For this reason, the third experiment was designed (Section 5.4). The main aim was to design a graphical user interface tailored to the needs of physiotherapists.

The biomechanical muscle parameters were studied on the basis of the three experiments. Thanks to the experience gained in practice, we have created a graphical user interface that facilitates the evaluation of measured data (Section 5.4.2.2).

6.2 Future Work

Regarding the representation of joint patterns, we would like to make progress in the analysis of muscle timing by multichannel SEMG mapping using an electrode grid. For the decomposition of the SEMG signal, the independent component analysis would be used, which could reveal the location of individual motor units and thus make it easier for us to find joint patterns and their changes when using reflective hell pads.

In future work, we would also like to concentrate on development of our graphical user interface for RSWA detection. We would like to put this interface into practice. This will require further improvements and modifications proposed methods. Our detector is based on semi-automation and is still dependent on a neurologist who detects REM sleep phases in advance. This opens up the next stages of the process. We would like to fully automate the proposed detector, which will include: automatic REM sleep phase detection, accelerating QRS complex detection, for example by removing cardiac artifacts directly from the SEMG signal using wavelet filtering along with independent component analysis. We will test detection capability in future studies that will include data analysis

from healthy subjects as well as subjects suffering from sleep disorders. We will also try to get scored data from more neurologist experts to achieve better detector accuracy.

Furthermore, we will develop a graphical user interface for the analysis of myotonometric parameters and its use in rehabilitation practice. Additional modules will be added to select the measurement and select the necessary analysis. We would also like to create a mobile application on this basis. The increasingly rapid development of technical equipment currently provides us with several aspects that we would like to use for future work. In particular, the development of wireless SEMG measurement, which would allow extending the use of this method outside the laboratory. The wireless device also provides better usability during motion, allowing continuous measurement directly during physical exercise without any movement restrictions.

Another useful sector is the so-called smart textiles. However, their development is at the beginning and so far there is no perfect solution to prevent, for example, the movement of electrodes on the tissue during movement and sweating. However, it is one of the ways to move our development forward.

Bibliography

[1] Milerská, I.; Saifutdinová, E.; Jelínek, M.; et al. Representation of Joint Patterns in HD SEMG: A Case Study. *Proceedings*, volume 31, no. 1, Nov 2019: p. 45, ISSN 2504-3900, doi:10.3390/proceedings2019031045. Available from: `http://dx.doi.org/10.3390/proceedings2019031045`

[2] Novotná, I.; Křemen, V.; Holub, M.; et al. Case Study: Functional Verification of Multichannel Surface Electrode for Joint Patterns Investigation. In *LHOTSKÁ, L., et al., eds. Proceedings of BioDat 2014 - Conference on Advanced Methods of Biological Data and Signal Processing. 3rd Conference on Advanced Methods of Biological Data and Signal Processing BioDat 2014*, Praha: Czech Technical University in Prague, 2014, ISBN 978-80-01-05624-0.

[3] Lieber, R. *Skeletal Muscle Structure, Function, and Plasticity*. Skeletal muscle structure, function and plasticity: the physiological basis of rehabilitation, Lippincott Williams & Wilkins, 2002, ISBN 9780781730617. Available from: `https://books.google.cz/books?id=T0fbq_b89cAC`

[4] Smith, D. L.; Plowman, S. A. Chapter 2 - Understanding Muscle Contraction**Based on Plowman SA, Smith DL: Exercise physiology for health, fitness, and performance, ed 2, San Francisco, 2003, Benjamin Cummings. In *Sports-Specific Rehabilitation*, edited by R. Donatelli, Saint Louis: Churchill Livingstone, 2007, ISBN 978-0-443-06642-9, pp. 15 – 38, doi:https://doi.org/10.1016/B978-044306642-9.50005-8. Available from: `http://www.sciencedirect.com/science/article/pii/B9780443066429500058`

[5] Merletti, R.; Parker, P. *Electromyography: Physiology, Engineering, and Non-Invasive Applications*. IEEE Press Series on Biomedical Engineering, Wiley, 2004, ISBN 9780471675808. Available from: `https://books.google.cz/books?id=SQthgVMil3YC`

[6] Calder, K. M.; Gabriel, D. A.; McLean, L. Differences in EMG spike shape between individuals with and without non-specific arm pain. *Journal of Neuroscience Methods*, volume 178, no. 1, 2009: pp. 148 – 156, ISSN 0165-0270, doi:https://doi.org/10.1016/j.jneumeth.2008.11.015. Available from: http://www.sciencedirect.com/science/article/pii/S0165027008006614

[7] Bailey, L.; Samuel, D.; Warner, M.; et al. Parameters representing muscle tone, elasticity and stiffness of biceps brachii in healthy older males: symmetry and within-session reliability using the MyotonPRO. *Journal of Neurological Disorders*, volume 1, no. 1, April 2013: pp. 1–7. Available from: https://eprints.soton.ac.uk/352058/

[8] Novotná, I.; Holub, M.; Křemen, V.; et al. Případová studie: Kloubní vzorce při využití povrchového EMG. In *Sborník příspěvků MEDSOFT 2014*, Praha: Creative Connections, 2014, ISBN 978-80-86742-38-0, ISSN 1803-8115, pp. 173–183. Available from: http://creativeconnections.cz/medsoft/2014/Medsoft_2014_Novotna.pdf

[9] Milerska, I.; Kremen, V.; Gerla, V.; et al. Semi-automated detection of polysomnographic REM sleep without atonia (RSWA) in REM sleep behavioral disorder. *Biomedical Signal Processing and Control*, volume 51, May 2019: pp. 243–252, ISSN 1746-8094, doi:10.1016/j.bspc.2019.02.023.

[10] Milerska, I.; Lhotská, L.; Macas, M. Biomechanical Parameters of Muscles, Objective Assessment Using MyotonPRO. *2018 IEEE International Conference on Bioinformatics and Biomedicine (BIBM)-Proceedings*, 2018: pp. 1522–1525, doi:10.1109/BIBM.2018.8621074.

[11] Daniel, M.; Tomanová, M.; Hornová, J.; et al. Biomechanical analysis of INFINITY rehabilitation method for treatment of low back pain. *Journal of physical therapy science*, volume 29, no. 5, 2017: pp. 832–838.

[12] Textbook Equity College Edition. An Open Education Resource. *Anatomy and Physiology*. sv. 1, Lulu.com, 2014, ISBN 9781304834621. Available from: https://books.google.cz/books?id=eFhkBgAAQBAJ

[13] Rizzo, D. *Fundamentals of Anatomy and Physiology*. Cengage Learning, 2015, ISBN 9781305445420. Available from: https://books.google.cz/books?id=vfeoBAAAQBAJ

[14] Slater, C. R. The Structure of Human Neuromuscular Junctions: Some Unanswered Molecular Questions. *International Journal of Molecular Sciences*, volume 18, no. 10, 2017, ISSN 1422-0067, doi:10.3390/ijms18102183. Available from: http://www.mdpi.com/1422-0067/18/10/2183

[15] Vincent, A.; Buckley, C.; Burke, G. CHAPTER 90 - NEUROMUSCULAR JUNCTION DISORDERS. In *Neurology and Clinical Neuroscience*, edited by A. H. Schapira; E. Byrne; S. DiMauro; R. S. Frackowiak; R. T. Johnson; Y. Mizuno; M. A. Samuels; S. D. Silberstein; Z. K. Wszolek, Philadelphia: Mosby, 2007, ISBN 978-0-323-03354-1, pp. 1223 – 1234, doi:https://doi.org/10.1016/B978-0-323-03354-1.50094-8. Available from: `http://www.sciencedirect.com/science/article/pii/B9780323033541500948`

[16] Clancy, E. A.; Morin, E. L.; Merletti, R. Sampling, noise-reduction and amplitude estimation issues in surface electromyography. *Journal of electromyography and kinesiology : official journal of the International Society of Electrophysiological Kinesiology*, volume 12, no. 1, 2002: pp. 1–16, doi:10.1016/S1050-6411(01)00033-5.

[17] Penhaker, M.; Imramovský, M.; Tiefenbach, P.; et al. *Lékařské diagnostické přístroje*. Ostrava: VŠB - Technická univerzita Ostrava, 2004, ISBN 80-248-0751-3 (brož.), 320 pp.

[18] Stegeman, D.; Hermens, H. Standards for suface electromyography: The European project Surface EMG for non-invasive assessment of muscles (SENIAM). volume 1, 01 2007.

[19] Hermens, H. J.; Freriks, B.; Disselhorst-Klug, C.; et al. Development of recommendations for SEMG sensors and sensor placement procedures. *Journal of Electromyography and Kinesiology*, volume 10, no. 5, 2000: pp. 361 – 374, ISSN 1050-6411, doi:https://doi.org/10.1016/S1050-6411(00)00027-4. Available from: `http://www.sciencedirect.com/science/article/pii/S1050641100000274`

[20] Mesin, L.; Merletti, R.; Rainoldi, A. Surface EMG: the issue of electrode location. *Journal of Electromyography and Kinesiology*, volume 19, no. 5, 2009: pp. 719–726.

[21] Rainoldi, A.; Nazzaro, M.; Merletti, R.; et al. Geometrical factors in surface EMG of the vastus medialis and lateralis muscles. *Journal of Electromyography and Kinesiology*, volume 10, no. 5, 2000: pp. 327–336.

[22] Merletti, R.; Bottin, A.; Cescon, C.; et al. Multichannel surface EMG for the non-invasive assessment of the anal sphincter muscle. *Digestion*, volume 69, no. 2, 2004: pp. 112–122.

[23] Zwarts, M. J.; Stegeman, D. F. Multichannel surface EMG: basic aspects and clinical utility. *Muscle & Nerve: Official Journal of the American Association of Electrodiagnostic Medicine*, volume 28, no. 1, 2003: pp. 1–17.

[24] Merletti, R.; Farina, D.; Gazzoni, M. The linear electrode array: a useful tool with many applications. *Journal of Electromyography and Kinesiology*, volume 13, no. 1, 2003: pp. 37 – 47, ISSN 1050-6411, doi:https://doi.org/10.1016/S1050-6411(02)00082-2. Available from: `http://www.sciencedirect.com/science/article/pii/S1050641102000822`

[25] Merletti, R.; Muceli, S. Tutorial. Surface EMG detection in space and time: Best practices. *Journal of Electromyography and Kinesiology*, volume 49, 2019: p. 102363, ISSN 1050-6411, doi:https://doi.org/10.1016/j.jelekin.2019.102363. Available from: `http://www.sciencedirect.com/science/article/pii/S1050641119302536`

[26] Robbins, D. An Introduction to EMG Signal Processing Using MatLab and Microsoft Excel. In *Applications, Challenges, and Advancements in Electromyography Signal Processing*, IGI Global, 2014, pp. 95–112.

[27] Navarro, X.; Krueger, T. B.; Lago, N.; et al. A critical review of interfaces with the peripheral nervous system for the control of neuroprostheses and hybrid bionic systems. *Journal of the Peripheral Nervous System*, volume 10, no. 3, 2005: pp. 229–258.

[28] Chowdhury, R.; Reaz, M.; Ali, M.; et al. Surface electromyography signal processing and classification techniques. *Sensors*, volume 13, no. 9, 2013: pp. 12431–12466.

[29] Kappenman, E. S.; Luck, S. J. The effects of electrode impedance on data quality and statistical significance in ERP recordings. *Psychophysiology*, volume 47, no. 5, 2010: pp. 888–904.

[30] Reaz, M. B. I.; Hussain, M.; Mohd-Yasin, F. Techniques of EMG signal analysis: detection, processing, classification and applications. *Biological procedures online*, volume 8, no. 1, 2006: p. 11.

[31] Willigenburg, N. W.; Daffertshofer, A.; Kingma, I.; et al. Removing ECG contamination from EMG recordings: A comparison of ICA-based and other filtering procedures. *Journal of electromyography and kinesiology*, volume 22, no. 3, 2012: pp. 485–493.

[32] Prutchi, D.; Norris, M. *Design and development of medical electronic instrumentation: a practical perspective of the design, construction, and test of medical devices*. John Wiley & Sons, 2005.

[33] Piskorowski, J. Powerline interference rejection from sEMG signal using notch filter with transient suppression. In *2012 IEEE International Instrumentation and Measurement Technology Conference Proceedings*, IEEE, 2012, pp. 1447–1451.

[34] Gabriel, D. A.; Basford, J. R.; An, K.-N. Assessing fatigue with electromyographic spike parameters. *IEEE engineering in medicine and biology magazine*, volume 20, no. 6, 2001: pp. 90–96.

[35] González-Izal, M.; Malanda, A.; Gorostiaga, E.; et al. Electromyographic models to assess muscle fatigue. *Journal of Electromyography and Kinesiology*, volume 22, no. 4, 2012: pp. 501 – 512, ISSN 1050-6411, doi:https://doi.org/10.1016/j.jelekin.2012.02.019. Available from: `http://www.sciencedirect.com/science/article/pii/S1050641112000508`

[36] Zhang, Y.; Li, P.; Zhu, X.; et al. Extracting time-frequency feature of single-channel vastus medialis EMG signals for knee exercise pattern recognition. *PloS one*, volume 12, no. 7, 2017: p. e0180526.

[37] Kilby, J.; Prasad, K. Analysis of Surface Electromyography Signals Using Discrete Fourier Transform Sliding Window Technique. *International Journal of Computer Theory and Engineering*, 01 2013: pp. 321–325, doi:10.7763/IJCTE.2013.V5.702.

[38] Vogel, F.; Holm, S.; Lingjærde, O. C. Spectral moments and time domain representation of photoacoustic signals used for detection of crude oil in produced water. In *Proc. Nordic Symp. on Physical Acoustics, Ustaoset, Norway*, 2001.

[39] Phinyomark, A.; Limsakul, C.; Phukpattaranont, P. Application of wavelet analysis in EMG feature extraction for pattern classification. *Measurement Science Review*, volume 11, no. 2, 2011: pp. 45–52.

[40] Hussain, M.; Mamun, M. Effectiveness of the Wavelet Transform on the Surface EMG to Understand the Muscle Fatigue During Walk. *Measurement Science Review*, volume 12, no. 1, 2012: pp. 28 – 33. Available from: `https://content.sciendo.com/view/journals/msr/12/1/article-p28.xml`

[41] Unser, M.; Aldroubi, A. A review of wavelets in biomedical applications. *Proceedings of the IEEE*, volume 84, no. 4, 1996: pp. 626–638.

[42] Jobert, M.; Tismer, C.; Poiseau, E.; et al. Wavelets—a new tool in sleep biosignal analysis. *Journal of Sleep Research*, volume 3, no. 4, 1994: pp. 223–232, doi:10.1111/j.1365-2869.1994.tb00135.x, `https://onlinelibrary.wiley.com/doi/pdf/10.1111/j.1365-2869.1994.tb00135.x`. Available from: `https://onlinelibrary.wiley.com/doi/abs/10.1111/j.1365-2869.1994.tb00135.x`

[43] Kumar, D. K.; Pah, N. D.; Bradley, A. Wavelet analysis of surface electromyography. *IEEE Transactions on neural systems and rehabilitation engineering*, volume 11, no. 4, 2003: pp. 400–406.

[44] Vain, A. The Phenomenon of Mechanical Stress Transmission in Skeletal Muscles. *Acta Academiae Olympiquae Estoniae*, volume Vol. 14, 01 2006: pp. 38–48.

[45] Wright, D. *Human Physiology and Health*. Human Physiology and Health Series, Pearson Education, 2000, ISBN 9780435633042. Available from: `https://books.google.cz/books?id=b7cLhsrd3KAC`

[46] Mullix, J.; Warner, M.; Stokes, M. Testing muscle tone and mechanical properties of rectus femoris and biceps femoris using a novel hand held MyotonPRO device: relative ratios and reliability. *Working Papers in Health Sciences*, volume 1, no. 1, 2012: pp. 1–8.

[47] Davidson, M. J.; Bryant, A. L.; Bower, W. F.; et al. Myotonometry Reliably Measures Muscle Stiffness in the Thenar and Perineal Muscles. *Physiotherapy Canada*, volume 69, no. 2, 2017: pp. 104–112, doi:10.3138/ptc.2015-85, https://doi.org/10.3138/ptc.2015-85. Available from: https://doi.org/10.3138/ptc.2015-85

[48] Aird, L.; Samuel, D.; Stokes, M. Quadriceps muscle tone, elasticity and stiffness in older males: Reliability and symmetry using the MyotonPRO. *Archives of Gerontology and Geriatrics*, volume 55, no. 2, 2012: pp. e31 – e39, ISSN 0167-4943, doi:https://doi.org/10.1016/j.archger.2012.03.005. Available from: http://www.sciencedirect.com/science/article/pii/S0167494312000520

[49] Ditroilo, M.; Hunter, A. M.; Haslam, S.; et al. The effectiveness of two novel techniques in establishing the mechanical and contractile responses of biceps femoris. *Physiological Measurement*, volume 32, no. 8, jul 2011: pp. 1315–1326, doi:10.1088/0967-3334/32/8/020. Available from: https://doi.org/10.1088%2F0967-3334%2F32%2F8%2F020

[50] Schneider, S.; Peipsi, A.; Stokes, M.; et al. Feasibility of monitoring muscle health in microgravity environments using Myoton technology. *Medical & Biological Engineering & Computing*, volume 53, no. 1, Jan 2015: pp. 57–66, ISSN 1741-0444, doi:10.1007/s11517-014-1211-5. Available from: https://doi.org/10.1007/s11517-014-1211-5

[51] Tichý, M.; Jelínek, M.; Macková, E. Funkční blokáda kloubu a její příznaky. *Kontakt, 2010a, roč*, volume 12, 2010: pp. 472–479.

[52] Véle, F. *Kineziologie: přehled klinické kineziologie a patokineziologie pro diagnostiku a terapii poruch pohybové soustavy.* Triton, 2006.

[53] Lewit, K. *Manipulační léčba v myoskeletální medicíně.* Sdělovací technika, spol. s.r.o. ve spolupráci s Česká lékařská společnost J.E. Purkyně, 2015, ISBN 9788086645049. Available from: https://books.google.cz/books?id=7AMqCgAAQBAJ

[54] Rychlíková, E. Manuální medicína: průvodce diagnostikou a léčbou vertebrogenních poruch, 3. rozš. vyd., Praha: Maxdorf, 2004, 530 s. Technical report, ISBN 80–7345–010–0, 2004.

[55] Novotná, I.; Křemen, V.; Čeřovský, Z.; et al. 53. Representation of joint patterns in surface EMG. In *Clinical Neurophysiology*, volume 125, 2014, ISSN 13882457, doi:10.1016/j.clinph.2013.12.091. Available from: https://linkinghub.elsevier.com/retrieve/pii/S1388245713013278

[56] Novotná, I.; Křemen, V.; Čeřovský, Z.; et al. Surface EMG Signal Processing for Evaluation of Isometric Voluntary Extension of the Knee Joint. In *LHOTSKÁ, L. et al., eds. BioDat 2013 - Conference on Advanced Methods of Biological Data and Signal Processing. Conference on Advanced Methods of Biological Data and Signal Processing*, Praha: Czech Technical University, 2013, ISBN 978-80-01-05410-9.

[57] Öztürk, N.; Begovic, H.; Demir, P.; et al. Rectus Femoris and Vastus Medialis Muscles Exhibit Different Dynamics in Processing of Isometric Voluntary Contractions: A Fractal Analysis Study. 06 2019, pp. 1–6, doi:10.1109/MeMeA.2019.8802161.

[58] Rainoldi, A.; Melchiorri, G.; Caruso, I. A method for positioning electrodes during surface EMG recordings in lower limb muscles. *Journal of neuroscience methods*, volume 134, no. 1, 2004: pp. 37–43.

[59] Zwarts, M. J.; Stegeman, D. F. Multichannel surface EMG: Basic aspects and clinical utility. *Muscle & Nerve*, volume 28, no. 1, 2003: pp. 1–17, doi:10.1002/mus.10358, `https://onlinelibrary.wiley.com/doi/pdf/10.1002/mus.10358`. Available from: `https://onlinelibrary.wiley.com/doi/abs/10.1002/mus.10358`

[60] Zhou, S. H.; Helfenbein, E. D.; Lindauer, J. M.; et al. Philips QT interval measurement algorithms for diagnostic, ambulatory, and patient monitoring ECG applications. *Annals of Noninvasive Electrocardiology*, volume 14, 2009: pp. S3–S8.

[61] Kushida, C. A.; Littner, M. R.; Morgenthaler, T.; et al. Practice Parameters for the Indications for Polysomnography and Related Procedures: An Update for 2005. *Sleep*, volume 28, no. 4, 2005: pp. 499–523, doi:10.1093/sleep/28.4.499, `/oup/backfile/content_public/journal/sleep/28/4/10.1093_sleep_28.4.499/1/sleep-28-4-499.pdf`. Available from: `http://dx.doi.org/10.1093/sleep/28.4.499`

[62] Collop, N.; Anderson, W.; Boehlecke, B.; et al. Clinical Guidelines for the Use of Unattended Portable Monitors in the Diagnosis of Obstructive Sleep Apnea in Adult Patients Portable Monitoring Task Force of the American Academy of Sleep Medicine. *Journal of clinical sleep medicine : JCSM : official publication of the American Academy of Sleep Medicine*, volume 3, 01 2008: pp. 737–47.

[63] American Academy of Sleep Medicine. *International Classification of Sleep Disorders*. American Academy of Sleep Medicine, 2014, ISBN 9780991543410. Available from: `https://books.google.cz/books?id=aXb7oAEACAAJ`

[64] Odile, L.; Jacques, M. Polysomnographic features of REM sleep behavior disorder: Development of a scoring method. *Neurology*, volume 42, no. 7, 1992: p. 1371, doi:10.1212/WNL.42.7.1371, `http://www.neurology.org/content/42/7/1371.full.pdf+html`. Available from: `http://www.neurology.org/content/42/7/1371.abstract`

[65] Iranzo, A.; Frauscher, B.; Santos, H.; et al. Usefulness of the SINBAR electromyographic montage to detect the motor and vocal manifestations occurring in REM sleep behavior disorder. *Sleep Medicine*, volume 12, no. 3, 2011: pp. 284 – 288, ISSN 1389-9457, doi:https://doi.org/10.1016/j.sleep.2010.04.021. Available from: `http://www.sciencedirect.com/science/article/pii/S1389945710003813`

[66] Louis, E. K. S.; Boeve, B. F. REM Sleep Behavior Disorder: Diagnosis. Clinical Implications. and Future Directions. *Mayo Clinic Proceedings*, volume 92, no. 11, 2017: pp. 1723 – 1736, ISSN 0025-6196, doi:https://doi.org/10.1016/j.mayocp.2017.09.007. Available from: `http://www.sciencedirect.com/science/article/pii/S0025619617306882`

[67] Mayer, G.; Kesper, K.; Ploch, T.; et al. Quantification of tonic and phasic muscle activity in REM sleep behavior disorder. *Journal of clinical neurophysiology : official publication of the American Electroencephalographic Society*, volume 25 1, 2008: pp. 48–55, doi:10.1097/WNP.0b013e318162acd7.

[68] Ferri, R.; Fantini, M. L.; Schenck, C. H. The role of REM sleep without atonia in the diagnosis of REM sleep behavior disorder: past errors and new challenges. *Sleep Medicine*, volume 15, no. 9, 2014: pp. 1007 – 1008, ISSN 1389-9457, doi:https://doi.org/10.1016/j.sleep.2014.05.006. Available from: `http://www.sciencedirect.com/science/article/pii/S1389945714002056`

[69] Bliwise, D. L.; He, L.; Ansari, F. P.; et al. Quantification of Electromyographic Activity During Sleep: A Phasic Electromyographic Metric. *Journal of Clinical Neurophysiology*, volume 23, no. 1, 2006: pp. 59–67, ISSN 0736-0258, doi:10.1097/01.wnp.0000192303.14946.fc.

[70] Burns, J.; Consens, F.; Little, R.; et al. EMG Variance During Polysomnography As An Assessment For REM Sleep Behavior Disorder. *Sleep*, volume 30, 2007: pp. 1771–1778, ISSN 0161-8105.

[71] Stieany, K.; Oertel, W.; Trenkwalder, C. Clinical symptomatology and treatment of restless legs syndrome and periodic limb movement disorder. *Sleep Medicine Reviews*, volume 6, no. 4, 2002: pp. 253–265, doi:10.1053/smrv.2001.0193.

[72] Luca, C. D. The use of surface electromyography in biomechanics. *Journal of Applied Biomechanics*, volume 13, no. 2, 1997: pp. 135–163. Available from: `https://web.njit.edu/~sengupta/IE665/EMG%20and%20biomechanics.pdf`

[73] Hodges, P.; Richardson, C. Inefficient Muscular Stabilization of the Lumbar Spine Associated With Low Back Pain. *Spine*, volume 21, no. 22, 1996: pp. 2640–2650, doi:10.1097/00007632-199611150-00014.

[74] Allison, G. Trunk muscle onset detection technique for EMG signals with ECG artefact. *Journal of Electromyography and Kinesiology*, volume 13, no. 3, 2003: p. 209–216, doi:10.1016/S1050-6411(03)00019-1.

[75] Studenski, S.; Duncan, P.; Chandler, J. Postural Responses and Effector Factors in Persons with Unexplained Falls: Results and Methodologic Issues. *Journal of the American Geriatrics Society*, volume 39, no. 3, 1991: pp. 229–234, doi:10.1111/j.1532-5415.1991.tb01642.x.

[76] Meigal, A.; Rissanen, S.; Tarvainen, M.; et al. Novel parameters of surface EMG in patients with Parkinson's disease and healthy young and old controls. *Journal of Electromyography and Kinesiology*, volume 19, no. 3, 2009: p. e206–e213, doi: 10.1016/j.jelekin.2008.02.008.

[77] Reaz, M. B. I.; Hussain, M. S.; Mohd-Yasin, F. Techniques of EMG signal analysis: detection. processing. classification and applications. *Biological Procedures Online*, volume 8, no. 1, 2006: p. 11–35, doi:10.1251/bpo115.

[78] Barzilay, O.; Wolf, A. A fast implementation for {EMG} signal linear envelope computation. *Journal of Electromyography and Kinesiology*, volume 21, no. 4, 2011: pp. 678 – 682, ISSN 1050-6411, doi:http://dx.doi.org/10.1016/j.jelekin.2011.04.004. Available from: `http://www.sciencedirect.com/science/article/pii/S1050641111000587`

[79] Pijnappels, M.; Bobbert, M. F.; van Dieën, J. H. EMG modulation in anticipation of a possible trip during walking in young and older adults. *Journal of Electromyography and Kinesiology*, volume 16, no. 2, 2006: p. 137–143, doi: 10.1016/j.jelekin.2005.06.011.

[80] Staudenmann, D.; Idsart Kingma; Daffertshofer, A.; et al. Improving EMG-based muscle force estimation by using a high-density EMG grid and principal component analysis. *IEEE Engineering in Medicine and Biology Society*, volume 53, no. 4, 2006: pp. 712 – 719, doi:10.1109/TBME.2006.870246.

[81] Chowdhury, R.; Reaz, M.; Ali, M.; et al. Surface Electromyography Signal Processing and Classification Techniques. *Sensors*, volume 13, no. 9, 2013: pp. 12431–12466, doi: 10.3390/s130912431.

[82] Willigenburg, N.; Daffertshofer, A.; Kingma, I.; et al. Removing ECG contamination from EMG recordings: A comparison of ICA-based and other filtering procedures. *Journal of Electromyography and Kinesiology*, volume 22, no. 3, 2012: p. 485–493, doi:10.1016/j.jelekin.2012.01.001.

[83] Sobahi, M. Denoising of EMG Signals Based on Wavelet Transform. *Asian Transactions on Engineering*, volume 1, no. 5, 2011: pp. 17–23. Available from: `http://citeseerx.ist.psu.edu/viewdoc/download?doi=10.1.1.675.8997&rep=rep1&type=pdf`

[84] Phinyomark, A.; Limsakui, C.; Phukpattaranont, P. EMG denoising estimation based on adaptive wavelet thresholding for multifunction myoelectric control. *Innovative Technologies in Intelligent Systems and Industrial Applications*, 2009: pp. 171 – 176, doi:10.1109/CITISIA.2009.5224220.

[85] McCarter, S. J.; St.Louis, E. K.; J.Duwell, E.; et al. Diagnostic Thresholds for Quantitative REM Sleep Phasic Burst Duration. Phasic and Tonic Muscle

Activity. and REM Atonia Index in REM Sleep Behavior Disorder with and without Comorbid Obstructive Sleep Apnea. *Sleep*, volume 37, no. 10, 2014: pp. 1649–1662, doi:10.5665/sleep.4074, /oup/backfile/content_public/journal/sleep/37/10/10.5665_sleep.4074/1/aasm.37.10.1649.pdf. Available from: +http://dx.doi.org/10.5665/sleep.4074

[86] McCarter, S. J.; St.Louis, E. K.; Sandness, D. J.; et al. Diagnostic REM sleep muscle activity thresholds in patients with idiopathic REM sleep behavior disorder with and without obstructive sleep apnea. *Sleep Medicine*, volume 33, no. Supplement C, 2017: pp. 23 – 29, ISSN 1389-9457, doi:https://doi.org/10.1016/j.sleep.2016.03.013. Available from: http://www.sciencedirect.com/science/article/pii/S1389945716300132

[87] Frauscher, B.; Ehrmann, L.; Zamarian, L.; et al. Validation of the Innsbruck REM sleep behavior disorder inventory. *Movement Disorders*, volume 27, no. 13, 2012: pp. 1673–1678, doi:10.1002/mds.25223, https://onlinelibrary.wiley.com/doi/pdf/10.1002/mds.25223. Available from: https://onlinelibrary.wiley.com/doi/abs/10.1002/mds.25223

[88] Frauscher, B.; Iranzo, A.; Gaig, C.; et al. Normative EMG Values during REM Sleep for the Diagnosis of REM Sleep Behavior Disorder. *Sleep*, volume 35, no. 6, 2012: pp. 835–847, doi:10.5665/sleep.1886, /oup/backfile/content_public/journal/sleep/35/6/10.5665_sleep.1886/1/aasm.35.6.835.pdf. Available from: http://dx.doi.org/10.5665/sleep.1886

[89] Iber, C.; Ancoli-Israel, S.; Chesson, A.; et al. Westchester. IL: American Academy of Sleep Medicine; 2007. *The AASM manual for the scoring of sleep and associated events: rules. terminology and technical specifications*, 2007: pp. 48–49.

[90] Jacques, M.; Jean-Francois, G.; Livia, F. M.; et al. Polysomnographic diagnosis of idiopathic REM sleep behavior disorder. *Movement Disorders*, volume 25, no. 13, 2010: pp. 2044–2051, ISSN 1531-8257, doi:10.1002/mds.23257. Available from: http://dx.doi.org/10.1002/mds.23257

[91] Stegeman, D.; Hermens, H. Electromyography: the European project "Surface EMG for non-invasive assessment of muscles (SENIAM)". Januar 2007. Available from: http://www.med.uni-jena.de/motorik/pdf/stegeman.pdf

[92] Elgendi, M.; Jonkman, M.; De Boer, F. Frequency bands effects on QRS detection. In *BIOSIGNALS 2010 - Proceedings of the 3rd International Conference on Bio-inpsired Systems and Signal Processing*, volume 1, edited by V. Mahadevan; J. Zhou, Institute for Systems and Technologies of Information, Control and Communication (INSTICC), 2010, ISBN 978-989-674-018-4, pp. 428–431, 3rd International Conference on Bio-inspired Systems and Signal Processing, BIOSIGNALS 2010 ; Conference date: 20-01-2010 Through 23-01-2010.

[93] Moraes, J. C. T. B.; Freitas, M. M.; Vilani, F. N.; et al. A QRS complex detection algorithm using electrocardiogram leads. In *Computers in Cardiology*, Sep. 2002, ISSN 0276-6547, pp. 205–208, doi:10.1109/CIC.2002.1166743.

[94] Chen, H.; Chen, S. A moving average based filtering system with its application to real-time QRS detection. In *Computers in Cardiology, 2003*, IEEE, 2003, pp. 585–588.

[95] Mahmoodabadi, S.; Ahmadian, A.; Abolhasani, M. ECG feature extraction using Daubechies wavelets. In *Proceedings of the fifth IASTED International conference on Visualization, Imaging and Image Processing*, 2005, pp. 343–348.

[96] Benitez, D. S.; Gaydecki, P.; Zaidi, A.; et al. A new QRS detection algorithm based on the Hilbert transform. In *Computers in Cardiology 2000*, IEEE, 2000, pp. 379–382.

[97] Ondráček, O.; Púčik, J.; Cocherová, E. Filters for ECG digital signal processing. In *International Conference Trends in Biomedical Engineering: Žilina, Slovak Republic*, volume 7, 2005.

[98] Sörnmo, L.; Laguna, P. *Bioelectrical Signal Processing in Cardiac and Neurological Applications*. Academic Press series in biomedical engineering, Elsevier Science, 2005, ISBN 9780124375529. Available from: `https://books.google.cz/books?id=RQv7tFFXYyIC`

[99] Lutovac, M.; Tošić, D.; Evans, B. *Filter Design for Signal Processing Using MATLAB and Mathematica*. Prentice Hall, 2001, ISBN 9780201361308. Available from: `https://books.google.cz/books?id=h_MxJeVdWw8C`

[100] Parák, J.; Havlík, J. ECG signal processing and heart rate frequency detection methods. *Proceedings of Technical Computing Prague*, volume 8, 2011: p. 2011.

[101] Arzeno, N.; Deng, Z.; Poon, C. Analysis of First-Derivative Based QRS Detection Algorithms. *IEEE Transactions on Biomedical Engineering*, volume 55, no. 2, 2008: pp. 478–484, doi:10.1109/TBME.2007.912658.

[102] Tikkanen, P. Nonlinear wavelet and wavelet packet denoising of electrocardiogram signal. *Biological cybernetics*, volume 80, no. 4, 1999: pp. 259–267.

[103] Hussain, M. S.; Reaz, M. B. I.; Mohd-Yasin, F.; et al. Denoising and Analysis of Surface EMG Signals. 2006: p. 306.

[104] Zucconi, M.; Ferri, R.; Allen, R.; et al. The official World Association of Sleep Medicine (WASM) standards for recording and scoring periodic leg movements in sleep (PLMS) and wakefulness (PLMW) developed in collaboration with a task force from the International Restless Legs Syndrome Study Group (IRLSSG). *Sleep Medicine Reviews*, volume 7, no. 2, 2006: pp. 175–183, doi:10.1016/j.sleep.2006.01.001.

[105] Bailenson, J.; Pontikakis, E.; Mauss, I.; et al. Real-time classification of evoked emotions using facial feature tracking and physiological responses. *International Journal of Human-Computer Studies*, volume 66, no. 5, 2008: p. 303–317, doi: 10.1016/j.ijhcs.2007.10.011.

[106] Frigerio, A.; Cavallari, P.; Frigeni, M.; et al. Surface Electromyographic Mapping of the Orbicularis Oculi Muscle for Real-Time Blink Detection. *JAMA Facial Plastic Surgery*, volume 16, no. 5, 2014: pp. 335–342, doi:10.1001/jamafacial.2014.283.

[107] Basmajian, J. V. Muscles alive. Their functions revealed by electromyography. *Academic Medicine*, volume 37, no. 8, 1962: p. 802.

[108] Mayer, G.; Penzel, T.; Kesper, K.; et al. New findings on the pathogenesis and pathophysiology of REM sleep behaviour disorder (RBD). *J Sleep Res*, volume 15, no. Suppl 1, 2006: p. 29.

[109] Kempfner, J.; Sorensen, G.; Zoetmulder, M.; et al. REM Behaviour Disorder detection associated with neurodegenerative diseases. In *2010 Annual International Conference of the IEEE Engineering in Medicine and Biology*, Aug 2010, ISSN 1094-687X, pp. 5093–5096, doi:10.1109/IEMBS.2010.5626212.

[110] Ferri, R.; Manconi, M.; Plazzi, G.; et al. A quantitative statistical analysis of the submentalis muscle EMG amplitude during sleep in normal controls and patients with REM sleep behavior disorder. *Journal of Sleep Research*, volume 17, no. 1: pp. 89–100, doi:10.1111/j.1365-2869.2008.00631.x, `https://onlinelibrary.wiley.com/doi/pdf/10.1111/j.1365-2869.2008.00631.x`. Available from: `https://onlinelibrary.wiley.com/doi/abs/10.1111/j.1365-2869.2008.00631.x`

[111] Jeppesen, J.; Otto, M.; Frederiksen, Y.; et al. Observations on muscle activity in REM sleep behavior disorder assessed with a semi-automated scoring algorithm. *Clinical Neurophysiology*, volume 129, no. 3, 2018: pp. 541 – 547, ISSN 1388-2457, doi:https://doi.org/10.1016/j.clinph.2017.12.029. Available from: `http://www.sciencedirect.com/science/article/pii/S1388245717312166`

[112] Frauscher, B.; Iranzo, A.; Gaig, C.; et al. Normative EMG Values during REM Sleep for the Diagnosis of REM Sleep Behavior Disorder. *Sleep*, volume 35, no. 6, 2012: pp. 835–847, doi:10.5665/sleep.1886, `/oup/backfile/content_public/journal/sleep/35/6/10.5665_sleep.1886/1/aasm.35.6.835.pdf`. Available from: `http://dx.doi.org/10.5665/sleep.1886`

[113] Hackner, H.; Biermayr, M.; Stefani, A.; et al. Validation of an Integrated Software for the Detection of Rapid Eye Movement Sleep Behavior Disorder. *Sleep*, volume 37, no. 10, 10 2014: pp. 1663–1671, ISSN 0161-8105, doi:10.5665/sleep.4076, `http://oup.prod.sis.lan/sleep/article-pdf/37/`

10/1663/26668836/aasm.37.10.1663.pdf. Available from: https://dx.doi.org/10.5665/sleep.4076

[114] Fukunaga, T.; Kawakami, Y.; Kubo, K.; et al. Muscle and tendon interaction during human movements. *Exercise and Sport Sciences Reviews*, volume 30, no. 3, 2002: pp. 106–110, ISSN 0091-6331.

[115] O'Sullivan, S.; Schmitz, T.; Fulk, G. *Physical Rehabilitation*. F.A. Davis Company, 2014, ISBN 9780803625792. Available from: https://books.google.cz/books?id=3fxskQEACAAJ

[116] Meerits, T.; Bacchieri, S.; Pääsuke, M.; et al. Acute effect of static and dynamic stretching on tone and elasticity of hamstring muscle and on vertical jump performance in track-and-field athletes. *Acta Kinesiologiae Universitatis Tartuensis*, volume 20, 2014: pp. 48–59.

[117] Lin, C.-F.; Chen, C.-Y.; Lin, C.-W. Dynamic Ankle Control in Athletes With Ankle Instability During Sports Maneuvers. *The American Journal of Sports Medicine*, volume 39, no. 9, 2011: pp. 2007–2015, doi:10.1177/0363546511406868, pMID: 21622814, https://doi.org/10.1177/0363546511406868. Available from: https://doi.org/10.1177/0363546511406868

[118] Finlayson, M. A. *MyotonPRO Digital Palpation, User Manual*. MYOTON AS. Available from: https://www.myoton.com/

[119] Daneshmandi, H.; Choobineh, A.; Ghaem, H.; et al. The effect of musculoskeletal problems on fatigue and productivity of office personnel: A cross-sectional study. *Journal of Preventive Medicine and Hygiene*, volume 58, 09 2017: pp. E252–E258.

[120] Wise, C. Back Pain and Common Musculoskeletal Problems. *ACP Medicine, Sec*, volume 17, 2011.

[121] Tomanova, M.; Lippert-Grüner, M.; Lhotska, L. Specific rehabilitation exercise for the treatment of patients with chronic low back pain. *Journal of Physical Therapy Science*, volume 27, no. 8, 2015: pp. 2413–2417, doi:10.1589/jpts.27.2413.

[122] Špringrová, I. P. *Funkce - diagnostika - terapie hlubokého stabilizačního systému*. Česko: I. Palaščáková Špringrová, first edition, c2010, ISBN 978-80-254-7736-6.

[123] Tichý, M. *Funkční diagnostika pohybového aparátu*. V Praze: Stanislav Juhaňák - Triton, second edition, 2017, ISBN 978-80-7553-307-4.